Examining the Effects of Applied Potential on the Surface Charge of Functionalized Monolayers for Site-Directed Ionic Self Assembly

Wesley Crowell Sanders

Dissertation submitted to the faculty of the Virginia Polytechnic Institute and State University in partial fulfillment of the requirements for the degree of

Doctor of Philosophy
In
Chemistry

Mark R. Anderson, Chair
John R. Morris, Co-Chair
Karen J. Brewer
Gary L. Long
Brian M. Tissue

November 4, 2008
Blacksburg, VA

Keywords: Ionic self assembly, polyelectrolytes, electrochemical impedance, quartz crystal microbalance, scanning electrochemical microscopy, redox probe

Examining the Effects of Applied Potential on the Surface Charge of Functionalized Monolayers for Site-Directed Ionic Self Assembly

Wesley C. Sanders

ABSTRACT

The focus of this dissertation research involves surface charge manipulation of functionalized monolayers. Application of potential to acid or base terminated organic films immobilized on electrodes results in the ionization of the terminal groups. The ionization of these groups using applied potential provides conditions favorable the control of polyelectrolyte deposition to the monolayer surface.

Research is presented that asserts that the interfacial pH of acid or base terminated monolayers responds to applied potential as a result of the accumulation of phosphate counterions to the monolayer-solution interface. Results obtained from applied potential modulation of surface charge endeavors strongly suggest that manipulation of terminal group ionization with applied potential "turns on" or "turns off" the charge of the monolayer. Switching on the surface charge of functionalized monolayers using applied potential yields conditions that make it possible for the promotion or inhibition of electrostatic attachment of polyelectrolyte to the monolayer surface.

Electrostatic interactions between immobilized polyelectrolytes and redox probes result in changes in electron transfer that can be monitored with electrochemical impedance measurements. Impedance measurements provide a qualitative assessment of the degree of potential-driven polyelectrolyte self assembly. The electrostatic interactions between the redox probe in solution and the terminal region of monolayers directly affects the extent of charge-transfer between the electrode and the redox probe in solution. For this reason, impedance measurements are able to provide an indication of whether or not potential drives to electrostatic deposition to the terminal region of a functionalized monolayer.

Unlike impedance measurements, quartz crystal microbalance measurements provide quantitative mass assessments that confirm polyelectrolyte deposition of inhibition under the direction of applied potential.

Application of appropriate potentials is shown to induce variations in the electrostatic interactions between redox probes in solution and terminal groups of monolayers. Variations in the electrostatic interactions between the modified electrode and the redox probe modulate electron transfer that produces varying current. Since scanning electrochemical microscopy (SECM) relies on modulation of feedback current underneath a ten-micrometer platinum tip, SECM provides a means for monitoring of potential-driven surface charge modulation. Experiments presented in this dissertation will show that in addition to monitoring the effect of applied potential on the charge of ionizable surface groups, SECM can also be used to selectively deposit a polyelectrolyte to the surface of a carboxylic acid terminated monolayer. The SECM tip was rastered over the surface of a functionalized monolayer in the form of a simple pattern while the electrode was immersed in a dilute polyelectrolyte solution. As the SECM tip was moved and potential stepped more positive than the PZC, ionization was confined ionization to one spot encouraging localized ionic self assembly.

Table of Contents

List of Figures

List of Tables

List of Abbreviations

AAO – anodic alumina oxide

AFM – atomic force microscopy

CYS – cysteine

EFDLA - electric field directed layer-by-layer assembly

HRP – horseradish peroxidase

ITO – indium tin oxide

MHDA – mercaptohexadecanoic acid

MPA - mercaptoproprionic acid

MUA - mercaptoundecanoic acid

PZC - potential of zero charge

PDDA - polydiallydimethyl ammonium chloride

PSS - polystyrene sulfonate

QCM - quartz crystal microbalance

SAM - self-assembled monolayer

SECM - scanning electrochemical microscope

SEM - scanning electron microscope

SERS – surface enhanced Raman spectroscopy

STM – scanning tunneling microscopy

Chapter 1. Interfacial Double-Layer Structure of Functionalized Self-Assembled Monolayers and Its Role in Ionic Self Assembly

1.1 Introduction

The research described in this dissertation demonstrates that ionic self assembly of polyelectrolytes onto the surface of functionalized monolayers can be controlled using applied potential. Potential-driven modulation of surface charge was encouraged to promote a change in the interfacial pH of acid or base terminated monolayers. When acid groups are present at the solution-monolayer interface, the groups are deprotonated, creating conditions favorable for the electrostatic attraction of polycations. Work presented in following chapters will demonstrate that application of applied potential to modified electrodes provided a means to control the extent of polyelectrolyte deposition and when combined with scanning electrochemical microscopy, allows the regioselective ionic self assembly of polyelectrolytes. For this reason, the focus of the research presented involves proof-of-concept application of potential-driven deposition of polyelectrolytes to functionalized self-assembled monolayers, not the molecular structure of the adsorbed polyelectrolyte.

1.2 The Structure of the Electrical Double-layer

Self-assembled monolayers (SAMs) refer to highly organized organic films assembled on gold substrates that form close-packed hexagonal arrangements with a $\sqrt{3} \times \sqrt{3}$ R30° overlayer structure (Figure 1a)[1]. One of the driving forces for assembly of monolayers is the 1-2 kcal mol^{-1} van der Waals interaction between neighboring alkanethiol chains of the molecules used to prepare the monolayer; this promotes the formation of a film that serves as an effective barrier to electron transfer and ion permeation (Figure 1b). The passivating ability of these films decreases with shorter chain length thiols, such as 3-mercaptopropionic acid due to the formation of domains containing thiols with different orientations within the monolayer; it is reported that monolayers of 3-mercaptopropionic acid can contain domains that differ in rotational or translational arrangement[2-4]. Additional assertions made by Giz and coworkers attribute the

disorder within monolayers prepared with short chain thiols to the inability of the lateral van der Waals forces to align the molecules in a parallel arrangement[5]. Adjacent domains within a short chain monolayer with different orientations border each other along a domain boundary, a defect site where it is reported that the diffusion of redox probes is uninhibited[4] (Figure 1c).

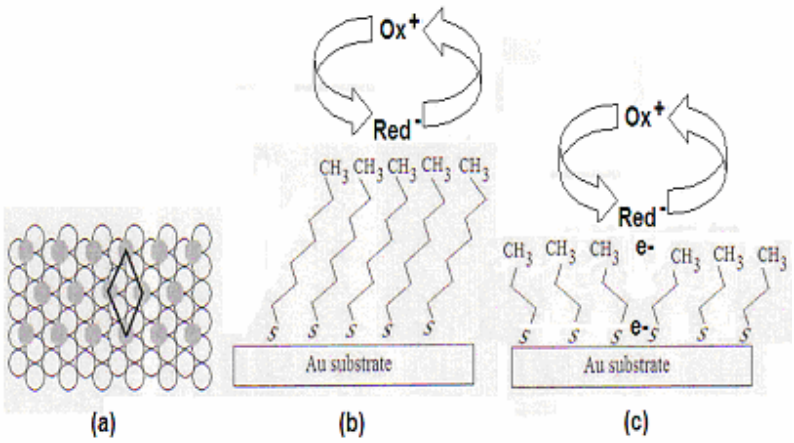

Figure 1: √3√3×R30° alkanethiol structure (a). Electron transfer through long chain (b) and short chain monolayers (c).

Although the nature of the packing density of monolayers is a parameter that researchers seek to optimize in self-assembled monolayer studies, the behavior of the interfacial region of monolayers under the influence of applied potential is the focus of this dissertation. The following thiols, 3-mercaptopropionic (Figure 2a), L-cysteine (Figure 2b), and 11-mercaptoundecanoic acid (Figure 2c), were used in these experiments in order to assess the feasibility of surface group ionization with applied potential. Preparing monolayers with functionalized surface groups offers the opportunity to tailor the electrostatic properties of the terminal region of the monolayer.

It was believed that modulation of counterion concentration at the monolayer-solution interface of functionalized monolayers can be made to differ from the bulk when potential is applied, having a direct effect on surface group ionization[6]. Surface groups such as COOH or NH_2 reside in a region know as the plane of acid dissociation, PAD[7, 8]. The extent of dissociation of the ionizable surface groups is governed by the pH of the solution and the potential applied to the modified electrode[9]. The behavior of counterions adjacent to ionizable

surface groups exposed to changes in pH and applied potential can be used to explain similar behavior when the charged surface groups are immersed in solutions containing polyelectrolytes.

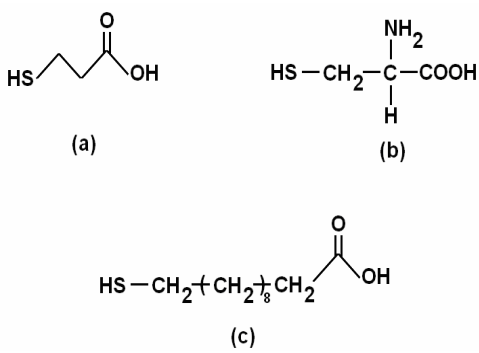

Figure 2: Structures of 3-mercaptopropionic acid (a), L-cysteine (b), and 11-mercaptounecationic acid (c).

1.2.1 The Helmholtz Model of the Electrical Double-layer

The Helmholtz model of the electrical double-layer states that application of charge to an electrode promotes the accumulation of counterions of opposite polarity at the electrode-electrolyte interface to compensate for the externally applied charge [10]. The resulting planes of opposite charge are separated by a thin layer of solvent molecules that act as a dielectric[11, 12]. This model states that any excess charge that accumulates on a metal surface resides strictly at the metal-solution interface (Figure 3)[13]. More specifically, a counter charge in the solution resides at the surface of the electrode separated by a layer of water one molecule thick. This structure is similar to that of a parallel plate capacitor whose capacitance is expressed using the Helmholtz equation (Equation 1) where the C term represents the capacitance of the double-layer, ε_0 represents vacuum permittivity (8.85419×10^{-12} J^{-1} C^2 m^{-1})[14], ε represents the dielectric constant of the insulating medium (2.1 for alkanethiol chains)[15], and d represents the thickness of the medium acting as the dielectric. The weakness of this model is the assumption that the capacitance of the double-layer is constant. This is not the case because variations in applied potential result in variations in the concentration of ions at the interface, this has an effect on the distance between the sheets of ions, d.

$$C = \frac{\varepsilon\varepsilon_0}{d} \quad (1)$$

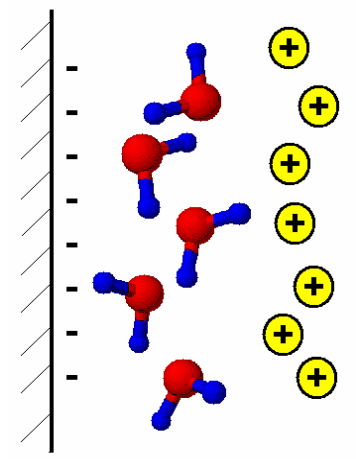

Figure 3: Structures of 3-mercaptopropionic acid (a), L-cysteine (b), and 11-mercaptounecationic acid (c).

1.2.2 Gouy - Chapman Theory

Rather than describing ions adjacent to the electrode surface as a stationary region of charge with a fixed thickness, the Gouy-Chapman Theory describes the electrical double-layer as a three dimensional area of ions in random thermal motion that extends out into the bulk solution (Figure 4)[10, 12]. The buildup of the diffuse layer is responsible for balancing the charge that exists on the surface of the electrode. This theory relates the double-layer to diffusion layer thickness[13]; a highly charged electrode results in a more compact diffuse layer and consequently, an increase in the double-layer capacitance. The shortcoming of the Gouy-Chapman model of the double-layer is the fact that this theory ignores the physical dimensions of the ions by placing no restrictions on how closely the ions in the diffuse region approach the electrode surface[16].

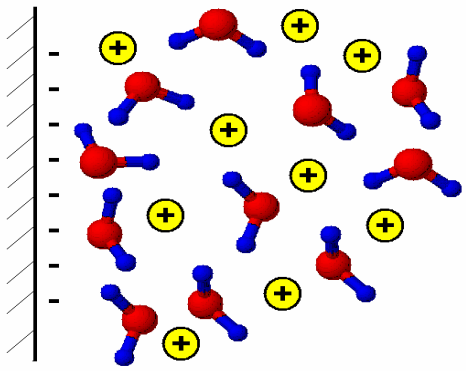

Figure 4: Gouy-Chapman diffuse layer at the surface of a metal electrode.

1.2.3 Stern Modification to the Double-layer Structure

The ions that migrate from the diffuse layer to the electrode surface to balance charge are considered point charges that can approach the surface very closely[13]. With extremely high charge at the electrode surface, the Gouy-Chapman model states that the effective separation between the electrode and solution phase is zero. The Stern model was developed to refine this aspect of the double-layer description because the proximity of the ions to the electrode surface is limited by the ionic radius. The Stern model asserts that a plane of closest approach exists. This model further asserts that the electrical double-layer consists of a loosely bound diffuse layer and a tightly bound Stern layer (Figure 5)[17]. The Stern layer is divided into two parts: a compact inner layer of directly adsorbed ions and a diffuse layer of ions adjacent to the contact adsorbed species[10, 16]. In the case of an ω-functionalized monolayer assembled on gold; the ionizable surface groups lie in the inner Helmholtz plane (IHP) and are surrounded by a thin layer of water molecules serving as a dielectric[9]. The outer Helmholtz plane (OHP) lies on the opposite side of the dielectric, and is described a layer of solvated ions where the nature of this layer is governed by charge and concentration of counterions in the electrolyte[9]. In addition to serving as the interface between the Stern layer and the diffuse Gouy-Chapman layer[9], the outer Helmholtz plane contains ions that diffuse from the bulk and are limited in the distance they can approach the electrode surface[13]. Due to the limited approach of ions at the outer Helmholtz plane to the electrode surface, the interaction between these ions and the electrode surface results from long range Coulombic forces[13].

For this reason, the ions that lie in the outer Helmholtz plane are said to be nonspecifically adsorbed[10, 13]. This theory is inclusive of the Gouy-Chapman layer because nonspecifically adsorbed ions, separated from the Stern layer by the outer Helmholtz plane[9] but not associated with this plane, are in random motion, and comprise of a three-dimensional region referred to as the diffuse layer[13].

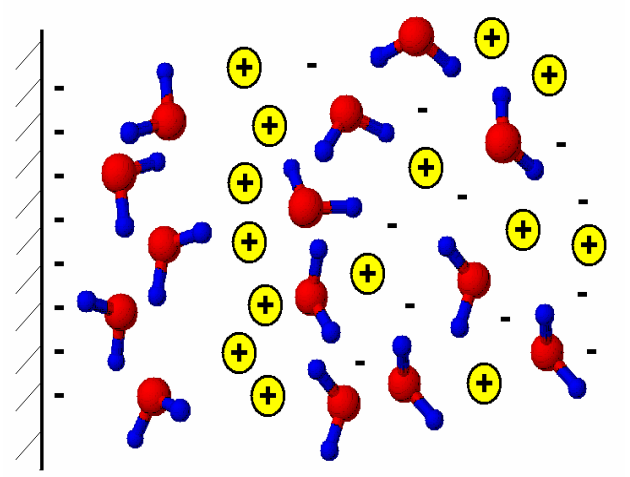

Figure 5: Gouy-Chapman Stern layer at the surface of a metal electrode.

1.2.4 Quantifying effects of pH on the electrical double-layer

The ionizable groups that lie in the inner Helmholtz plane of the Stern layer are often referred to as the plane of acid dissociation (PAD)[7, 8]. Since the control of the dissociation of the terminal groups is one of the main objectives of this research, the extent of acid dissociation in the PAD needed to be described. Double-layer capacitance is a parameter that is sensitive to the charged state of functionalized monolayers[18]. Double-layer capacitance is a value that is used to model the capacitive behavior of the electric double-layer at the terminal region of the electrode[13]. Mendes et al. demonstrated that modulation of double-layer capacitance with solution pH was possible due to interactions between the ionizable groups in the IHP and an anionic redox probe[19]. The total capacitance of an electrochemical system is the sum of individual capacitances associated with the electrical double-layer (Equation 2)[20] where the total capacitance, C_T^{-1}, is the sum of the monolayer film capacitance, C_F^{-1}, and the double-layer capacitance, C_{DL}^{-1} which is inclusive of the IHP and the OHP. The sensitivity of the double-layer capacitance is based on fluctuations due to the degree of surface group dissociation[8, 18, 21, 22].

$$C_T^{-1} = C_F^{-1} + C_{DL}^{-1} \quad (2)$$

Schweiss et al. assert that in the absence of redox-active molecules, the lack of electron transfer establishes conditions where double-layer capacitance is influenced by double-layer

charging[21]. This charging arises from the release of protons from acidic terminal groups and the association of protons with basic terminal groups where both conditions lead to the accumulation of charges in the electric double-layer and an increase in double-layer capacitance.

1.2.5 Applied potential affects on the electric double-layer

Previously it was stated that double-layer capacitance is used to quantify the extent of the effects of surface group ionization on the electrical double-layer. It was later discovered that double-layer capacitance serves as an effective measure of the effect of potential on the interfacial charge of functionalized surfaces because potentials positive or negative of the potential of zero charge modulate the concentration of counterions in the double-layer region adjacent to the interface[23]. Potential of zero charge (PZC) is defined as the potential where no excess surface charge exists in the terminal region of a monolayer[24] and is reported to be the potential where ion adsorption is absent[25].

Early analyses of the potential of zero charge arose from studies of the electrocapillary effect, which involves the study of the surface tension of Hg as a function of applied potential[10]. This analysis was conducted using a mercury drop electrode due to the non-rigidity of the electrode surface, making potential effects on the surface tension of the drop easy to identify[10]. Both Wang[10] and Bard et al.[13] report the appearance of a maximum in an electrocapillary curve. At potentials below or above the potential of zero charge, accumulation of excess charge resulted in repulsion of charges along the surface of the mercury drop electrode. This repulsion along the "skin" of the electrode resulted in a decrease in the tendancy of the surface to contract. This surface contraction produces a decrease in surface tension. However, when there is no excess charge present, repulsion between like charges is absent, and surface tension is optimized. A plot of surface tension versus potential, referred to as an electrocapillary curve, contains a maximum which marks the PZC. The maximum denotes the PZC because at this point, surface tension is maximized due to the absence of excess charge[10, 13]. The minimum in capacitance vs potential plots is the potential of zero charge as shown in previous reports[23, 26, 27]. At potentials

at or near the PZC, no excess charge exists at the monolayer surface, resulting in an increase in Stern layer thickness in the double-layer region leading to a decrease in double-layer capacitance. Although the behavior of the counterions in the double-layer at potentials relative to the PZC effects the double-layer capacitances used to determine the PZC, the actual PZC value is independent of ionic strength[23, 28]. Reports however, show that application of potentials positive or negative of the PZC modulates the ionic strength at the terminal region of the monolayer producing counterion concentration at the monolayer-solution interface that can differ significantly from the bulk[23].

For potentials positive of the PZC, anions are adsorbed; and, at potentials negative of the PZC, cations accumulate at the interface[29]. This effect was observed during surface enhanced Raman spectroscopy experiments conducted by Anderson and Evans[30]. They report that applying potentials more negative than -0.4 V to silver electrodes immersed in solutions of 4-pyridine carboxaldehyde encouraged accumulation of the protonated form of the aldehyde at the electrode surface[30].

Kutnetsov et al. applied potentials negative to the PZC of a glassy carbon electrode in order to orient and bind cytochrome c molecules to the electrode surface as pretreatment for covalent attachment[31]. Iwasita and coworkers report on the adsorption of water molecules on platinum electrodes in an “H –down” or “O – down” orientation based on the application of appropriate potentials[32]. Nosal-Wiercinska et al. report that thiourea adsorbed to the surface of mercury electrodes from both neutral and acidic solutions due to the excess charge existing on the surface due to the application of the appropriate potential relative to the PZC[33]. An example of surface charge manipulation via potential is also described in work reported by Cao[34]. This report presents Raman spectra of an energized electrode modified with an amine terminated SAM immersed in sodium perchlorate solution. The Raman spectra show a decrease ClO_4^- intensity due to the decrease in the local hydrogen ion concentration at the interface resulting in a neutral

surface. The lack of charge at the interface promoted no electrostatic interaction between the terminal region of the amine terminated monolayer and the ClO_4^- counterion.

An additional applied potential effect on interfacial pH, reported by Sugihara and coworkers, show that the interfacial pH of 16-mercaptohexadecanoic acid monolayers in pH 5.3 phosphate buffer solutions can vary significantly from the bulk pH under applied potential conditions[35].

1.3 Ionic Self Assembly

The electrical double-layer is a collection of counterions that accumulate adjacent to a surface in response to surface charge via ionizable surface groups or the application of applied potential. The accumulation of counterions in response to the surface charge is a version of ionic self assembly. Ionic self assembly is a process that can encapsulate electro-active polymers, dyes, quantum dots, and redox probes in multilayer films[36]. This makes ionic self assembly an affordable and facile method for the fabrication of flat transparent films, organic LEDs, and conductive polymer materials[37]. Modification of the surface charge of functionalized monolayers by modulating the interfacial pH of the monolayers has been used to assemble polyelectrolytes to the charged surface[38-41]. Decher and coworkers were among the first to report ionic self assembly of polyelectrolytes onto functionalized monolayers[38]. They reported the use of a cationic monolayer, 3-aminopropyldimethyl siloxane, for the immobilization of anionic polyelectrolytes such as polystyrene sulfonate, followed by subsequent attachment of polydiallydimethyl ammonium chloride, a cationic polyelectrolyte[42]. This result stresses an important point, that electrostatic attraction between the opposite charges of ionized surface groups and polyelectrolytes is the impetus for ionic self assembly (Figure 6). FT-IR analyses conducted by Jordan et al.[43] show that successful cationic polyelectrolyte deposition accomplished through ionic pairing between the ammonium groups of poly-L-lysine and a deprotonated carboxylic acid monlayer. Wu and coworkers report the use of carboxylic acid terminated monolayers for the ionic self assembly of cationic polydiallyldimethyl ammonium chloride and urease for urea detection[40].

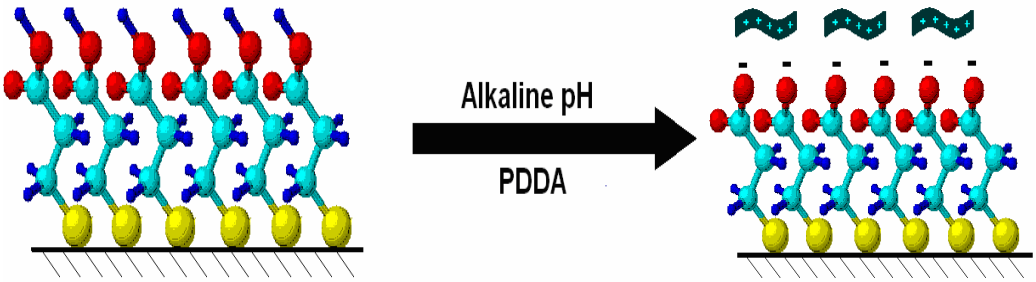

Figure 6: Ionic self assembly of polydiallyldimethyl ammonium chloride on a deprotonated carboxylic acid terminated surface.

Although electrostatic attraction plays a major role in ionic self assembly, there are assertions that short-range hydrophobic interactions play a secondary role in the ionic self assembly process[36, 44]. Support of these assertions comes from literature that claim the assembly of proteins such as myoglobin and lysozyme onto an oppositely charged polymer, such as polystyrene sulfonate, occurs readily because due to the hydrophobic environment within charged polyelectrolytes[44]. The short range van der Waals forces between the hydrocarbon regions of protein and the polymer aide in effective binding[44].

The same report shows that adsorption of these proteins to substrates of negatively charged aluminosilicates is blocked. Protein adsorption to aluminosilicates is inhibited due to the lack of short range van der Waals forces along the extremely hydrophilic surface of aluminosilicates. Weak electrostatic binding between proteins and aluminosilicate surfaces allows removal of proteins by simply by rinsing the substrate with water. When considering both electrostatic and hydrophobic interactions in the ionic self assembly process, electrostatic interactions between the polyelectrolyte and the substrate are responsible for the structure of the polyelectrolyte film and the short range hydrophobic forces are responsible for film properties such as thickness, morphology, and stability[36].

Molecular weight also plays a role in polyelectrolyte adsorption as a report by Clark et al. indicates[37]. These researchers used a patterned polymeric stamp coated with trichloralkylsilane solution to deposit alternating bands of monolayers on a substrate[37]. This technique, known as microcontact printing, allowed selective deposition of polyelectrolytes to functionalized surfaces

via ionic self assembly. Their AFM analysis showed that increasing the molecular weights of polydiallyldimethyl ammonium chloride and polystyrene sulfonate used in the ionic self assembly resulted in a decrease of edge resolution of the patterned domains. They assert that higher molecular weight polyelectrolytes result in an extension of the ionically adsorbed polyelectrolyte past the edge patterned domain.

In addition to decreasing molecular weight of polyelectrolytes to increase patterned domain resolution, there are reports that state ionic strength can be used to control the resolution of the patterned domains[37, 45]. Results of their studies indicate that low ionic strengths result in polyelectrolytes with extended conformations. At low ionic strengths, polyelectrolytes are rigid due to repulsion between charged monomer units. Increasing ionic strength results in a decrease in the charge density around the polyelectrolyte resulting in an increase in the hydrophobic interactions between the nonpolar regions of the polyelectrolyte[37, 45]. Consequently, adsorption of polyelectrolytes from solutions with high ionic strengths results in the formation of thick layers due to increased interchain interactions between monomer units.

Although reports have shown that molecular weight[37] and ionic strength[37, 45] play a pivotal role in the ionic self assembly of polyelectrolytes, the main focus of this research is centered around the interaction between terminal acid and base groups of monolayers and polyelectrolytes in solution. Encouraging ionic self assembly to the surface of carboxylic acid terminated monolayers using applied potential was one of the main objectives of this dissertation research. For this reason, no change in molecular weight of the polyelectrolyte or ionic strength of the assembling solution was made during the course of the experiments presented in this dissertation. Use of a single polyelectrolyte, polydiallyldimethyl ammonium chloride (PDDA), and 0.05 $mol \cdot L^{-1}$ phosphate buffer solutions provided constant experimental conditions for the assessment of polyelectrolyte deposition driven by the application of potentials relative to the PZC.

1.4 Electric field driven ionic self assembly

The driving force behind ionic self assembly is immersion of a functionalized surface in a solution with a pH that ionizes the surface group, leading to the adsorption of an oppositely charged polyelectrolyte to the monolayer surface (Figure 6). Other reports describe the use of applied potential to adsorb polyelectrolytes to electrode surfaces[46-51]. This process is known as the electric field directed layer-by-layer assembly method (EFDLA) and was first demonstrated Gao and coworkers[46]. This process involves applying a potential to an electrode which either serves to accelerate or decelerate the deposition of polyeletrolytes to the electrode surface; deposition is encouraged when the applied potential and the polyelectrolyte have opposite polarities, and is inhibited when the polarities are the same[48]. Ionic self assembly by solution adsorption limits control over the sites of polyelectrolyte deposition[48], however electric field driven deposition allows spatial control over the deposition of polyelectrolytes and makes possible the formation of lateral, binary patterns of adsorbates of opposite polarity on the same substrate[46, 48-50]. Gao and coworkers first demonstrated the ability of the EFDLA process to selectively deposit polyelectrolytes by successfully depositing polydiallydimethyl ammonium chloride/glucose isomerase bilayers onto two indium tin oxide (ITO) strips on a glass substrate separated 2 mm apart[46]. In a later report, the EFDLA method was used to deposit two different bilayers on indium tin oxide substrates assembled on glass; polyelectrolyte bilayers consisting of glucose oxidase and catalase bilayers were immobilized on the separate indium tin oxide strips separated by 2 mm[49]. Although EFDLA allows researchers to control the spatial deposition and the extent of the assembly of polyelectrolytes on the surface of electrodes, the patterns deposited on substrates is limited to lateral structures. In order to address the limited range of patterns formed with the EFDLA process, Wu et al. attempted to use this technique to produce enzyme nanotubes[47]. These researchers used an indium tin oxide substrate coated with anodic alumina oxide (AAO) as the working electrode and an Au electrode as the counter electrode. Nanotube fabrication proceeded upon application of a negative potential to the ITO/AAO electrode while

immersed in polydiallyldimethyl ammonium chloride. The ITO/AAO electrode was then immersed in horseradish peroxidase (HRP) while a positive potential was applied to the electrode. Phosphoric acid solution was used to dissolve the AAO membrane and the remaining structures were PDDA/HRP nanotubes.

Ionic self assembly is a versatile, economical, and effective method for the fabrication of multilayer films[38], producing multicomponent structures on a single substrate[49], and for the immobilization of enzymes for biomolecule detection[40, 52]. However, it is difficult to use solution driven ionic self assembly to create microscale and nanoscale structures with definite dimensions because placement of polyelectrolytes are randomly deposited. This is the motivation behind the research presented in this dissertation; it was believed that potential induced modulation of the surface charge of functionalized monolayers would offer better control over the extent and ultimately the location of polyelectrolytes during ionic self assembly.

1.5 Conceptual Basis of Dissertation

It is reported in the literature that potential can control the interfacial pH of surfaces with functional groups[29, 34]. The concept of potential-driven manipulation of surface charge is the focus of the research presented in this dissertation. This dissertation demonstrates that excess charge applied to electrodes modified with monolayers terminated with acid or base groups encourages the accumulation of phosphate ions at the interface. The phosphate ions behave as conjugate bases that result in the deprotonation of the surface acid groups. Once deprotonated, ionic self assembly of a cationic polyelectrolyte to the resulting carboxylate surface is encouraged. This allows control over the extent of ionic self assembly by controlling the ionization of terminal surface groups using potential, making it possible to turn on or turn off ionic self assembly.

Attachment of polyelectrolytes (polydiallyldimethyl ammonium chloride and polystyrene sulfonate) to the surface of 3-mercaptopropionic acid (3-MPA), 11-mercaptoundecanoic acid (11-MUA), and cysteine monolayers via applied potential was confirmed using electrochemical

impedance measurements. This was possible due to the electrostatic interactions between the charged polymer and an anioic redox couple, $[Fe(CN)_6]^{3-/4-}$. The quantity of polyelectrolytes deposited on the functionalized monolayers was assessed using quartz crystal microbalance measurements. Dissociation of ionizable surface groups via applied potential is also monitored using scanning electrochemical microscopy (SECM).

During imaging with scanning electrochemical microscopy (SECM), the potential of 3-mercaptopropionic acid (3-MPA) and 11-mercaptoundecanoic acid (11-MUA) modified electrodes is stepped to values more positive than the PZC in solutions buffered to pH values below the surface pK_a of the monolayers. The resulting electrostatic attraction between the deprotonated carboxylic acid groups and the cationic redox probe, $[Ru(NH_3)6]3^+$, was imaged.

The secondary objective of this research was to attempt potential-driven, site- directed ionic self assembly of polyelectrolytes to the surface of functionalized monolayers. The most common method used to deposit polyelectrolytes onto the surface of functionalized monolayers is solution adsorption. Deposition using solution adsorption involves immersion of a functionalized monolayer in a solution with a pH that promotes surface group ionization driving the deposition of an oppositely charged polyelectrolyte[38-41]. However, this technique allows no control over the spatial deposition of polyelectrolytes. Polymer deposition promoted in this fashion results in the immobilization of a film that coats the entire substrate with a polymer film[53]. A secondary goal of the research presented in this dissertation involves using an SECM tip was used to localize the applied potential on the surface of functionalized monolayers to a region tens of micrometers across. Localizing the potential step to a specific region on a functionalized monolayer, and promoting surface group ionization at that location makes it possible to selectively deposit polyelectrolytes onto monolayer surfaces. Site-directed deposition of PDDA to the surface of a functionalized monolayer is demonstrated by depositing simple patterns on the monolayer surface. This process has the potential to be used to pattern an array

of microdots on the surface of a functionalized monolayer for the purpose of creating a biosensor with the capability of multiple sensing specificities.

This dissertation describes the outcomes of the major objectives of this work as follows. Chapter 3 describes surface pK_a and PZC determination of 3-mercaptopropionic acid (3-MPA) and 11-mercaptoundecanoic acid (11-MUA) using electrochemical impedance. This chapter will also discuss how electrochemical impedance measurements were used to confirm the deposition or inhibition of polydiallydimethyl ammonium chloride via applied potential. Included in this chapter is a discussion pertaining to the use of charge-transfer resistance values obtained from impedance data to reflect the electrostatic interactions between the polyelectrolyte layer assembled by potential-driven ionic self assembly and the redox couple. A description of quartz crystal microbalance measurements for the purpose of determining the mass of polyelectrolyte deposited using applied potential is included in this chapter also.

Chapter 4 describes applied potential experiments using surfaces modified with cysteine monolayers. Surface pK_a and PZC determinations for cysteine monolayers are included in this chapter. This chapter will also discuss how electrochemical measurements were used to confirm the deposition or inhibition of polydiallydimethyl ammonium chloride and polystyrene sulfonate to cysteine surfaces via applied potential. Included in this chapter is a discussion pertaining to the use of charge-transfer resistances obtained from impedance data to reflect the electrostatic interactions between the polyelectrolyte layer assembled by potential-driven ionic self assembly and the redox couple. Mass determinations of polydiallyldimethyl ammonium chloride and polystyrene sulfonate adsorbed to cysteine monolayers using QCM is reported in this chapter as well.

Surface charge imaging of 3-MPA and 11-MUA monolayers under the influence of applied potential will be discussed in chapter 5. The discussion will include how SECM was used to localize a pH change and how the resulting electrostatic attraction between the carboxylate surface and the redox probe generates a current change underneath the SECM probe.

Images produced from stepping the potential to values positive and negative of the PZC will be presented.

Chapter 6 will describe site-directed ionic self assembly of PDDA to the surface of functionalized monolayers using SECM. A description of how the SECM tip is used to localize the electric field for the purpose of modifying the interfacial pH for site directed ionic self assembly of PDDA will be discussed. Chapter 7 will provide a summary of major conclusions drawn from the experiments and future endeavors of the project.

Chapter 2. Experimental Methods

2.1 Introduction

Since potential induced manipulation of the electrical double-layer for the purpose of spatial control over polyelectrolyte deposition is the focus of the dissertation research, electroanalytical techniques sensitive to electrostatic interactions in the interfacial region of the monolayer were selected. The most frequently used techniques used to monitor the effect of potential on interface-electrolyte interactions were electrochemical impedance measurements and quartz crystal microbalance measurements. A general description of these techniques and experimental conditions associated with these measurements is included in this chapter.

A secondary objective of this dissertation project involves using scanning electrochemical microscopy to direct the ionic self assembly of polyelectrolytes to the surface of functionalized monolayers. For this reason, this chapter also includes a description of the scanning electrochemical microscope and experimental details associated with imaging with the SECM.

2.2 Chronoamperometry

In order to induce surface group ionization for ionic self assembly, chronoamperometry was used to alter the potential of modified electrodes between values where ionization of the monolayer is expected or it not expected. Chronoamperometry is a potential step technique that manipulates of the electrical double-layer to create a concentration gradient near the surface of the electrode[10]. Depletion of the electroactive reactant adjacent to the surface produces the diffusion layer[11]. At the onset of the potential step, there is a steep concentration gradient resulting in a low double-layer thickness[10]. The progression of the potential step experiment results in the expansion of the diffusion layer and a decrease in the concentration gradient due to the decreasing concentration of the electroactive reactant. In a chronoamperometry experiment, the potential is stepped from an initial potential to a final potential. The potential is held at the final potential for a predetermined amount of time while current is measured. Since these

measurements involve the use of a stationary electrode in a cell where stirring is absent, the mass transport of electroactive species from the bulk solution is governed by diffusion.

2.3 Electrochemical Impedance

Electrical impedance measurements are well suited for analysis of interfacial behavior because electrostatic interactions between charged surfaces and redox-active probes in solution can be quantified. It is reported that changes in charge-transfer resistance is an indicator of a film's passivating ability[54]. Electrochemical impedance measurements involve measuring the response of an electrochemical system to sinusoidal potential function applied to the modified substrate. The sinusoidal potential is in the form of an AC voltage with a 5 mV peak-to-peak voltage with frequencies ranging from 1.0×10^{6} Hz, to 1.0×10^{-3} Hz[55]. The current response to the sinusoidal potential function is shifted in time and amplitude[56]. Impedance data obtained from the perturbation of the applied voltage consists of a resistive (real) component (Z') that is in phase with the applied sinusoidal voltage and a capacitive (imaginary) component (Z'') that is out of phase with the applied sinusodal voltage (Figure 7).

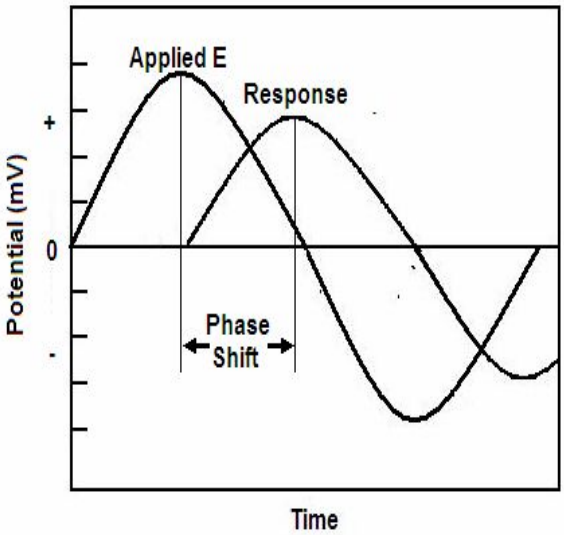

Figure 7: Response of an electrochemical system to an AC voltage during an impedance experiment.

The Randles circuit (Figure 8) is used to model the electrochemical systems analyzed by impedance measurements. The Randles circuit combines components that describe solution

resistance (R_S), self-assembled monolayer capacitance (C_{SAM}), double-layer capacitance (C_{DL}), charge-transfer resistance (R_{CT}), and Warburg impedance (R_W)[57], a parameter governed exclusively by mass transfer. The resistances obtained from impedance data provide information regarding the permeability of the film. Capacitance information obtained from impedance analyses provides information that describes the dielectric properties of the film.

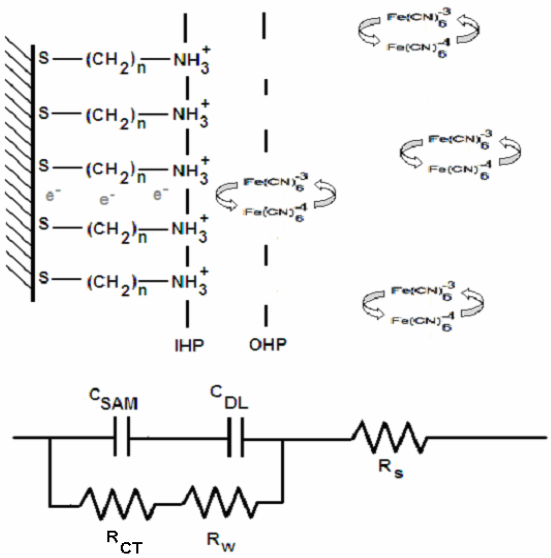

Figure 8: Randles equivalent circuit of a self-assembled monolayer and the correspondi Response of an electrochemical system to an AC voltage during an impedance experiment.

In the Randles equivalent circuit, one of the components of the overall impedance is described as two capacitors connected in series. There is a capacitance specific for the self-assembled monolayer (C_{SAM}) and another capacitance is specific for the double-layer capacitance (C_{DL}). The second component of the total impedance is the resistance of the system composed of one resistance that describes the ion permeability of the self-assembled monolayer (R_{CT}). The Warburg resistance arises from diffusional mass transport of the redox probe through defective regions within the monolayer (R_w).

These Randles circuit parameters can be graphically expressed in one of two ways. A Nyquist plot is a plot of the imaginary impedance (Z") vs the real impedance (Z')[54] (Figure 9).

Often there is a 45° line that appears that is representative of diffusional mass transfer that is obtained during impedance analyses of monolayers comprised of shorter chain thiols. The

semicircular response provides the most useful information on the resistances of the system. The intercept in the high frequency portion of the Nyquist plot yields resistance information regarding the solution resistance, which is governed by the concentration of the electrolyte used in the impedance experiment. The intercept at low frequency region of the Nyquist plot describes resistance associated with charge-transfer between redox probes in solution and the electrode. The most useful information gathered from Nyquist plots during the course of these investigations is the semicircle diameter. A qualitative assessment of the extent of the electrostatic interaction between the interface and the electrolyte is obtained by comparing the diameters of Nyquist plots produced from modified electrodes exposed to polyelectrolytes at various potentials. For example, in the presence of an anionic redox probe, a low semicircle diameter would indicate deposition of a cationic layer. Electrostatic attraction brings the negatively charged redox couple to the terminal region of the electrode containing the cationic layer, increasing the likelihood of electron transfer. This action would produce a lower charge-transfer resistance (R_{CT}) denoted by a lower R_{CT} intercept in the Nyquist plot. The converse would be true if an anionic layer were deposited on the monolayer surface.

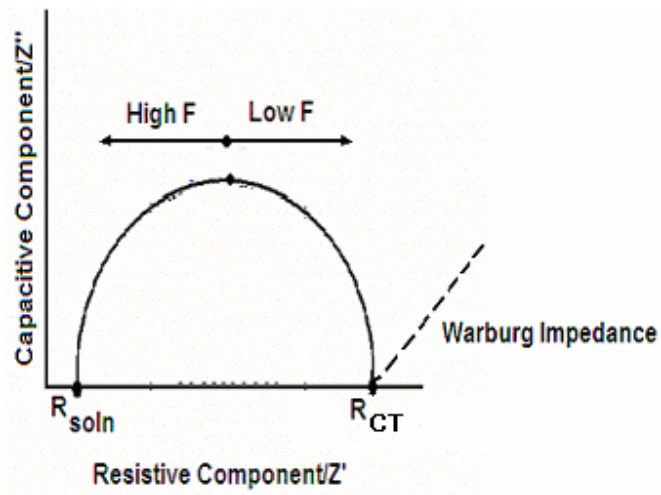

Figure 9: Example Nyquist plot.

Figure 10 contains Nyquist plots obtained with interfaces modified by self assembly of hexanethiol, heptanethiol, octanethiol, and nonanethiol. It is evident from these plots that the solution resistance (indicated by the left x intercept) is independent of thiol chain length.

However it is clearly obvious that there is a direct correlation between thiol chain length and charge-transfer resistance (right x intercept) based on increasing semicircle diameter.

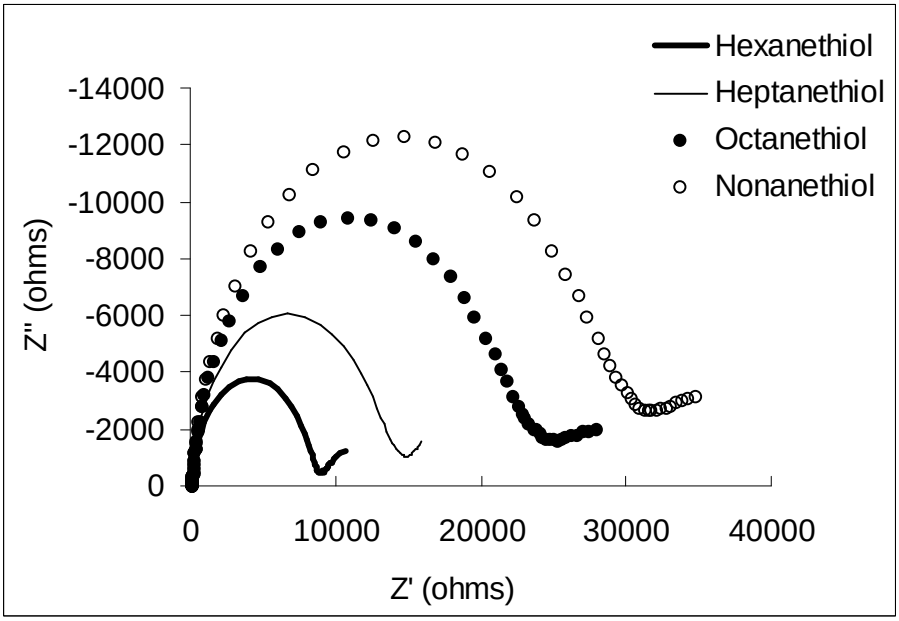

Figure 10: Nyquist plot for hexanethiol, heptanethiol, octanethiol, and nonanethiol. Impedance measurements were conducted in 0.005 mol·L^{-1} of $[Fe(CN)_6]^{3-/4-}$ containing 0.1 mol·L^{-1} KCl at a potential of 0.2 V vs Ag/AgCl.

A Bode plot (Figure 11) is a graphical representation of impedance data that provides a more explicit relationship between impedance data and frequency; this is the case because the logarithm of the total impedance (Z) versus the frequency is plotted. A horizontal line is present in the frequency regions where resistive effects dominate. This is due to the fact that the resistive component of the impedance data is frequency independent, so there is no response to changes in frequency[55]. Capacitive behavior is represented in Bode plots with a straight line with a slope of -1 because of the inverse relationship between capacitance and frequency[55]. Bode plots can be used to obtain values specific for double-layer capacitance. Extrapolating the linear region of the Bode plot to the y-axis yields a value of the double-layer capacitance, as illustrated in Figure 11. In this low frequency region, the total impedance of the system is governed exclusively by capacitive effects at the terminal region of the surface[56].

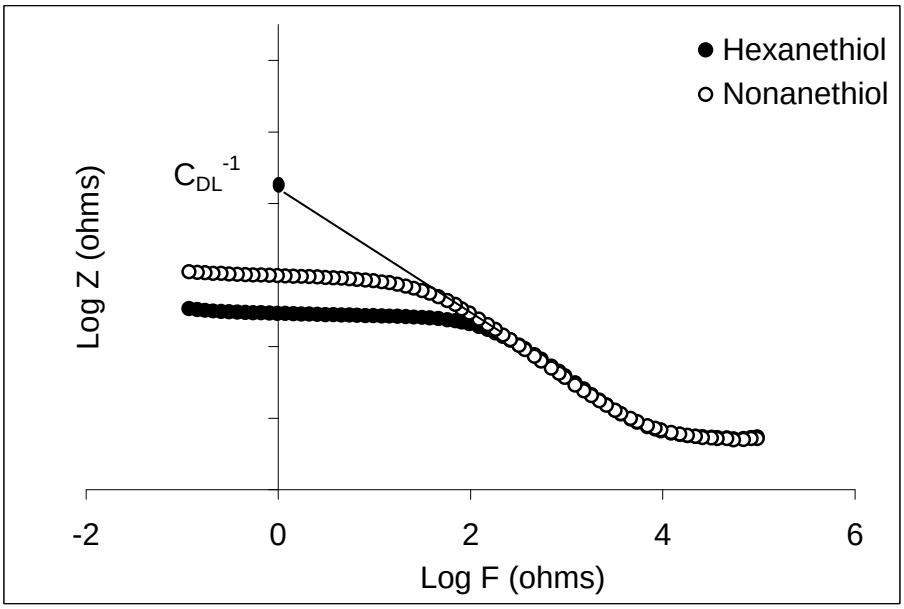

Figure 11: Double-layer capacitance determination for hexanethiol and nonanethiol. Impedance measurements were conducted in 0.005 mol·L-1 of $[Fe(CN)_6]^{3-/4-}$ containing 0.1 mol·L^{-1} KCl at a potential of 0.2 V vs Ag/AgCl.

Double-layer capacitance values and charge-transfer resistances for hexanethiol, heptanethiol, octanethiol, and nonanethiol are listed in Table 1. From this data it is seen that increasing chain length increases charge-transfer resistance due to denser packing of longer chain thiols resulting from increased lateral interactions between neighboring methylene chains. This dense packing inhibits ion permeation through the film.

Table 1: Charge-transfer resistance and double-layer capacitance for hexanethiol, heptanethiol, octanethiol, and nonanethiol.

Thiol	R_{CT} (Ω)
Hexanethiol	844.97
Heptanethiol	13,663
Octanethiol	22,422
Nonanethiol	28,754

Electrochemical impedance measurements have been used extensively to characterize the permeability[58-61] and thickness[62, 63] of alkanethiol self-assembled monolayers. There are also reports that use impedance measurements as the detection method for biosensing applications[64-66]. There are also several reports that describe the use of impedance measurements for analyzing the behavior of the double-layer structure[20, 21, 67-71]. Komura and coworkers report using impedance measurements to examine the charge-transfer at the interfacial region of at ionized

terminal groups[67]. Komura et al. demonstrate this by immersing a carboxylic acid terminated monolayer in solutions with pH ranging from 2 to 8 and measuring the charge-transfer resistance between the monolayer surface and $[Ru(NH_3)_6]^{3+}$, a cationic redox probe[67]. They show that charge-transfer resistance decreased by a factor of 300 when solution pH was changed from 2 to 8. This is attributed to the dissociation of carboxylic acid groups at high pH values. The resulting carboxylate groups exhibit strong repulsion between neighboring carboxylic acid groups while exhibiting electrostatic attraction with the cationic redox probe. The resulting open layer structure allows the redox probe to permeate the monolayer and exchange electrons with the electrode surface. At low pH values, it is reported that the van der Waals interactions between neutral carboxylic acid groups forms a more compact layer and prevents the redox probe from reaching the electrode surface.

These electrostatic interactions between ionizable surface groups and redox probes are the basis for Faradaic impedance titrations, which are titrations that involve recording impedance vs solution pH for the purpose of determining surface pK_a of functionalized self-assembled monolayers[68-70].

2.4 Quartz Crystal Microbalance

In addition to electrical circuit parameters of thin films, the mass of material deposited onto electrode surfaces were determined with a quartz crystal microbalance (QCM). Quartz crystal microbalances have been used to monitor the deposition and dissolution of monolayer films, changes in surface morphology of monolayer films, and changes in mass[72]. Qu and coworkers report that in addition to mass changes, viscoelastic changes of functionalized monolayers as a function of pH can be monitored with a quartz crystal microbalance[73]. Rocha and cowokers used a QCM to monitor the adsorption and desorption of thiols on gold surfaces[74]. QCM measurements have also been used to monitor the stability of polyamide films[54, 75]. The main component of a QCM device is a quartz plate housed between two electrodes[72, 76, 77]. The application of the voltage across the quartz plate produces a corresponding mechanical strain.

When an alternating current is applied to the quartz plate, the plate vibrates at the resonant frequency of the crystal[72, 76]. The vibrations travel through the crystal in a direction that is perpendicular to the crystal surface[76, 78] (Figure 12a). Buttry and coworkers assert that the transverse wave that propagates through the crystal will also propagate through uniformly distributed rigid adsorbates on the crystal surface[72] (Figure 12b). Addition of a rigid adsorbate to the crystal surface can be viewed as an extension of the crystal thickness and for every fractional change in film thickness there is a concurrent fractional change in the fundamental frequency of the QCM resonator[72].

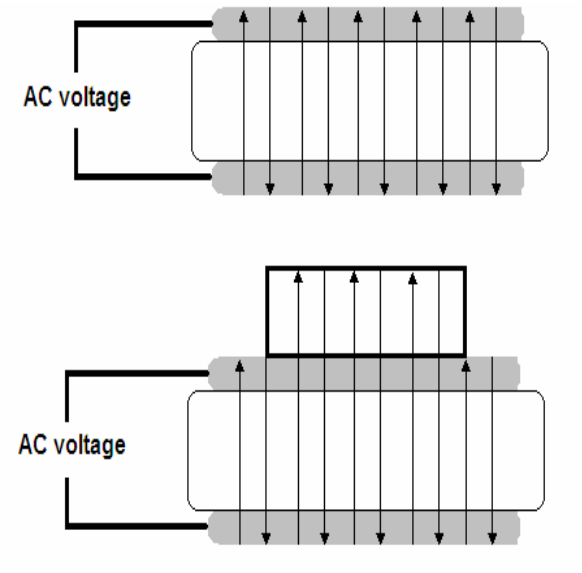

Figure 12: Behavior of transverse wave before (a) and after (b) film deposition.

The fundamental frequency of the QCM resonator changes as mass is adsorbed or removed from the resonator surface[79]. An example of this is shown in Figure 13. In this graph, a decrease in frequency is observed after deposition of a 3-mercaptopropionic acid monolayer, and after ionic self assembly of PDDA to the surface of the monolayer.

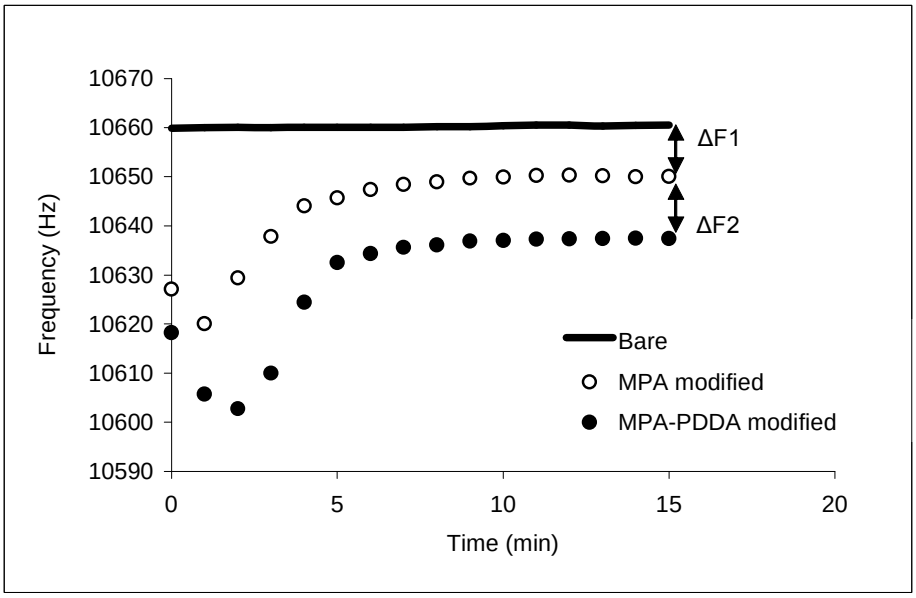

Figure 13: QCM frequencies of a bare electrode, 3-MPA modified electrode, and deposition of PDDA on a 3-MPA monolayer.

Buttry and coworkers assert that application of an alternating current across a quartz plate produces an acoustic transverse wave that travels through the thickness of the quartz plate, reflecting back and forth through the thickness of the quartz plate[72]. This vibration wave occurs due to the presence of dipoles in the crystal lattice[72]. Application of an electric field results in a reorientation of the dipoles leading to the generation of an elastic deformation (Figure 14). Application of the opposite polarity produces an identical deformation in the opposite direction. Melroy and coworkers report that the sensitivity of QCM devices are on the order of 1.1×10^{-9} g.

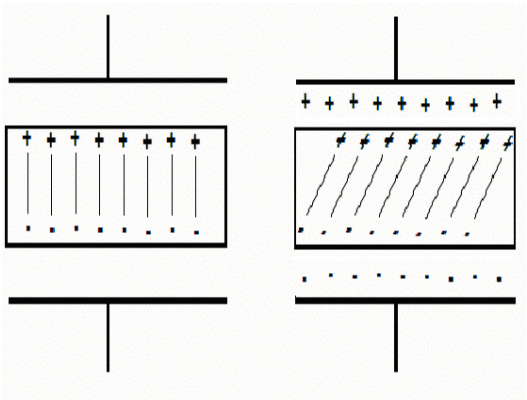

Figure 14: Response of dipoles of piezoelectric crystal to applied voltage.

The relationship between the mass adsorbed on the crystal surface and the fundamental frequency of the quartz resonator is expressed in the Sauerbrey equation (Equation 3)[72, 73, 77, 79]: Where the shear modulus of the quartz, μ_q, has a reported value of 2.947×10^{13} g·m^{-1}·s^{-2} and the density of quartz, ρ_q, has a value of 2.648 g·m^{-3} [79]. The area of the electrode surface is defined as A, f_o is the fundamental frequency of the quartz, Δm is the mass change, and Δf is the frequency change[79].

$$\Delta f = -\frac{2 f_o^2 \Delta m}{A\sqrt{\mu_q \rho_q}} \quad (3)$$

QCM measurements have been used for measuring the mass at the interface of a carboxylic acid monolayer under different pH conditions[35, 77]. Sugihara and coworkers used a QCM to perform a *surface mass titration*[35]. They observed a decrease in the frequency of QCM plates modified with 15-mercaptohexadecanoic acid in alkaline solutions, which translates to an increase in mass which they attribute to the association of cations in solution to the deprotonated carboxylic acid groups. Wang et al. performed a similar experiment and observed a frequency increase, characteristic of a decrease in mass[77]. They assert that accumulation of ions do not account for the frequency change but the change can be attributed to an increase in the viscoelasticity and a decrease in viscosity of the hydrodynamic layer adjacent to the quartz resonator as the resonator is exposed to increasingly alkaline solutions. This decrease in the viscoelasticity of the hydrodynamic layer is a direct result of the electrostatic repulsion of the newly deprotonated carboxylic acid groups.

2.5 Scanning electrochemical microscopy

Scanning electrochemical microscopy is a technique that measures current flow through a very small electrode tip, 10 µm in diameter, brought in close proximity to a conductive, non-conductive, or semiconducting substrate[80]. SECM measurements are used to characterize redox events and structural hills at the surface of substrates. In addition, SECM provides topographical information on substrates, potential distributions, and can be used for microfabrication[80]. One

reported aspect of microfabrication involves electropolymerization initiated by the SECM tip; there are reports of using the SECM tip to polymerize polythiopene[81], polyaniline[53, 82], and polypyrrole[83] at electrode surfaces. The SECM tip generally serves as the current detector of redox events that occur between the tip and substrate. Diffusion to the tip of this small electrode when the electrode is far from the electrode surface (≥100 μm) is hemispherical (Figure 15a)[84, 85]. The most attractive feature of the SECM tip is the quick formation of a diffusion layer with a fixed thickness directly under the SECM tip[85]. The rapid buildup of a diffusion layer thickness enables the SECM tip to scan a substrate and obtain topographic and chemical reactivity profiles with minimal perturbation from convection in the solution[85]. In a SECM measurement, a redox probe experiences reduction or oxidation at the SECM tip. The resultant products diffuse away from the SECM tip towards the substrate where these products are re-oxidized or re-reduced leading to an enhancement of the current at the SECM tip[84].

The tip can operate under one of two conditions; it can act as a passive tip, which means it only detects electrochemical information at a particular region on the substrate, or it can serve as an active tip which means it interacts with the target analyte on the substrate surface to detect the resulting signal[86]. When the tip is close to the surface (~10μm), the current response (feedback) depends on the conductive nature of the substrate[87]. The most commonly used operating mode for SECM is the feedback mode[86]. In the positive feedback mode, close proximity to the electrode surface results in an increase in tip current as long as the redox event between the tip and the substrate is electrochemically reversible. In this mode, the substrate regenerates the species that is reacted at the tip (Figure 15b). In the positive feedback mode, an increase in current indicates close proximity to a conductive surface and rapid electron transfer between the redox probe and the substrate[87]. Negative feedback involves a decrease in the flow of redox-active species due to an inhibition of the regeneration of the redox probe over an insulator, producing a decrease in electron transfer[87]; this action produces a decrease in tip current (Figure 15c).

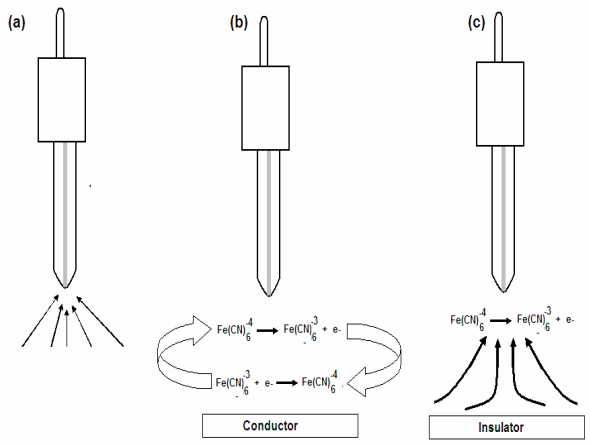

Figure 15: . Hemispherical diffusion away from electrode surface (a). regeneration of probe over a conductor (b). Probe regeneration is inhibited over an insulator (c).

Current versus distance profiles can be used to assess whether the SECM tip is above a conductor or an insulator as the SECM tip approaches the surface[85]. Bringing the SECM tip close to a conductive substrate increases current (Figure 16a). The opposite effect is observed when the SECM tip is close to a nonconductive substrate (Figure 16b).

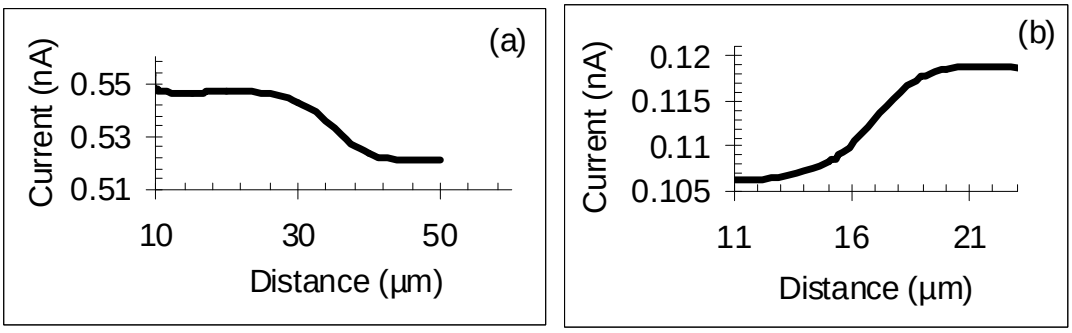

Figure 16: SECM approach curves in $[Fe(CN)_6]^{-4}$ over a conductor (a) and over an insulator (b). Approach curves were generated while a gold disk working electrode was immersed 0.005 mol·L^{-1} of $[Fe(CN)_6]^{-4}$ containing 0.1 mol·L^{-1} KCl.

There have been reports describing the use of SECM tips to localize potential over a region to promote the removal of alkanethiols in a specific region of a monolayer for patterning purposes[85, 88]. Reductive desorption is a process that involves using a cathodic voltammetric sweep in order to desorb thiols from electrode surfaces[89]. Application of appropriate negative potentials results in the reduction of the gold-sulfur bond which removes the thiol molecules from the surface of gold substrates (Figure 17). A 3-D surface and image map of localized

desorption in the shape of a square in a 2-methyl-1-propanethiol monolayer shown in Figures 24a and 24b.

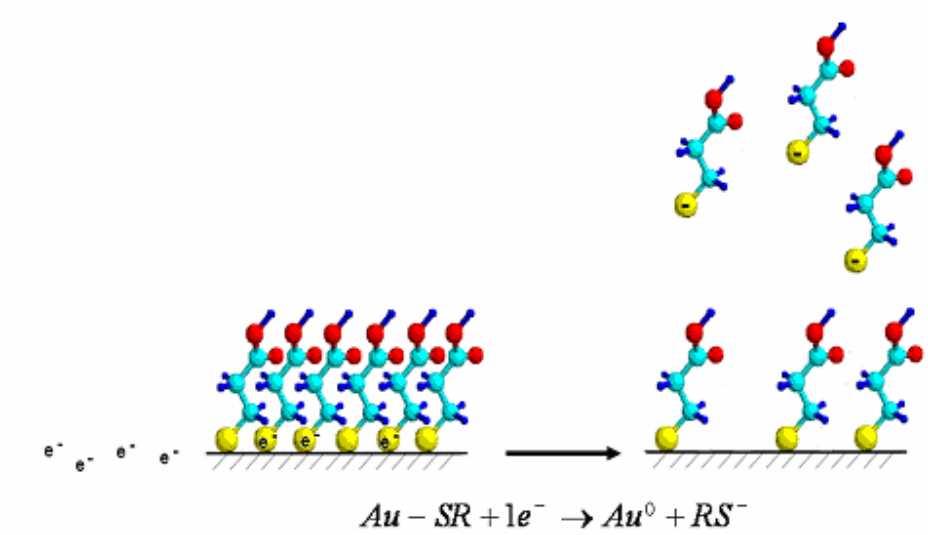

Figure 17: Mechanism for the reductive desorption of thiols from gold surfaces.

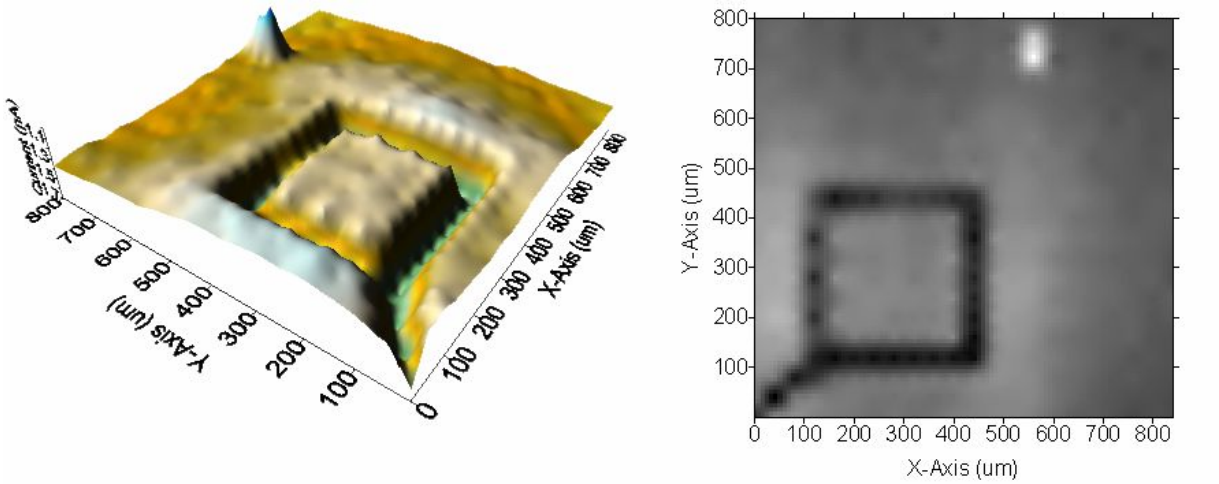

Figure 18: 3-D surface map (a) and image map (b) of a square desorbed in a 2-methyl-1-propanethiol monolayer. The images were generated using 0.005 mol·L^{-1} of $[Fe(CN)_6]^{-4}$ containing 0.1 mol·L^{-1} KCl.

In the work presented in this dissertation, SECM is used to image the electrostatic interaction between monolayers with terminal ionizable groups and redox probes. There have been many reports that describe the use of SECM in order to monitor the interaction between a redox probe and charged analytes on substrate surfaces[90-93]. Turcu[91] and Palchetti[90] report the use of the feedback mode of SECM for the purpose of imaging hybridized DNA. Both reports describe the occurrence of negative feedback when the SECM tip is moved across regions of immobilized DNA due to the electrostatic repulsion between the negatively charged $[Fe(CN)_6]^{-4}$

redox probe and the negatively charged phosphate groups on the oligonucleotide strands. Work conducted by Ye and coworkers show that approach curves can be used to study the interaction between 4-aminobenzoic acid immobilized on carbon electrodes immersed in alkaline solutions and both cationic ($[Ru(NH_3)_6]^{3+}$) and anionic ($[Fe(CN)_6]^{-4}$) redox probes[92]. Their work shows that negative feedback exists when an approach curve is generated using the anionic redox probe due to the electrostatic interaction between the negative charged redox probe and the deprotonated acid. The opposite trend was observed when Ye and coworkers used a cationic redox probe in their investigations[92].

Boldt et al.[93] also report that electrostatic interactions between functionalized monolayers and charged redox probes can be measured using SECM. When analyzing current distance curves generated from an SECM analysis of 11-mercaptoundecanoic acid monolayers on gold electrodes, they observed negative feedback between the anionic redox probe and the carboxylate surface and positive feedback between the cationic redox probe and the carboxylate surface. The aforementioned work described by Ye et al.[92] and Boldt et al.[93] is the basis behind the SECM portion of the research described in this dissertation. SECM is used to monitor the surface charge of carboxylic acid terminated monolayers in addition to depositing polyelectrolytes to the surface of these monolayers.

2.6 General Experimental Details

2.6.1 Experimental conditions for chronoamperometry

For all electrochemical measurements (chronoamperometry, impedance, and SECM), 3-MPA and 11-MUA modified electrodes were prepared in the same manner. A gold disk electrode purchased from Bioanalytical Systems (West Lafayette, IN) having a geometric area of 0.048 cm^2 was polished with alumina, sonicated in de-ionizaed water, and electrochemically cleaned. Electrochemically cleaning involved immersing the mechanically polished electrode in 0.1 $mol \cdot L^{-1}$ sulfuric acid and performing 15 potential sweeps from 2.0 V to -0.8 V (vs Ag/AgCl).

The pretreated electrodes were rinsed with de-ionized water, dried in a stream of nitrogen gas, and placed in a 0.005 mol·L^{-1} thiol/ethanol solution for 15 minutes. The assembling solutions were made from 3-mercaptopropionic acid or 11-mercaptoundecanoic acid; both purchased from Aldrich and used without further purification. Once monolayers were immobilized on electrode surfaces, the surfaces were rinsed with ethanol, de-ionized water, and dried in a stream of nitrogen. For cysteine monolayers, the same pretreatment procedure was used, but the adsorption solution was prepared differently. Cysteine was purchased from Aldrich and used with no further purification. Cysteine monolayers were prepared by immersing the electrodes in a 0.02 mol·L^{-1} cysteine solution prepared from hexanes for 5-10 minutes.

Promoting surface group ionization of COOH terminated monolayers with applied potential was achieved using a one-step chronoamperometry. The potential step was applied using a 604B electrochemical analyzer from CH Instruments (Austin, TX) interfaced to a personal computer. Solutions used in these experiments were prepared using poly diallyldimethylammonium chloride (MW~200,000-350,000 g·mol^{-1}) and poly sodium 4-syrene sulfonate (MW~200,000 g·mol^{-1}) both purchased from Aldrich and used with no further purification. A standard three electrode cell (Figure 19) was used to house the solution and the electrodes; an Ag/AgCl reference electrode and a Pt wire counter electrode was used during the measurements. During the potential step, the modified electrodes were immersed in 0.05 mol·L^{-1} pH 5 phosphate buffer solution containing 1.08×10^{-6} mol·L^{-1} PDDA. Phosphate buffer solutions with a pH of 5 and an ionic strength of 0.05 mol·L^{-1} were purchased from VWR Scientific. A 1.1×10^{-3} mol·L^{-1} PSS solution dissolved in pH 5 phosphate buffer solution from VWR Scientific was used to test the potential-driven deposition of an anionic polyelectrolyte to the surface of a cysteine monolayer. For applied potential experiments involving 3-MPA and 11-MUA monolayers, two separate Sixty-second potential steps to -0.15V vs Ag/AgCl and to -0.01 V vs AgAgCl were used to inhibit and promote ionic self assembly of PDDA, respectively. In the case of the cysteine monolayers, the potential steps were to -0.40 V vs Ag/AgCl and to -

0.05 V vs AgAgCl. Determining the values for the final potentials used in the one-step chronoamperometry experiment for 3-MPA, 11-MUA, and cysteine monolayers will be explained in chapters three and four.

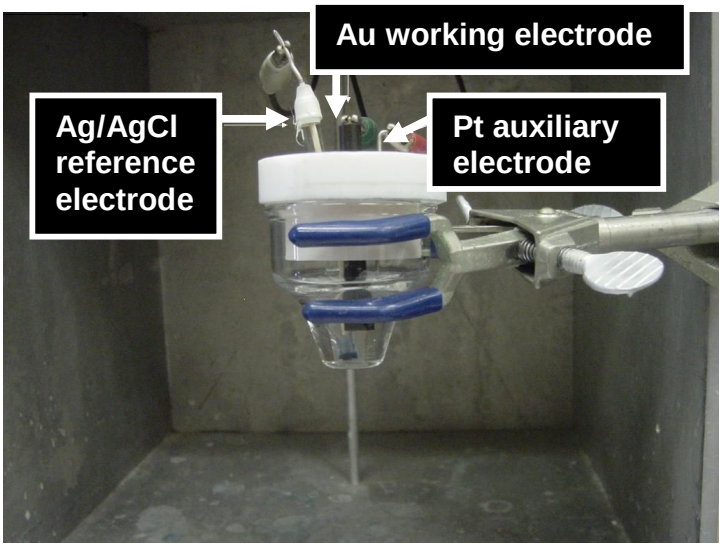

Figure 19: Three electrode electrochemical cell.

A three electrode cell arrangement was also used to perform applied potential deposition experiments on modified quartz crystal microbalance (QCM) plates (Figure 20). The polyelectrolyte assembling solutions described earlier were used in these QCM applied potential experiments. QCM plates modified with 3-MPA, 11-MUA, or cysteine were immersed in a 100 mL beaker containing approximately 50 mL of the appropriate assembling solution. The plates were connected as working electrodes, an Ag/AgCl reference electrode was used, and a Pt wire was used as the counter electrode.

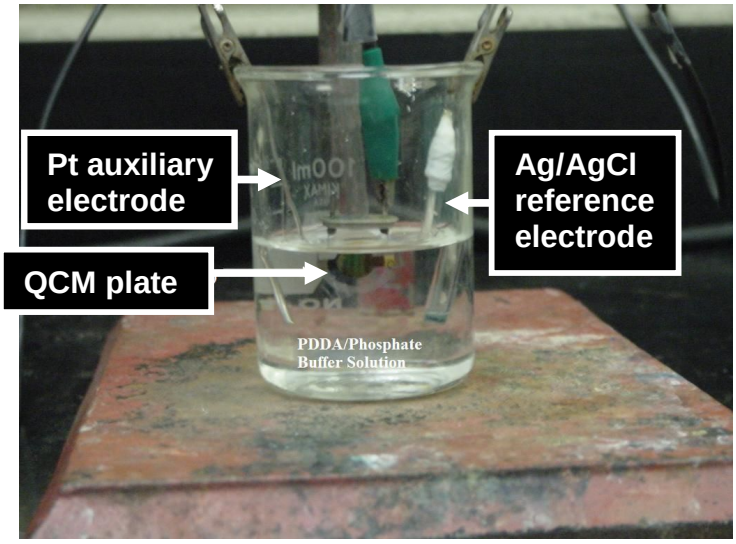

Figure 20: Applied potential deposition assembly for QCM analysis.

2.6.2 Experimental conditions for impedance

Electrochemical impedance measurements were performed using a model 604B electrochemical analyzer from CH Instruments (Austin, TX) interfaced to a personal computer. Modified electrodes were prepared according to the procedures listed in Section 2.6.1. Modified electrodes were placed in a standard three electrode cell (Figure 9) containing 0.005 mol·L^{-1} $[Fe(CN)_6]^{3-/4-}$ solutions prepared from potassium ferrocyanide and potassium ferricyanide from Fisher Scientific. The pH of the supporting electrolyte solution was maintained at 5 using 0.05 mol·L^{-1} phosphate buffers from VWR Scientific. Impedance data was obtained by applying a sinusoidal signal centered around 0.2 V vs Ag/AgCl using a range of frequencies from 1×10^5 Hz to 0.1 Hz. Quantitative estimates of the equivalent circuit parameters were obtained by fitting the experimental data using the nonlinear least squares fitting routines of the software package LEVM 7.0 (available from Solartron, www.solartronanalytical.com, written by James Ross Macdonald).

2.6.3 Experimental conditions for QCM

Quartz crystal microbalance measurements were preformed with an in-laboratory built QCM oscillator (Figure 21). Standard gold coated quartz plates from International Crystal

(Oklahoma City, Ok) were used for the substrate and the resonator. The electrode diameter on the quartz crystals was 0.13 cm.

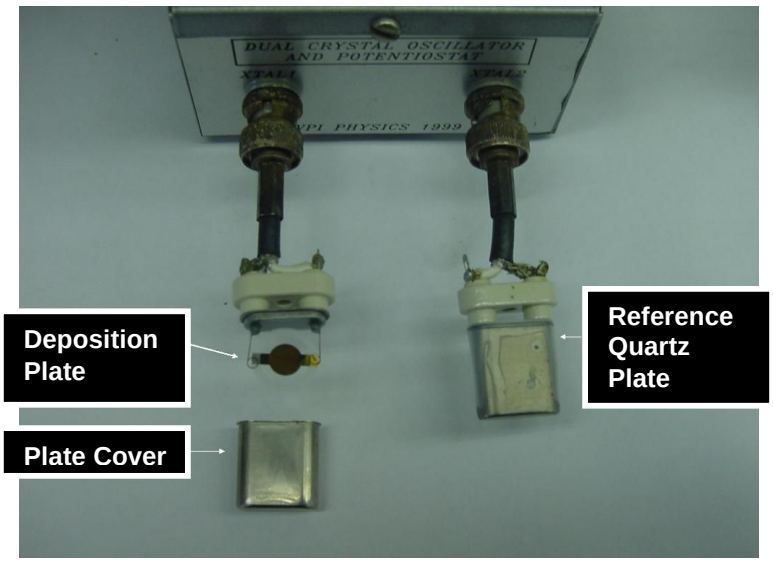

Figure 21: Quartz crystal microbalance.

Prior to thiol immobilization, the QCM plates were immersed in piranha solution (25% hydrogen peroxide/75% concentrated sulfuric acid) for less than a minute. They were then rinsed with copious amounts of de-ionized water, dried in a stream of N_2, and immersed in an ethanolic solution of 0.005 mol·L^{-1} thiol solution for at least 15-30 minutes.

2.6.4 Experimental conditions for SECM

Scanning electrochemical microscopy imaging was conducted with an in-laboratory built instrument with step resolution of approximately 40 nm (Figure 22). The SECM instrument consisted of a Thorlabs Inc. (Newton, NH) XYZ platform modified with Z600 series actuators. During imaging, the actuators are controlled with locally written Visual Basic software. Current was monitored using an EI-400 FCV bipotentiostat manufactured by Cypress Systems (Lawrence, KS).

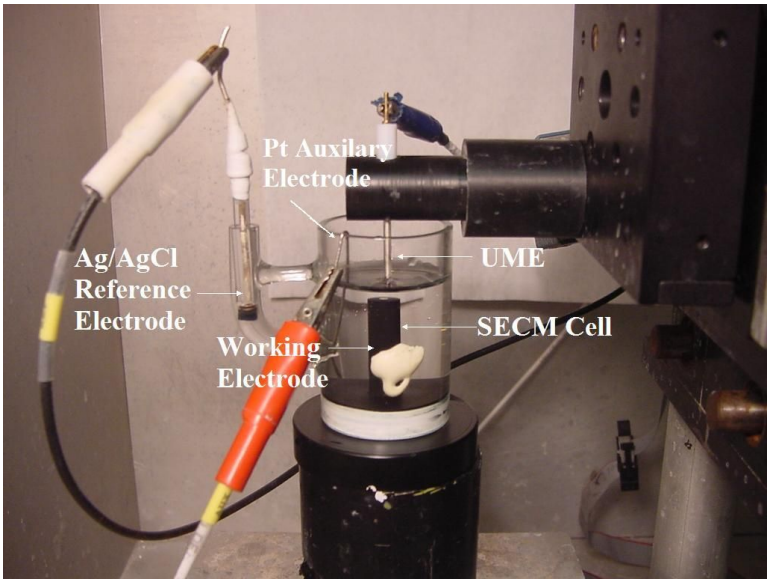

Figure 22: SECM set up.

Solutions used in SECM experiments were prepared using hexamine ruthenium (III) chloride from Aldrich with no further purification. The SECM cell (Figure 22) was filled with 0.005 mol·L^{-1} $[Ru(NH_3)_6]Cl_3$ prepared from 0.05 mol·L^{-1} pH 5 and pH 8 phosphate buffer solutions from VWR Scientific. A visual BASIC program was used to control the XYZ position of the SECM tip. The program was also used to collect current data during imaging. The Z position was manually controlled until the biopotentiostat registered a current overload, then the tip was brought away from the surface approximately 10 µm. The program was also used to collect data during scanning while the SECM tip was held at a constant height above the electrode surface. Tthe modified gold electrode was held at a potential near the PZC and the SECM tip was held at a potential that supported the reduction or oxidation of the redox probe.

Chapter 3. Impedance and Quartz Crystal Microbalance Measurements of Polyelectrolyte Deposition onto 3-Meracaptopropionic Acid and 11-Mercaptoundecanoic Acid Monolayers

3.1 Introduction

This chapter describes electrochemical impedance and quartz crystal microbalance measurements to monitor the extent of applied potential-driven ionic self assembly of polydiallyldimethyl ammonium chloride (Figure 23) onto the surface of 3-MPA and 11-MUA monolayers. These methods are well suited for assessing the feasibility of using applied potential to drive ionic self assembly because they are extremely sensitive to changes in the interfacial region of functionalized monolayers. Electrochemical impedance measurements can be used to monitor the electrostatic interactions between charged surfaces and redox probes[22,67]. The charge-transfer resistance values obtained from impedance analyses of the electrostatic attraction between the adsorbed PDDA layer and $[Fe(CN)_6]^{3-/4-}$ provide quantitative assessments of the extent of ionic self assembly driven by applied potential.

QCM measurements were used as an additional diagnostic tool to verify polyelectrolyte deposition to the surface of functionalized monolayers via applied potential. This technique was selected as an additional means to verify polyelectrolyte deposition and to quantify the amount of deposited polyelectrolyte during potential-driven ionic self assembly.

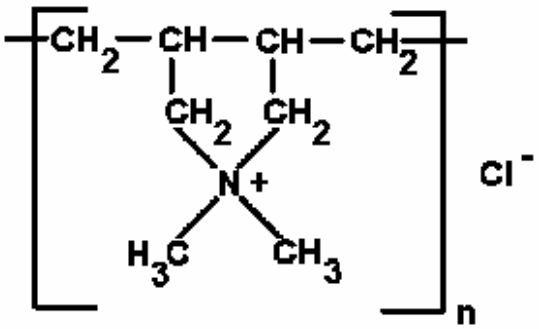

Figure 23: Structure of polydiallyldimethyl ammonium chloride.

3.2 Experimental

3.2.1 Polyelectrolyte deposition via solution pH

Monolayers of 3-MPA and 11-MUA were prepared as described in Section 2.6.1. Following monolayer immobilization, impedance analyses of the monolayers were conducted as described in Section 2.6.2. After an impedance analysis of the electrode modified with the pure monolayer, it was immersed in a solution containing 1.08×10^{-6} mol·L^{-1} PDDA in 0.1 mol·L^{-1} NaOH or 0.1 mol·L^{-1} HCl for approximately one minute. Sodium hydroxide and polydiallydimethyl ammonium chloride (PDDA) were purchased from Aldrich and used without further purification. After PDDA adsorption, the electrodes were rinsed and an impedance analysis was conducted.

For the QCM analysis, monolayers of 3-MPA and 11-MUA were assembled on gold coated quartz plates as described in Section 2.6.3. The modified QCM plates were then immersed in a solution containing 1.08×10^{-6} mol·L^{-1} PDDA in 0.1mol·L^{-1} NaOH or 0.1 mol·L^{-1} HCl for approximately one minute. The quartz plates were then removed, rinsed with de-ionized water, dried with a stream of nitrogen, and then connected to the QCM oscillator. The frequency of the modified plate was recorded every minute for 15 minutes. The results from the impedance and QCM measurements of solution adsorbed PDDA onto the surface of 3-MPA and 11-MUA monolayers were used as controls for comparison to the results obtained when using applied potential to deposit the PDDA. Prior to the applied potential deposition experiments, changes to the bulk solution were used to ionize the surface and create conditions favorable for the adsorption of PDDA. These experiments establish the system response using conditions known to favor the adsorption of PDDA.

3.2.2 pK_a determination

The 3-MPA and 11-MUA monolayers used for surface pK_a determination were prepared as described in Section 2.6.1. Impedance data was obtained for monolayers of 3-MPA and 11-

MUA immersed in 0.005 mol·L^{-1} $[Fe(CN)_6]^{3-/4-}$ solutions prepared with commercially available 0.05 mol·L^{-1} phosphate buffer solutions from VWR scientific with pH values ranging from 3 to 8. The impedance data was collected using the parameters listed in Section 2.6.2.

3.2.3 PZC determination

Once impedance titrations were complete, the PZC of the monolayers was determined in solutions buffered below the surface pK_a. The potential of zero charge of 3-MPA and 11-MUA monolayers was determined in commercially available pH 5 phosphate buffer solutions from VWR scientific. This pH was selected because impedance titration data found that pH 5 is below the surface pK_a of both monolayers which meant that the absence of surface ionization via solution pH was assured. The 3-MPA and 11-MUA monolayers used in these experiments were prepared following the procedure listed in Section 2.2.1. While immersed pH 5 phosphate buffer solutions, impedance analyses were conducted with the substrate at potential held at values between -0.6 V to 0.6 V vs Ag/AgCl. The impedance measurements were obtained in 0.1 V increments. The frequency range used in these measurements was 1×10^{6} Hz to 0.1 Hz.

3.2.4 Applied potential deposition

The monolayers used for the applied potential deposition experiments were prepared according to procedures listed in Section 2.6.1. Prior to application of applied potential in the presence of a polyelectrolyte, an impedance analysis was conducted on the pure monolayers using the procedures listed in Section 2.6.2. The monolayers were then immersed in pH 5 phosphate buffer solution containing 1.08×10^{-6} mol·L^{-1} PDDA. While in the polyelectrolyte solutions, a one-step chronoamperometry experiment was used to step the potential of the modified electrodes for approximately one minute as described in Section 2.6.1. A potential step to -0.15 V vs Ag/AgCl (3-MPA) or -0.130 V vs Ag/AgCl (11-MUA) was used to apply potentials near the PZC. Another potential step to -0.01 V vs Ag/AgCl (3-MPA) or -0.127 V vs Ag/AgCl (11-MUA) was used to apply potentials positive of the PZC. After the

chronoamperometry experiment, the electrodes were rinsed and a second impedance analysis was conducted. A new monolayer was used for each potential step experiment.

3.3 Results and discussion

3.3.1 pK_a values

A Faradaic impedance titration method reported by Kim et al.[68] was performed on 3-MPA and 11-MUA modified electrodes for the purpose of determining surface pK_a values. Electrochemical impedance measurements were conducted in 0.005 $mol \cdot L^{-1}$ $[Fe(CN)_6]^{3-/4-}$ solutions of varying pH. The Nyquist plots for 3-MPA (Figure 24) and 11-MUA (Figure 25) monolayer modified interfaces result in increasing impedance (e.g. larger semicircle diameters) with more basic solution pH. The semicircle diameter eventually reaches a constant value once all surface confined acid groups were ionized. This result is consistent with experiments conducted by Kim and coworkers[68]. They assert that low pH values less than five result in fully protonated surfaces resulting in a close approach of the$[Fe(CN)_6]_3^{-/4-}$ redox probe to the monolayer surface (Figure 26a) producing low electron transfer resistances. Higher pH values (>5) result in deprotonation of the monolayer and create conditions where electrostatic repulsion exists between the carboxylate surface and the anionic redox couple (Figure 26b). This condition yields larger electron transfer resistances and larger interfacial impedances, as evidenced by the increased diameters of the Nyquist plots. Quantitative estimates of the charge-transfer resistances are obtained by fitting the experimental data to the equivalent circuit via LEVM fitting software.

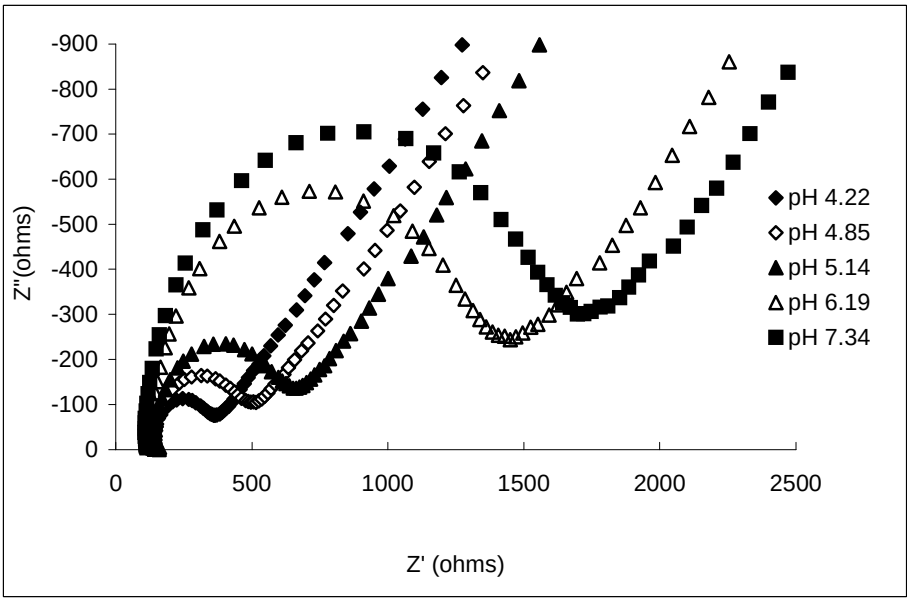

Figure 24: Impedance measurements of 3-mercaptopropionic acid modified electrode in phosphate buffer solutions with varying pH values. Impedance measurements were conducted in 0.005 mol•L^{-1}[Fe(CN)$_6$]$_3^{-/4-}$ in 0.1 mol·L^{-1} KCl at a potential of 0.2 V vs Ag/AgCl.

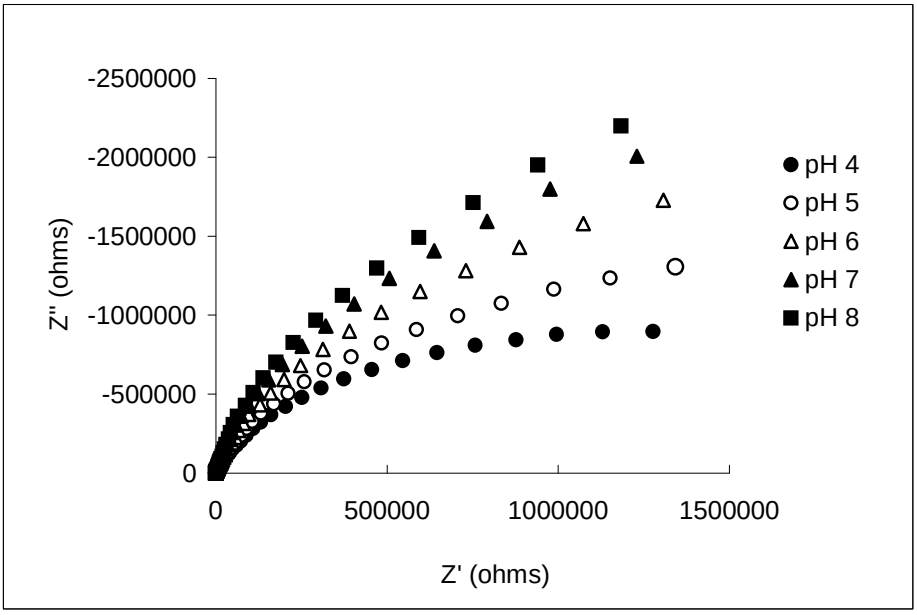

Figure 25: Impedance measurements of 11-mercaptoundecanoic acid modified electrode in phosphate buffer solutions with varying pH values. Impedance measurements were conducted in 0.005 mol•L^{-1}[Fe(CN)$_6$]$_3^{-/4-}$ in 0.1 mol·L^{-1} KCl at a potential of 0.2 V vs Ag/AgCl.

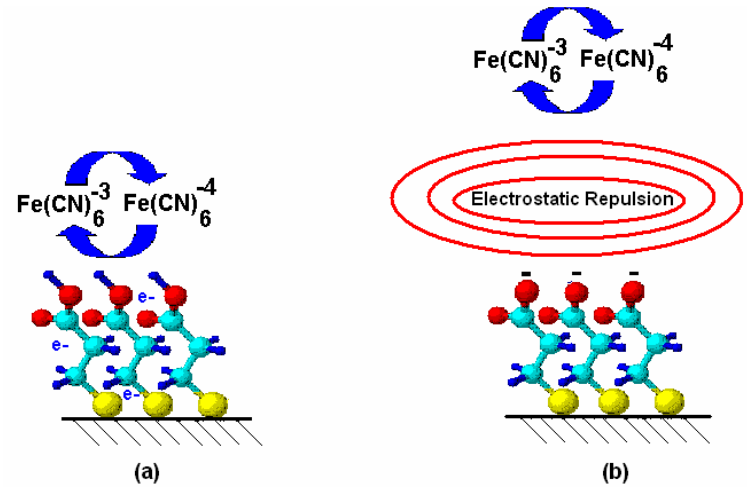

Figure 26: Schematic representing the likely electrostatic interaction between an anionic redox probe and neutral (a) and deprotonated (b) 3-MPA surfaces.

In accordance with reports by Kim and Kwak[68], charge-transfer resistances were plotted against solution pH to produce impedance titration curves for 3-MPA (Figure 27) and 11-MUA (Figure 28). The surface pK_a values were determined by estimating the midpoint of the steep increase in the titration curve[94]. The experimentally determined surface pK_a value for 3-MPA, 5.6$\pm$0.2, is consistent with the pK_a value of 3-MPA monolayers of 5.2 reported elsewhere[68, 95]. Impedance titrations conducted on 11-MUA resulted in a surface pK_a value of ~6.7$\pm$0.1. The 11-MUA pK_a is slightly over one pH unit larger than the surface pK_a value for 3-MPA. This is thought to be due to the packing density of the 11-MUA monolayer relative to the 3-MPA monolayer. The longer alkyl chain of the 11-MUA monolayer provides increased lateral van der Waals interactions between neighboring chains which increases the stability of the monolayer. The increased stability, however, decreases the ease of acid dissociation. This effect can be observed by comparing the cyclic voltammograms of the reductive desorption of long chain and short chain alkyl thiol monolayers.

Reductive desorption involves application of an increasingly negative potential to thiol modified electrodes for the purpose of reducing the gold sulfur bond to facilitate the removal of the thiol from the gold surface[96]. Previous studies show a direct correlation between packing density and reductive desorption potential. Less densely packed monolayers desorb at less negative potentials[89, 96]. Voltammograms resulting from the desorption of 3-MPA, 11-MUA, and

CYS monolayers (Figure 29) illustrate that 11-MUA requires a much more negative potential (-1.241 V vs Ag/AgCl) to desorb from the electrode surface than 3-MPA (-0.902 V vs Ag/AgCl). Cysteine requires the least negative potential to desorb from the gold electrode (-0.734 V vs Ag/AgCl). The voltammograms shown in Figure 29 illustrate the dependence of desorption potential on chain length. There are reports that state increasingly negative desorption potential with increasing chain length is the result of increased lateral interactions between methlyene groups. These interactions promote in plane hydrogen bonding which minimizes the degree of acid dissociation. This is consistent with reports by Creager and Clark who state that a positive shift in surface pK_a is expected due to the inhibition of solvation of the terminal carboxylic acid groups due to increased in-plane hydrogen bonding[94]. An approximation of the surface pK_a of monolayers, the point where approximately half of the confined carboxylic acid groups are deprotonated,[8, 21] is needed so that solution pH could be buffered below this value. Buffering solution pH below the surface pK_a of the monolayer ensures that the surface charge of the terminal groups is neutral prior to application of the potential step.

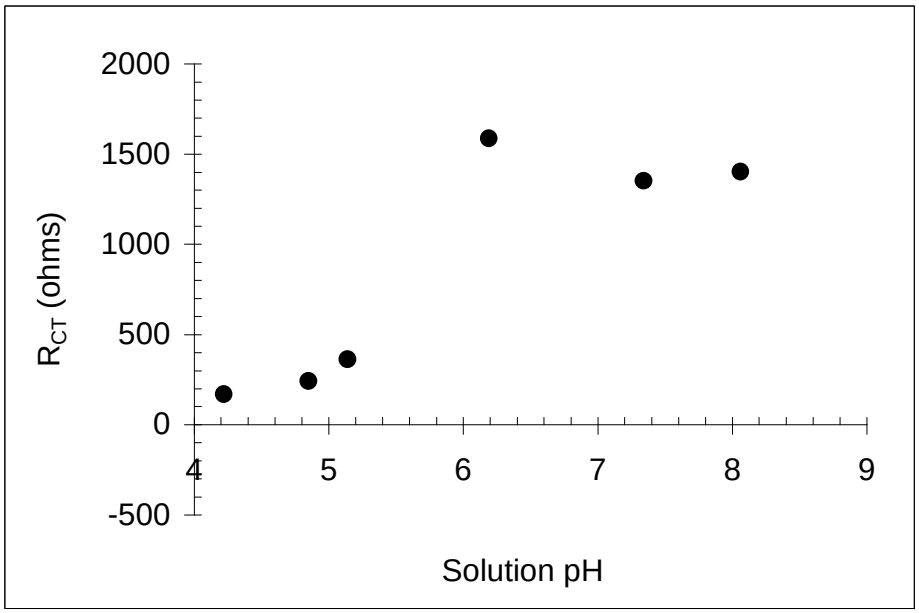

Figure 27: Electrochemical impedance titration of 3-mercaptopropionic acid monolayers assembled on gold. Impedance measurements were conducted in 0.005 mol•L^{-1}[Fe(CN)$_6$]$_3^{-/4-}$ in 0.1 mol·L^{-1} KCl at a potential of 0.2 V vs Ag/AgCl.

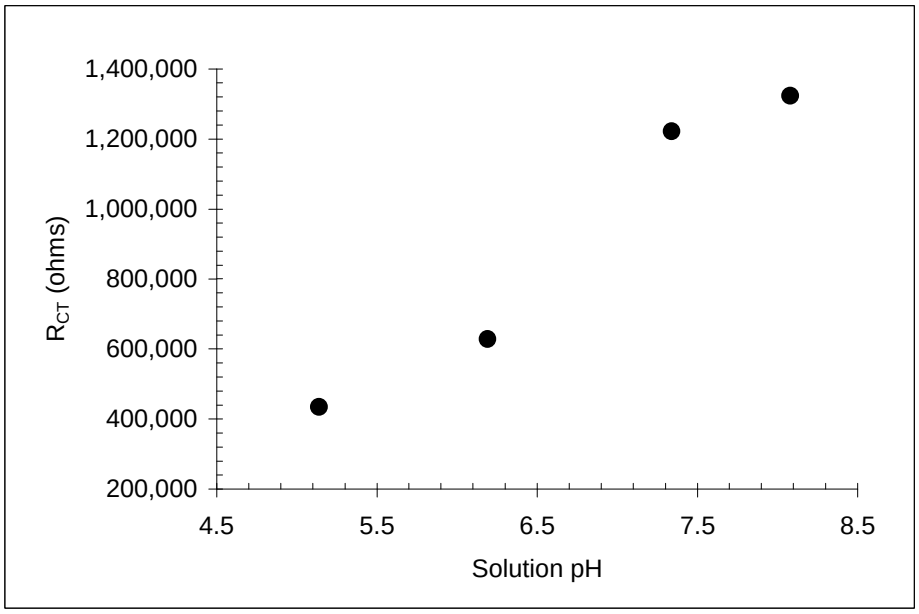

Figure 28: Electrochemical impedance titration of 11-mercaptoundecanoic acid monolayers assembled on gold. Impedance measurements were conducted in 0.005 mol•L^{-1}[Fe(CN)$_6$]$_3^{-/4-}$ in 0.1 mol·L^{-1} KCl at a potential of 0.2 V vs Ag/AgCl.

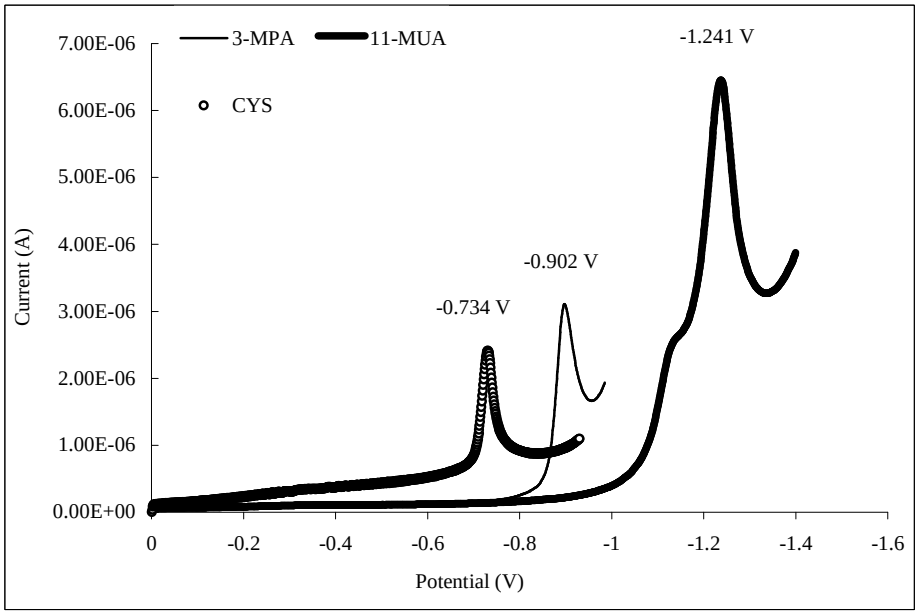

Figure 29: Voltammograms for the reductive desorption of 3-MPA, CYS, and 11-MUA on gold. Desorption was conducted in 0.5 mol·L^{-1} NaOH purged for 1 minute using nitrogen.

In addition to performing an impedance titration of 3-MPA and 11-MUA monolayers using an anionic redox probe, similar experiments were conducted using a cationic redox probe, hexaammine ruthenium chloride. Hexaammine ruthenium chloride was obtained from Adrich and used without further purification. It is clear that the pK$_a$ estimates from the impedance

titrations using hexaammine ruthenium chloride are shifted to higher pK_a values for both 3-MPA (~6) and 11-MUA (~7.2) as shown in Figures 30 and 31 respectively. The increase in pK_a values can be attributed to the differences in potential during the impedance analyses. When the$[Fe(CN)_6]_3^{-/4-}$ redox couple was used, the AC voltage applied to the modified electrodes was centered around the formal potential of the redox couple, 0.2 V vs Ag/AgCl. When the hexaammine ruthenium chloride redox probe was used, the AC voltage was centered around the reduction potential of the cationic redox probe, -0.3 V vs Ag/AgCl. The shift in pK_a values with varying potentials provides an early indication that potential can affect the extent of acid dissociation of terminal carboxylic acid groups. This effect was first reported by Sugihara and Shimazu while conducting surface mass titrations of mercaptohexadecanoic acid monolayers under the influence of increasingly negative potentials[35]. The behavior of the titration curve is reversed as a result of the behavior of the cationic redox probe in response to the anionic surface. At pH values below the pK_a, the acid groups are not charged and no electrostatic attraction exists between the surface and the cationic redox probe (Figure 32a). At pH values exceeding the pK_a of the monolayers, the cationic redox probe is attracted to the carboxylate surface (Figure 32b). Decreased proximity between the redox probe and the surface increases the likelihood of electron transfer between the redox probe and the surface resulting in a decrease in charge-transfer resistance.

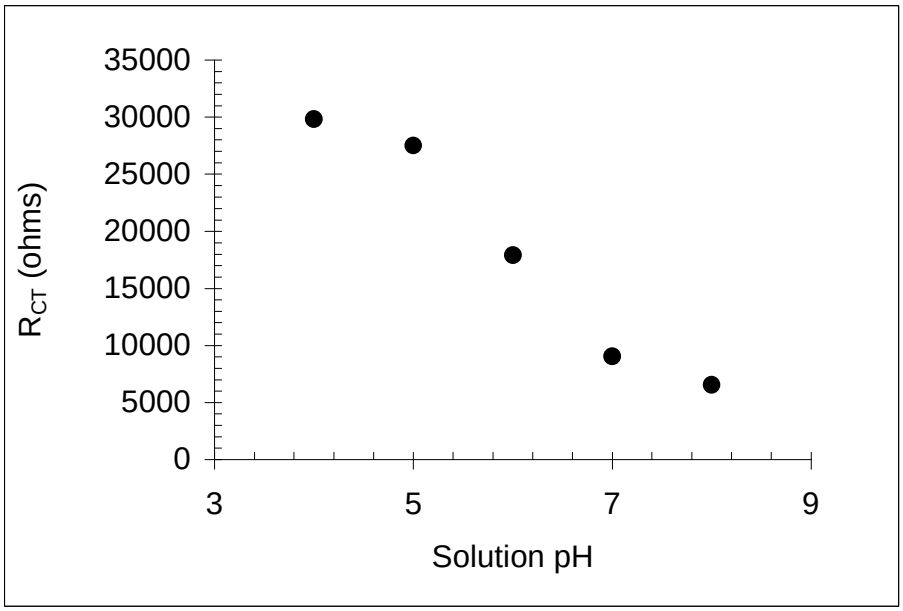

Figure 30: Electrochemical impedance titration of 3-mercaptopropionic acid monolayers assembled on gold. Impedance measurements were taken in 0.005 mol•L-1 $[Ru(NH_3)_6]^{3+}$ containing 0.1 mol·L^{-1} KCl at a potential of -0.3 V vs Ag/AgCl.

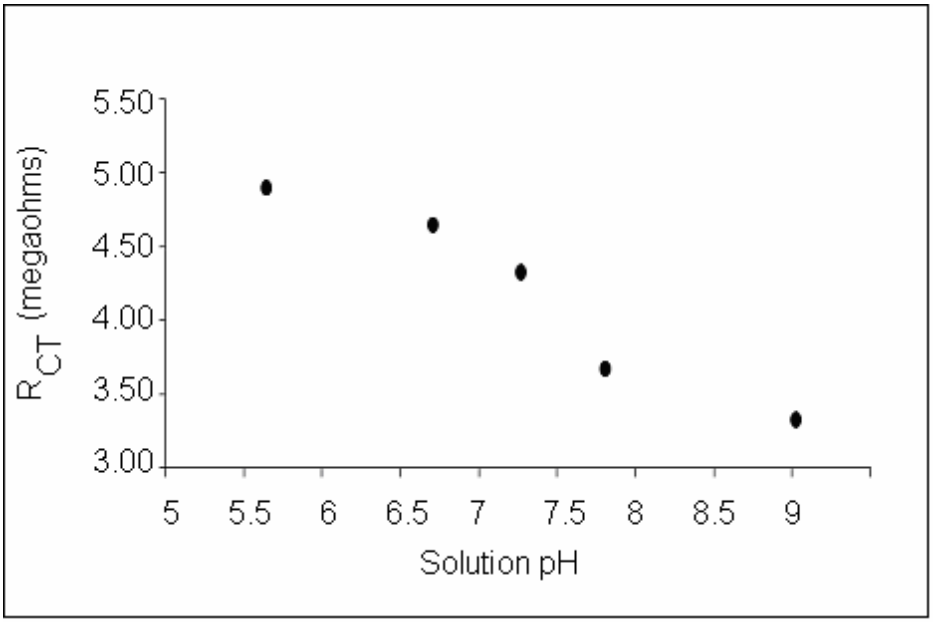

Figure 31: Electrochemical impedance titration of 11-mercaptoundecanoic acid monolayers assembled on gold. Impedance measurements were taken in 0.005 mol•L^{-1} $[Ru(NH_3)_6]^{3+}$ at a potential of -0.3 V vs Ag/AgCl.

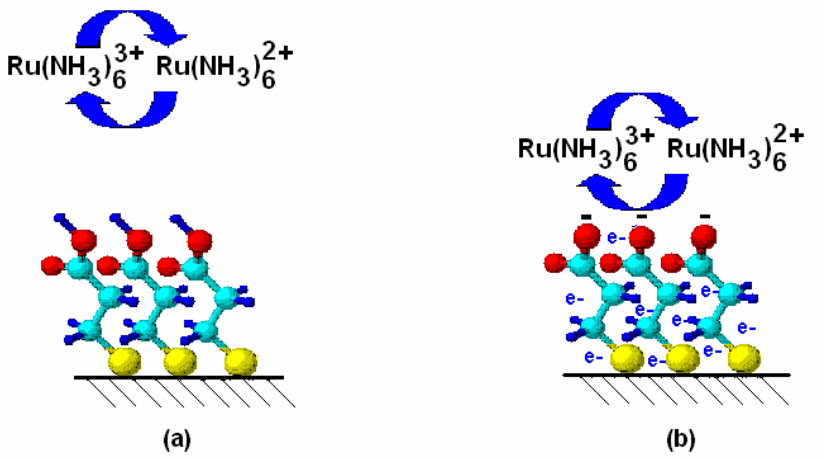

Figure 32: Schematic representing the likely electrostatic interaction between cationic redox probe and neutral (a) and deprotonated (b) 3-MPA surfaces.

3.3.2 Potential of zero charge

Application of appropriate potential to functionalized monolayers to promote surface group ionization while immersed in solutions buffered below the surface pK_a of the monolayer is the major objective of this dissertation research. That is why it was important to determine the point where potential affects surface charge, the potential of zero charge (PZC). The conditions used to collect impedance data for PZC determination were different than impedance measurements used in the Faradiac impedance titrations in two ways. Impedance measurements used to determine PZC values were conducted at different potentials instead of one, and the measurements were performed in a solution absent of a redox probe. Conducting impedance measurements in the absence of a redox probe provided data that solely reflects the behavior of the double-layer. When electrochemically active redox probes are excluded from the solution, no charge-transfer takes place and the dissociation of the terminal acid or base groups results in changes in the double-layer capacitance[21].

Double-layer capacitance serves as a measure of the effect of potential on the interfacial charge of functionalized surfaces because potentials positive or negative of the potential of zero charge influences the concentration of counterions in the double-layer region adjacent to the interface[23]. Kakiuchi et al. report that double-layer capacitance is a function the surface charge and the extent of dissociation of the surface acid groups[18]. Double-layer capacitance values were

determined by plotting log of the total impedance (Z) vs log frequency. Figure 33 is a example of a log Z vs log F plot that contains data for impedance analyses at various potentials. The y-intercepts of Log Z vs Log F plots provided values that are proportional to $\frac{1}{C_{DL}}$. Plots similar to these were generated for each potential and the y-intercepts were used to generate C_{DL} vs potential plots for the determination of the potential of zero charge for 3-MPA (Figure 34) and 11-MUA (Figure 35). The minimum in plots of double-layer capacitance vs potential denotes the potential of zero charge as reported by Becka and Miller[23].

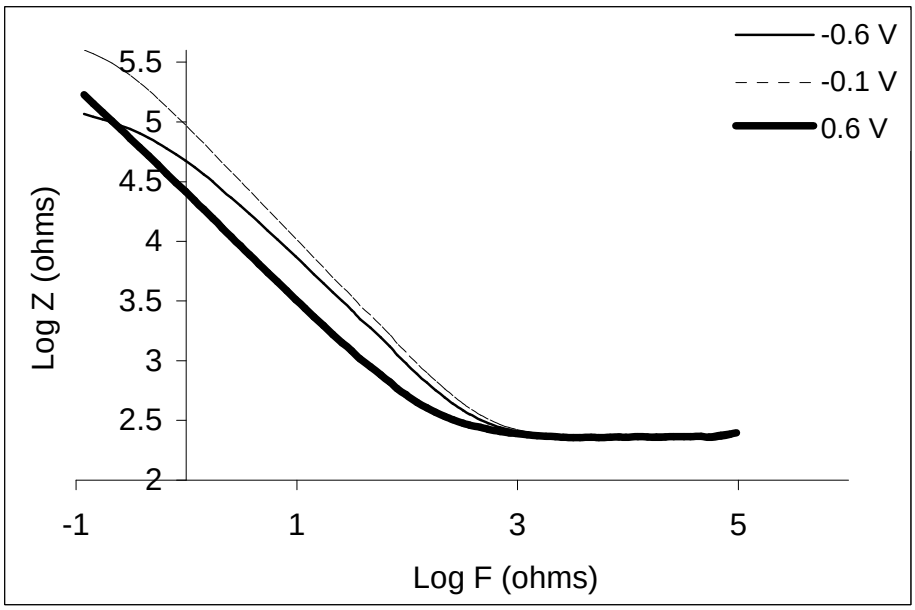

Figure 33: Double-layer capacitance determination of 3-MPA at -0.6 V, -0.1V, and 0.6 V. Impedance measurements were conducted in 0.05 mol·L^{-1} pH 5 phosphate buffer solution from -0.6 V to 0.6 V vs Ag/AgCl.

The potential of zero charge was determined to be -0.13 V vs Ag/AgCl for 3-MPA and -0.13 V vs Ag/AgCl for 11-MUA. At potentials equal to the PZC, no excess charge exists at the monolayer surface. The absence of excess charge at the terminal region of the monolayer produces an increase in the Stern layer thickness which leads to a decrease in the double-layer capacitance, and is the origin of the minimum in double-layer capacitance vs potential curves. At potentials positive of the PZC, anion binding decreases the proximity of ions to the monolayer surface resulting in a decrease in the Stern layer in the double-layer region producing an increase in apparent double-layer capacitance in accordance with the Helmholtz equation (Equation 1).

The counterion binding effect is also observed at potentials negative of the PZC due to cation accumulation at the interface.

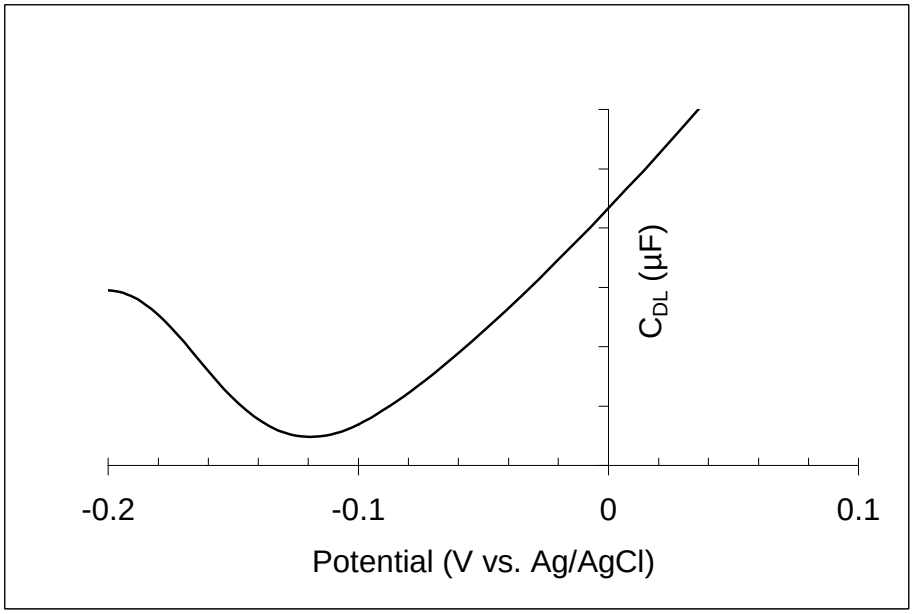

Figure 34: Potential of zero charge determination of 3-mercaptopropionic acid monolayers.

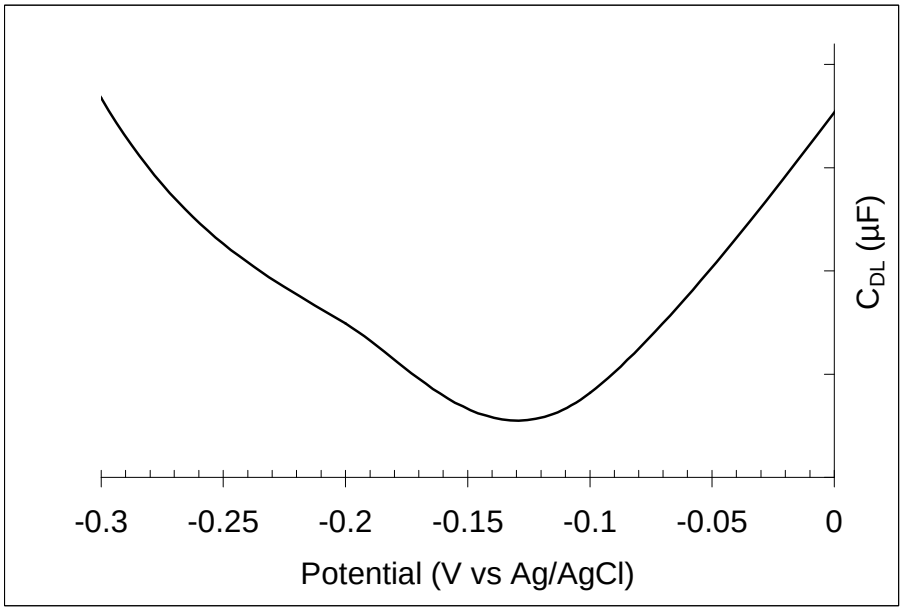

Figure 35: Potential of zero charge determination of 11-MUA.

3.3.3 pH Driven Deposition

As stated in the previous sections, two preliminary pieces of information, surface pK_a and PZC, were determined with impedance measurements. Impedance measurements were also

used to measure the extent of ionic self assembly driven by solution pH. LEVM fitting software was used to extract charge-transfer resistance values from impedance data which provided a more explicit quantative measure of pH driven ionic self assembly.

Nyquist plots of 3-MPA (Figure 36) and 3-MUA (Figure 37) monolayers immersed in 0.1 $mol \cdot L^{-1}$ NaOH containing1.08×10^{-6} $mol \cdot L^{-1}$ PDDA solutions show smaller diameters of the complex impedance plots after PDDA exposure; this result is indicative of lower charge-transfer resistance values providing evidence of ionic self assembly of PDDA to the surface of 3-MPA. Average LEVM fits of the impedance data yield charge-transfer resistance values for 3-MPA and 11-MUA monolayers before and after PDDA exposure in 0.1 $mol \cdot L^{-1}$ NaOH; these values are listed in Table 2. The large differences in charge-transfer resistances before and after PDDA exposure are the result of the electrostatic interaction between the anionic redox probe and the cationic PDDA layer. In the absence of electrostatic attraction between the terminal region of the monolayer and the redox probe, the proximity between the probe and the monolayer surface is governed by diffusional effects (Figure 38a). However, deposition of a cationic PDDA layer allows the anionic redox probe a closer approach to the interfacial region of the monolayer and lowers the measured impedance due to increased electron transfer (Figure 38b).

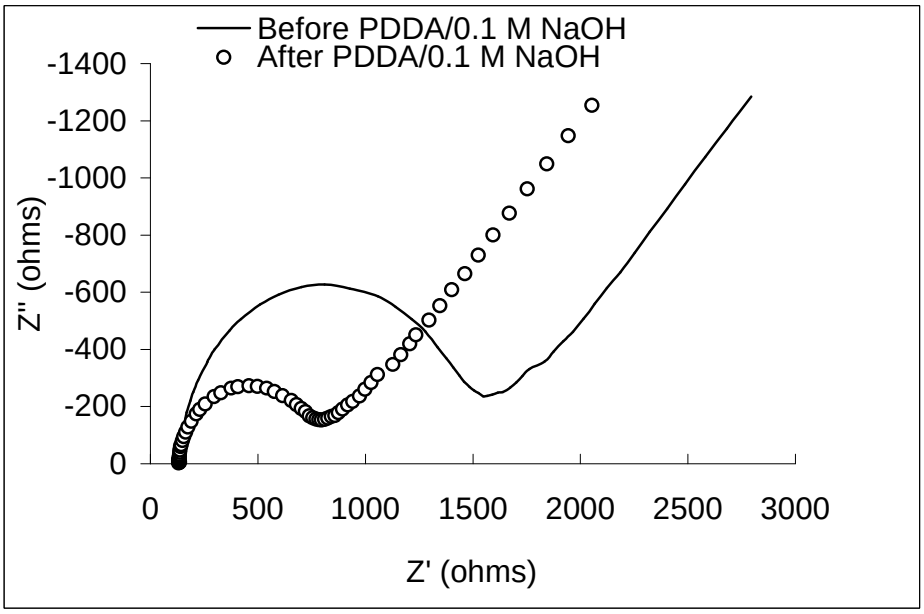

Figure 36: Nyquist plots of 3-MPA monolayers before and after polydiallydimethyl ammonium chloride 0.1 mol·L^{-1} NaOH. Impedance measurements were conducted in 0.005 mol·L^{-1}[Fe(CN)$_6$]$_3^{-/4-}$ containing 0.1 mol·L^{-1} KCl at a potential of 0.2 V vs Ag/AgCl.

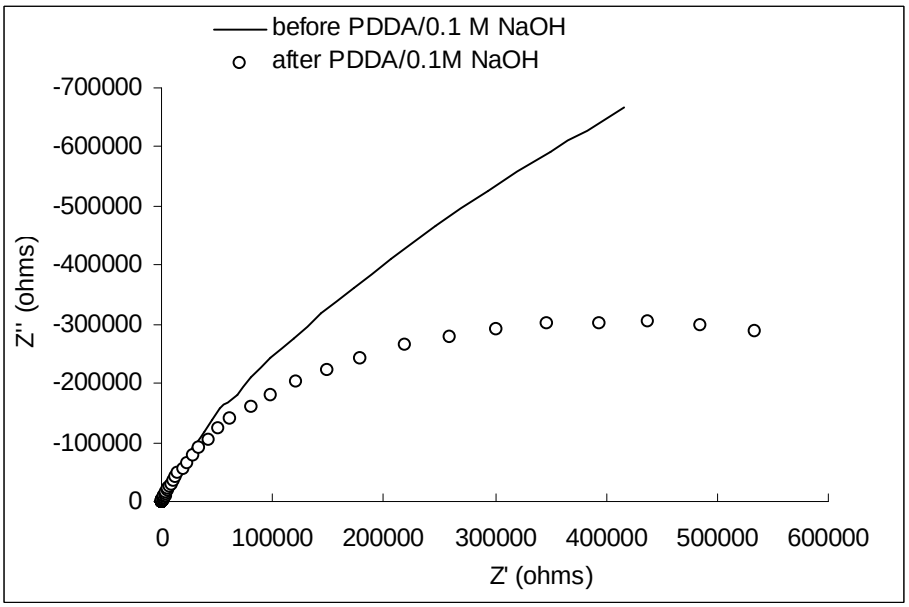

Figure 37: Nyquist plots of 11-MUA monolayers before and after polydiallydimethyl ammonium chloride 0.1 mol·L^{-1} NaOH. Impedance measurements were conducted in 0.005 mol·L^{-1}[Fe(CN)$_6$]$^{3-/4-}$ containing 0.1 mol·L^{-1} KCl at a potential of 0.2 V vs Ag/AgCl.

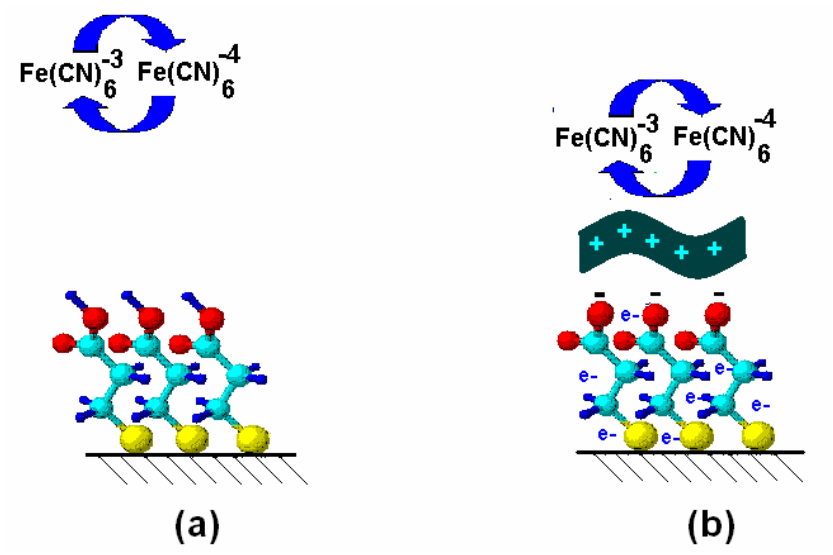

Figure 38: Schematic representing the likely interaction of the$[Fe(CN)_6]^{3-/4-}$ redox couple with neutral 3-MPA surfaces (a) and 3-MPA surfaces modified with PDDA.

Control experiments involving solution driven ionic self assembly were conducted to obtain data for the promotion and inhibition of ionic self assembly. Solution adsorption of PDDA to the surface of 3-MPA and 11-MUA was attempted in 0.1 $mol \cdot L^{-1}$ HCl. Nyquist plots of 3-MPA (Figure 39) and 11-MUA (Figure 40), show minimal change in the diameters of the complex impedance plots before and after exposure of the modified electrodes to PDDA in dilute acid solutions. The minimal change in charge-transfer resistances listed in Tables 2 and 3 provide further evidence of the inhibition of polyelectrolyte deposition to the surface of carboxylic acid terminated monolayers in acidic solutions. In acidic solutions, the acid groups are fully protonated and no charge exists in the terminal region (Figure 41). The lack of electrostatic interactions between the surface and PDDA results in a small change in charge-transfer resistance. It is believed that the small decrease in charge-transfer resistance is attributed to the nonspecific adsorption that is promoted by the hydrophobic interactions between the polymer backbone of the polyelectrolyte and the methlylene chains of the thiol.

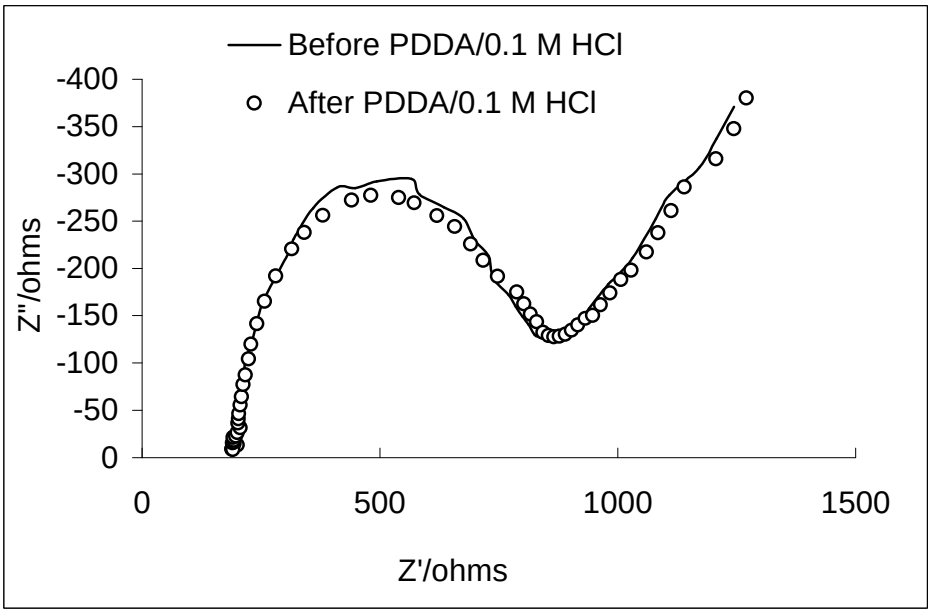

Figure 39: . Nyquist plots of 3-MPA monolayers before and after PDDA exposure in 0.1 mol·L^{-1} HCl. Impedance measurements were conducted in 0.005 mol·L-1[Fe(CN)$_6$]$^{3-/4-}$ containing 0.1 mol·L^{-1} KCl

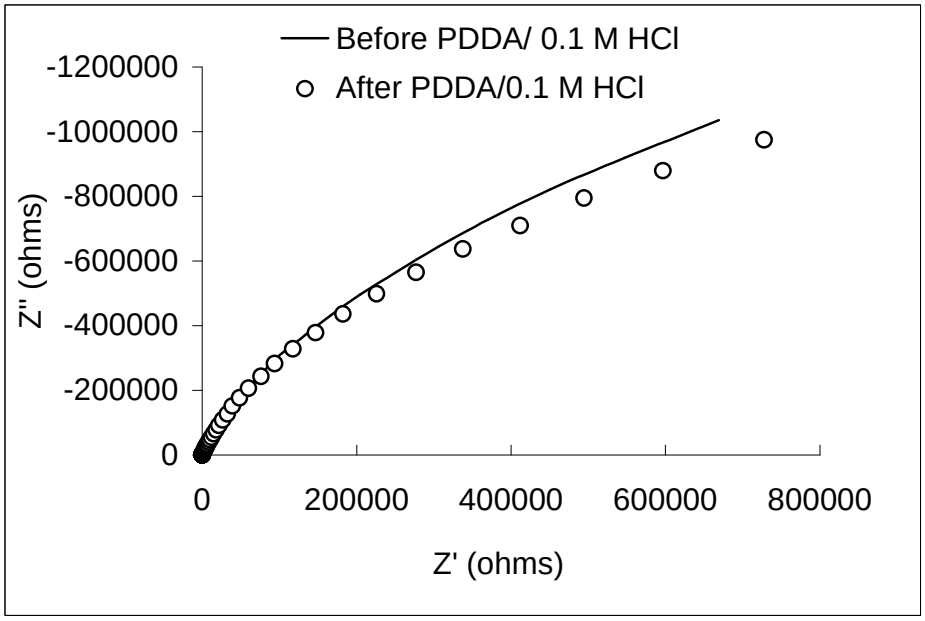

Figure 40: Nyquist plots of 11-MUA monolayers before and after polydiallydimethyl ammonium chloride 0.1 mol·L^{-1} HCl. Impedance measurements were conducted in 0.005 mol·L^{-1}[Fe(CN)$_6$]$^{3-/4-}$ containing 0.1 mol·L^{-1} KCl at a potential of 0.2 V vs Ag/AgCl.

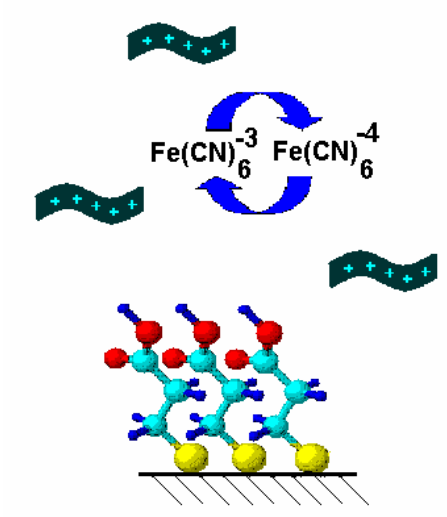

Figure 41: Schematic representing the likely interaction of the$[Fe(CN)_6]^{3-/4-}$ redox couple with PDDA deposited in 0.1 mol·L^{-1} HCl.

Table 2: Charge-transfer resistances before and after solution adsorption of PDDA onto 3-MPA monolayers in basic and acidic solutions.

	0.1 mol·L^{-1} NaOH (Ω)	0.1 mol·L^{-1} HCl (Ω)
Before PDDA exposure	520±78	600±76
After PDDA exposure	180±12	613±59
ΔR	340	13

Table 3: Charge-transfer resistances before and after solution adsorption of PDDA onto 11-MUA monolayers in basic and acidic solutions.

	0.1 mol·L^{-1} NaOH (MΩ)	0.1 mol·L^{-1} HCl (MΩ)
Before PDDA exposure	2.2±0.059	2.418
After PDDA exposure	0.750±0.0068	2.148
ΔR	1.450	0.269

Although charge-transfer resistance provides an indication of the extent of PDDA adsorption based on electrostatic interactions between the anionic redox probe and the cationic surface, it does not provide a measure of the quantity of PDDA adsorbed. Quartz crystal microbalance measurements were used to quantify the amount of PDDA deposited on the surface of 3-MPA and 11-MUA from solutions with acidic or basic pH. The most substantive piece of information obtained in a QCM analysis is a shift in the resonant frequency of a gold coated quartz plate when material is adsorbed to the gold. The resulting frequency change (ΔF) is used in the Sauerbrey equation (Equation 3) in order to determine the mass of PDDA adsorbed via ionic self assembly. Solution driven PDDA deposition onto 3-MPA and 11-MUA monolayers was examined using QCM by immersing the monolayer modified quartz plates in 0.1 mol·L^{-1}

NaOH containing 1.08×10^{-6} mol·L^{-1} PDDA. The trends observed in the QCM experiments were consistent with the trends observed in the impedance experiments. The average ΔF for PDDA deposition in 0.1 mol·L^{-1} NaOH was 9.5±2.4 Hz for 3-MPA and 12±2.5 Hz for 11-MUA; by employing the Sauerbrey equation to determine the mass from ΔF, these frequency changes correspond to masses of 130±40 ng for 3-MPA and 140±20 ng for 11-MUA. These mass approximations are in agreement with reported QCM analyses of the deposition of PDDA on bare gold under the influence of applied potential (125.6 ng and 190.6 ng)[51]. It is believed that these values provide further evidence of the deposition of PDDA to the surface of carboxylic acid functionalized monolayers in alkaline solutions.

As discussed above, ionic self assembly is promoted due to the deprotonation of the terminal acid groups and the resulting electrostatic attraction between the carboxylate surface and the cationic polyelectrolyte. QCM analyses were also conducted in a solution of 0.1 mol·L^{-1} HCl containing 1.08×10^{-6} mol·L^{-1} PDDA. The average frequency change for PDDA adsorbed to 3-MPA in dilute HCl was 3.4±0.18 Hz and for 11-MUA the average frequency change was 2.2 Hz. Inserting these frequency changes in the Sauerbrey equation results in the calculation of considerably lower amounts of PDDA deposited onto 3-MPA (6.43±0.5 ng) and 11-MUA (42 ng). It was expected for frequency and mass determinations of modified QCM plates exposed to PDDA in dilute HCl to be lower than plates exposed to the polyelectrolyte in NaOH. In dilute HCl, the surface groups of acid terminated monolayers are not charged, therefore electrostatic interaction between the terminal region of the monolayer and the cationic redox probe is absent. Therefore no significant accumulation of PDDA is detected with QCM measurements when modified plates are exposed to PDDA in 0.1 mol·L^{-1} HCl.

3.4 Applied potential deposition

The previous section describes behavior of impedance and QCM data when ionic self assembly is promoted and inhibited using alkaline and acidic solutions, respectively. Terminal

acid groups are deprotonated upon exposure to dilute NaOH solutions resulting in conditions favorable for the ionic self assembly of a cationic polyelectrolyte. Ionic self assembly of a cationic polyion was evident by the decrease in the charge-transfer resistance, which is a direct result of the electrostatic attraction between the cationic polyelectrolyte on the surface of the monolayer and the anionic redox probe in solution. Further evidence of PDDA deposition in NaOH was observed in the QCM data. A few hundred nanograms of material were deposited on the surface of the monolayer while exposed to dilute NaOH. The impedance and QCM data for modified plates exposed to PDDA in dilute HCl behaved as expected. It is believed that the neutrality of the monolayers in dilute acid solutions inhibits ionic self assembly of a cationic polyelectrolyte, therefore charge-transfer resistance of monolayers exposed to PDDA in acid solutions experienced minimal change, and QCM analyses only showed a few tens of nanograms of polyelectrolyte deposited. This section describes impedance and QCM data that reflect ionic self assembly that is promoted or discouraged using applied potential. To ensure that surface group ionization was a direct result of applied potential, experiments described in this section were conducted in pH 5 phosphate buffer solutions. Impedance and QCM data was once again used to verify ionic self assembly and to quantify the extent of ionic self assembly driven by applied potential.

The behavior of the modified electrodes exposed to PDDA while under the influence of potential equivalent to or near the PZC is reflected in the Nyquist plots shown in Figures 42 and 43. Both plots show that there is no change in the diameter of the complex impedance plot before and after exposure to PDDA at potentials equal to or slightly negative of the PZC. The charge-transfer resistances obtained from the LEVM fitting program (Tables 4 and 5) also show minimal change when potential is held near the PZC. This behavior is consistent with impedance analysis of solution deposition of PDDA in 0.1 $mol \cdot L^{-1}$ HCl which showed minimal change in charge-transfer resistance values resulting from the neutrality of the surface while immersed in acidic media.

Since Nyquist plots of modified electrodes exposed to PDDA at potential near the PZC show a minimal change, the inference can be made that at the potential of zero charge, surface group ionization is absent and ionic self assembly of PDDA is inhibited.

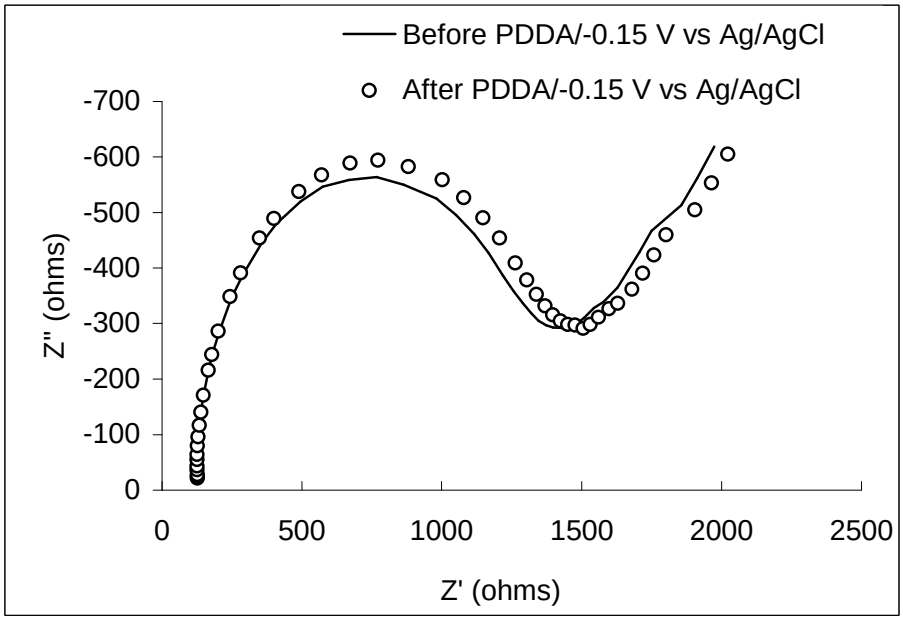

Figure 42: Nyquist plots for 3-MPA monolayers exposed to PDDA before and after application of -0.15 V vs Ag/AgCl (E = PZC). Impedance measurements were conducted in 0.005 mol·L-1$[Fe(CN)_6]^{3-/4-}$ containing 0.1 mol·L^{-1} KCl at a potential of 0.2 V vs Ag/AgCl.

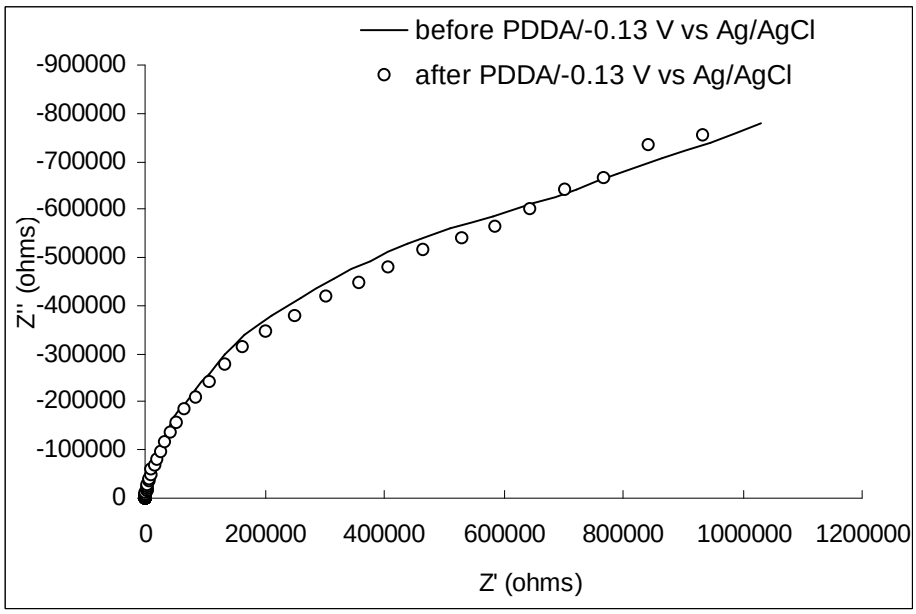

Figure 43: Nyquist plots for 11-MUA monolayers exposed to PDDA before and after application of -0.13 V vs Ag/AgCl. (E = PZC). Impedance measurements were conducted in 0.005 mol·$L^{-1}$$[Fe(CN)_6]^{3-/4-}$ containing 0.1 mol·L^{-1} KCl at a potential of 0.2 V vs Ag/AgCl.

After control experiments involving solution adsorption, applied potential-driven ionic self assembly of polyions commenced. Impedance analyses were conducted on modified electrodes exposed to PDDA at potentials positive of the PZC; this data is shown in Figures 44 and 45. There is an apparent decrease in the diameter of the complex impedance plot in both figures; charge-transfer resistances obtained via a fitting program (Tables 4 and 5) also show an apparent decrease at potentials positive of the PZC. This impedance response is similar to the behavior of the modified electrodes exposed to 0.1 $mol \cdot L^{-1}$ NaOH solutions containing diluted PDDA. In NaOH, the terminal acid groups are deprotonated promoting ionic self assembly of cationic polyelectrolytes to the resulting carboxylate surface. The decrease in charge-transfer resistance is in response to the electrostatic attraction between the deposited PDDA layer and the$[Fe(CN)_6]^{3-/4-}$ redox probe. This decreased proximity between the redox probe and the deposited polyelectrolyte layer increased the likelihood of electron transfer between the electrode surface and the redox probe. Unlike the solution deposition experiments, applied potential experiments were conducted in pH 5 phosphate buffer solution; this pH is below the surface pK_a of both 3-MPA and 11-MUA which means that there is no surface group ionization encouraging ionic self assembly. However, impedance data clearly shows a decrease in charge-transfer resistance. The decrease in charge-transfer resistance is an indicator of a close proximity between the redox probe in solution and the terminal region of the electrode. Increased proximity of an anionic redox probe to the terminal region of a modified electrode can only occur under the impetus of electrostatic attraction. Therefore it is believed that at potentials more positive than the PZC for both 3-MPA and 11-MUA the interfacial pH is changed in a way that encouraged ionic self assembly of cationic polyelectrolyte despite the fact that the modified electrode was immersed in a solution with a pH that discouraged surface group ionization

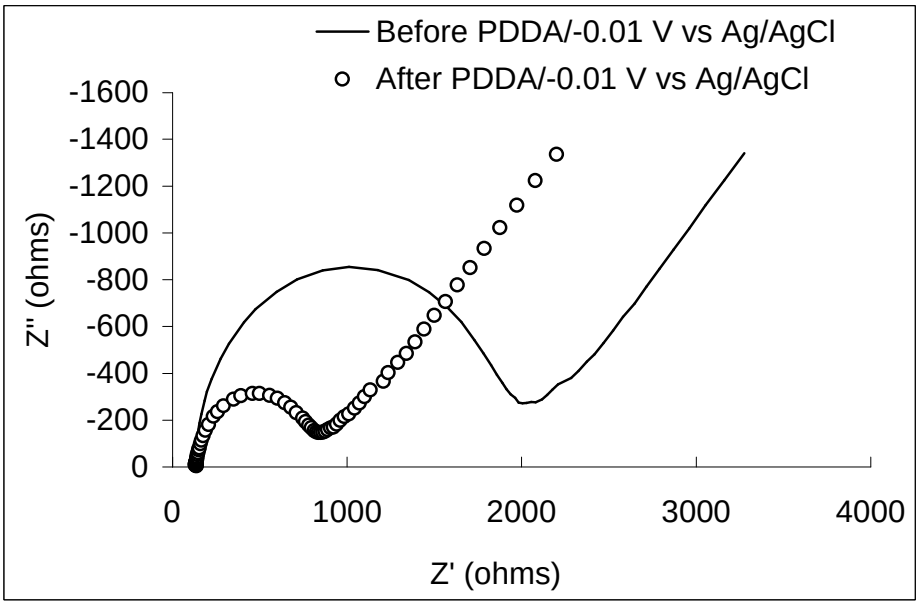

Figure 44: Nyquist plots for 3-MPA monolayers exposed to PDDA before and after application of -0.01 V vs Ag/AgCl (E > PZC). Impedance measurements were conducted in 0.005 mol·L^{-1}[Fe(CN)$_6$]$^{3-/4-}$ containing 0.1 mol·L^{-1} KCl at a potential of 0.2 V vs Ag/AgCl.

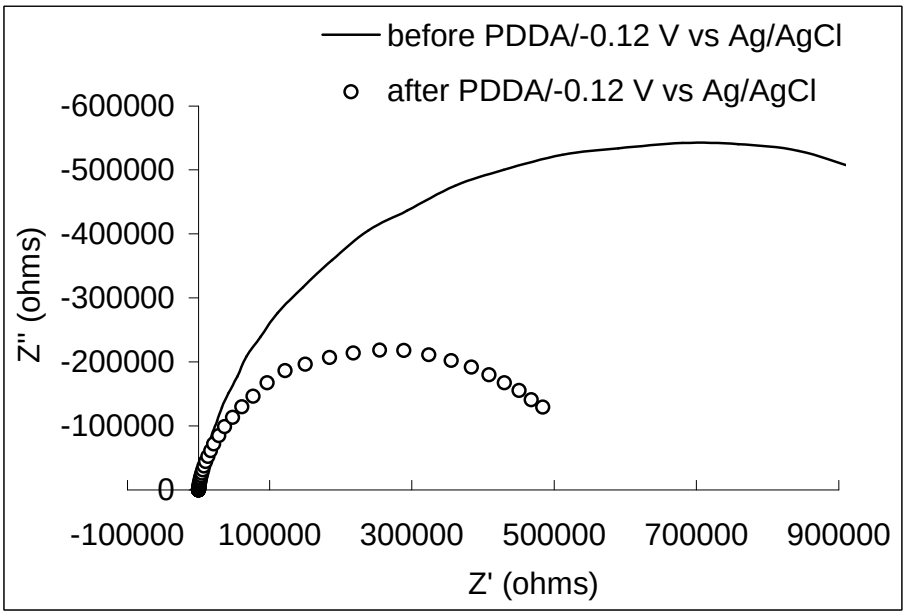

Figure 45: Nyquist plots for 11-MUA monolayers exposed to PDDA before and after application of -0.12 V vs Ag/AgCl (E > PZC). Impedance measurements were conducted in 0.005 mol·L^{-1}[Fe(CN)$_6$]$^{3-/4-}$ containing 0.1 mol·L^{-1} KCl at a potential of 0.2 V vs Ag/AgCl.

Table 4: Charge-transfer resistances before and after applied potential.

	E = PZC (Ω)	E > PZC (Ω)
Before PDDA Exposure	1,400±160	1,900±90
After PDDA Exposure	1,300±180	740±12
ΔR	100	1,160

Table 5: Charge-transfer resistances before and after applied potential.

	E = PZC M(Ω)	E > PZC (MΩ)
Before PDDA Exposure	1.6±0.3	1.2±0.02
After PDDA Exposure	1.7±0.5	0.67±0.53
ΔR	0.1	0.53

Mass changes were also used to confirm applied potential deposition of PDDA to the surface of 3-MPA and 11-MUA. At potentials close to the PZC the average frequency change was 2.5+0.2 Hz for 3-MPA and 4.3 Hz for 11-MUA. This corresponds to masses of 47±9 ng for 3-MPA and 50 ng for 11-MUA. This is consistent with the masses of PDDA deposited on the surfaces of modified surfaces exposed to solutions of 0.1 $mol \cdot L^{-1}$ HCl containing dilute PDDA. The lack of surface group charge of monolayers immersed in 0.1 $mol \cdot L^{-1}$ HCl allowed only tens of nanograms of PDDA to deposit due to hydrophobic interactions between exposed methylene chains of the monolayer and the polymer backbone. Application of potential near the PZC to modified electrodes produced similar QCM results due to the fact that there is no surface charge present to attract significant amounts of PDDA to the surface.

At potentials positive of the PZC, the average frequency change for modified QCM plates exposed to PDDA in pH 5 phosphate buffer solution was 29±6 Hz for 3-MPA and 11.2 Hz for 11-MUA. This corresponds to 552±106 ng for 3-MPA and 131 ng for 11-MUA. This behavior is consistent with the deposition of PDDA to modified electrodes in 0.1 $mol \cdot L^{-1}$ NaOH. In dilute alkaline solutions, the deprotonated carboxylic acid groups provided a template for the deposition of cationic polyelectrolytes; evidence of this was apparent by the hundreds of nanograms of PDDA that was deposited on the modified surfaces during the QCM analyses in 0.1 $mol \cdot L^{-1}$ NaOH. In pH 5 PBS, no ionic self assembly of cationic polyelectrolyte was encouraged because the solution pH is below the surface pK_a of both monolayers, but application of potential positive of the PZC to modified QCM plates in pH 5 phosphate buffer solution containing diluted PDDA clearly shows hundreds of nanograms of PDDA deposited. It can be inferred from these results that potential positive of the PZC lead to a change in the interfacial pH of the monolayer encouraging ionic self assembly of PDDA.

The control of ionic self assembly to the surface of carboxylic acid terminated monolayers via applied potential can be explained using observations reported by Dorain et al.[29] In their report, they present surface enhanced Raman intensities of phosphate ions in phosphate buffer system that vary with potential They illustrate that the ions accumulate at the surface of a silver electrode with increasingly positive potentials in the following order: $H_2PO_4^-$, HPO_4^{2-}, and PO_4^{3-}. Ebbing[97] reports that the literature pK_a values for the dihydrogen and monohydrogen phosphate ions are 6.2×10^{-8} and 4.8×10^{-13}; these values show that the anions that accumulate at the interface at potentials more positive than the PZC are increasingly basic. Therefore it is believed that holding the substrate potential at values more positive than the PZC lead to the accumulation of strong conjugate bases ($pK_b \geq 2.08\times10^{-2}$) at the interface and these deprotonate the surface carboxylic acid groups providing an anionic template for the deposition of a cationic polyelectrolyte.

3.5 Summary

The purpose of the research presented in this chapter was to determine if applied potential could control the deposition of polyelectrolytes to the surface of functionalized monolayers. Impedance and QCM data of PDDA deposited on the surface of functionalized monolayers in both 0.1 $mol\cdot L^{-1}$ NaOH and 0.1 $mol\cdot L^{-1}$ HCl show data of modified electrodes in conditions where ionic self assembly is promoted and discouraged. Applied potential deposition of polyelectrolytes was attempted in solutions with a pH of 5 to ensure that surface-confined acid groups were neutral, verifying that any significant deposition of polyelectrolytes would be a direct result of modifying the interfacial pH via applied potential. Impedance data showed that functionalized monolayers immersed in 0.1 $mol\cdot L^{-1}$ NaOH containing dilute PDDA experience a decrease in charge-transfer resistance. QCM experiments showed hundreds of nanograms of PDDA deposited to the surface of both 3-MPA and 11-MUA monolayers. This is direct evidence of the deprotonation of surface acid groups and the subsequent attachment of a cationic polyelectrolyte. Deposition of the cationic polyelectrolyte provided electrostatic attraction with

the anionic redox probe, leading to a decrease in charge-transfer resistance resulting from the decreased proximity of the redox probe to the terminal region of the monolayer. When potential positive of the PZC was applied to modified electrodes, similar behavior in the impedance and QCM data was witnessed, despite the fact that the supporting electrolyte solution pH was 5, well below the surface pK_a of the monolayers.

Impedance data of modified electrodes immersed in 0.1 $mol \cdot L^{-1}$ HCl containing dilute PDDA showed minimal change in charge-transfer resistance and QCM analyses only showed tens of nanograms of PDDA deposited. This is because the surface confined acid groups are neutral, inhibiting substantial ionic self assembly of PDDA to the surface of the functionalized monolayer. When potentials equal to the PZC were applied to the functionalized electrodes, charge-transfer resistance behaved similarly, only tens of nanograms of PDDA were deposited on 3-MPA and11-MUA surfaces.

Ionic self assembly is inhibited when solution deposition of PDDA is attemped in 0.1 $mol \cdot L^{-1}$ HCl, and when modified electrodes are exposed to potentials near the PZC while immersed in pH 5 phosphate buffer solution containing dilute PDDA. The inhibition of ionic self assembly is a result of the absence of surface charge at the terminal region of the monolayer. The slight changes in charge-transfer resistance and mass result from deposition of PDDA driven by hydrophobic interactions between the polymer backbone of the polyelectrolyte and the methylene chains of the monolayers. The results presented in this chapter demonstrate that application of potential relative to the PZC can be used to turn on or turn off ionic self assembly.

Chapter 4. Electrochemical Impedance and Quartz Crystal Microbalance Measurements of Polyelectrolyte Deposition onto Cysteine Monolayers

4.1 Introduction

Impedance and QCM data presented in the previous chapter demonstrate that application of potential positive of the PZC to electrodes modified with carboxylic acid terminated monolayers results in acid group deprotonation. This allows the activation and deactivation of ionic self assembly in solutions with pH values where ionizable surface groups are neutral. Evidence of potential-driven modification of cysteine surface charge was apparent from the decrease in charge-transfer resistance when modified electrodes exposed to PDDA were energized with potential positive of the PZC, and the minimal change in charge-transfer resistances when potential near the PZC was applied. The results of the applied potential deposition experiments with carboxylic acid terminated SAMs prompted a study to mirror these results with cysteine monolayers. Cysteine was chosen due to the presence of both carboxylic acid and amine groups yielding the possibility of potential-driven deposition of cationic and anionic polyelectrolytes.

This chapter describes the use of electrochemical impedance and quartz crystal microbalance measurements to examine the effects that varying solution pH and applied potential have on the interfacial charge of cysteine monolayers. Literature precedent involving the reversibility of the surface charge of monolayers include a report by Lahann and coworkers[98] that describes the use of 16-mercaptohexadecanoic acid (16-MHDA) monolayers in order to create surfaces that alternate between hydrophilic and hydrophobic character using applied potential. The authors induced changes in the conformation of the 16-MHDA monolayer by applying approximately +25 mV to attract the anionic end groups to the electrode surface. This produced a surface with hydrophobic characteristics due to exposed methylene chains. In the absence of applied potential, the 16-MHDA molecules were upright and the charged surface groups extended outwards producing a surface with hydrophilic properties. There are other reports that involve changing the surface polarity of monolayers by employing the use of mixed

SAMs containing both amine and carboxylic acid groups. Chuang and Lin report the use of a mixed 11-aminoundecanethiol/11-mercaptoundecanoic acid monolayer for the purpose of developing a surface to study variations in platelet adhesion to synthetic surfaces by adjusting the mole fraction of carboxylic acid terminated and amine terminated thiols [99]. The disadvantage of employing binary and ternary monolayers for the creation of monolayers with reversible surface characteristics is that careful control of the mole ratio of each thiol in the assembling solution is needed to produce a surface with the desired characteristics. There is also the possibility of phase aggregation of the mixture along the surface. An additional literature source involving producing reversible surface characteristics involves work reported by Homlin and coworkers[100]. They report the use of mixed zwitterionic monolayers consisting of terminal ammonium and sulfonic acid groups for inhibiting nonspecific adsorption of proteins[100]. It was show that mixed and single component zwitterionic SAMs consisting of ammonium and sulfonate groups resisted adsorption of fibrinogen and lysozyme proteins due to the electrical neutrality of the surface.

The possibility of reversing the surface charge of cysteine monolayers is based on reports that state the surface charge of cysteine is positive in solutions with a pH of approximately 1.71 due to protonation[101, 102] and is negative in solutions with pH values in excess of 11 due to deprotonation (Figure 46). Cysteine binds to gold via the Au-S bond[103-105] making the terminal NH_2 and COOH groups of cysteine accessible for ionization via solution pH or applied potential. The presence of both −NH2 groups and −COOH groups is expected to establish conditions that promote ionic self assembly of a cationic polyelectrolyte, polydiallyldimethyl ammonium chloride (PDDA) (Figure 23) and an anionic polyelectrolyte, polystyrene sulfonate (PSS) (Figure 47).

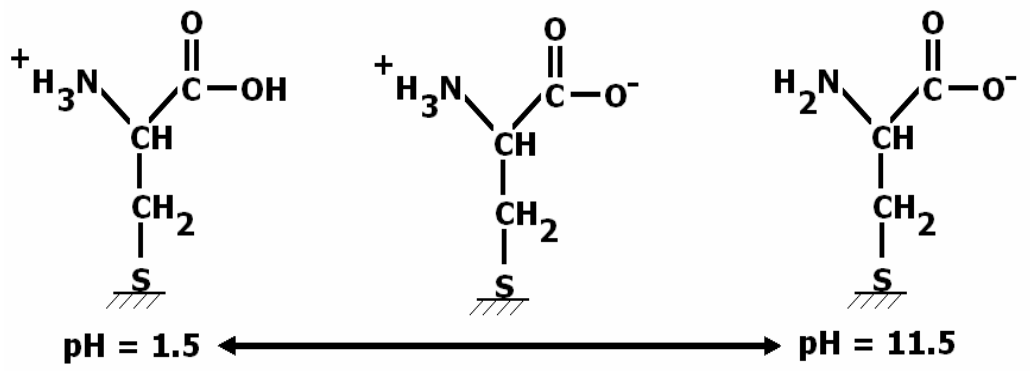

Figure 46: Surface charge of cysteine monolayers in acidic, neutral, and basic solutions.

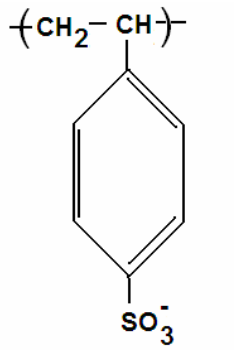

Figure 47: Structure of polystyrene sulfonate.

4.2 Experimental

4.2.1 Polyelectrolyte deposition via solution pH

Cysteine monolayers were prepared as described in Section 2.6.1. Cysteine was obtained from Aldrich and used without further purification. Impedance analyses were conducted on the modified electrodes following monolayer immobilization using impedance parameters described in Section 2.6.2. After conducting a preliminary impedance analysis of the modified electrodes, they were immersed in solutions of 1.08×10^{-6} mol·L^{-1} PDDA in 0.1 mol·L^{-1} NaOH or 0.1 mol·L^{-1} HCl for an impedance analysis of systems where ionic self assembly is encouraged and hindered. Polystyrene sulfonate was purchased from Aldrich and used without further purification. After Sixty-second polyelectrolyte exposure, the electrodes were rinsed with deionized water and a second impedance analysis commenced. The same procedure was used for the QCM analyses. Gold coated QCM plates were cleaned according to procedures listed in Section 2.6.3. Following the cleaning procedure, monolayers were immobilized on the plate

following procedures listed in 2.6.3. After monolayer immobilization, the modified plates were rinsed with ethanol and water, dried with a stream of nitrogen gas, and connected to the QCM oscillator. Once the modified plates were connected to the QCM oscillator, frequency measurements were obtained from the Hewlett Packard model 5334B universal counter every 15 minutes in 1 minute intervals. The impedance and QCM measurements of solution driven deposition of polyelectrolytes demonstrated known system responses for the encouragement and inhibition of ionic self assembly to cysteine monolayers.

4.2.2 pK_a determination

Cysteine monolayers used for surface pK_a determination were prepared as described in Section 2.6.1. The solutions used to collect impedance data for cysteine modified electrodes were 0.005 $mol \cdot L^{-1}[Fe(CN)_6]^{3-/4-}$ prepared using commercially available phosphate buffer solutions from VWR scientific. The pH values of the phosphate buffers ranged from 3 to 8. Impedance data was collected using the parameters listed in Section 2.6.2.

4.2.3 PZC determination

Impedance measurements were also used to determine PZC values for cysteine modified electrodes. Cysteine monolayers were prepared as described in Section 2.6.1. The PZC values were determined in pH 5 phosphate buffer solutions commercially available from VWR scientific. It is important to note that the solutions used in the PZC determination contained no redox probe. Solutions with a pH 5 were used for the PZC determination for cysteine monolayers because the reported isoelectric point of cysteine is approximately 5.06[104]. Cysteine monolayers were prepared as described in Section 2.6.1 Impedance analyses of cysteine monolayers immersed in pH 5 phosphate buffer were conducted at potentials ranging from -0.6 V to 0.6 V (vs Ag/AgCl) in 0.1 V increments with frequencies from 1.0×10^6 Hz to 0.1 Hz.

4.2.4 Applied potential deposition

Following surface pK_a and PZC determination of cysteine monolayers, attempts at applied potential deposition of polyelectrolytes commenced. The monolayers used for the applied potential deposition experiments were prepared according to procedures listed in Section 2.6.1. Initial impedance analyses were conducted on the modified electrodes before exposing the electrodes to potentials relative to the PZC; the impedance parameters used are listed in Section 2.6.2. Following the initial impedance analysis, the cysteine modified electrodes were immersed in 0.05 $mol \cdot L^{-1}$ pH 5 phosphate buffer solution containing 1.08×10^{-6} $mol \cdot L^{-1}$ PDDA or 1.2×10^{-3} $mol \cdot L^{-1}$ PSS. While in the polyelectrolyte solutions, a potential step experiment was used to apply the appropriate potential; the parameters that were used are described in Section 2.6.1. Sixty-second, potential steps to -0.05 V vs Ag/AgCl were used to apply potential positive of the PZC; potential negative of the PZC was applied using Sixty-second, potential steps to -0.40 V vs Ag/AgCl. After the potential step experiments, the electrodes were rinsed with de-ionized water and a second impedance analysis was conducted. It is important to note that before and after each potential step, the modified electrodes were rinsed with de-ionized water and immersed in 0.005 $mol \cdot L^{-1}[Fe(CN)_6]^{3-/4-}$/pH 5 phosphate buffer solution for impedance analyses. For each potential step experiment, a freshly prepared cysteine monolayer was used.

4.3 Results and Discussion

4.3.1 pK_a determination

Prior to confirming the applied potential deposition of polyelectrolytes, two preliminary experiments for the determination of the pK_a and PZC of the monolayers were conducted. Faradiac impedance titrations similar to titrations conducted on 3-MPA and 11-MUA monolayers were conducted on cysteine modified electrodes to determine the pK_a of cysteine monolayers. As shown in Figure 48, the Nyquist semicircle diameters increase with increasing solution pH. This behavior is also evident in the charge-transfer resistances listed in Table 6.

This result is similar to the results observed with 3-MPA and 11-MUA monolayers. In this case, lower pH values result in the protonation of the amine group of the cysteine monolayer encouraging electrostatic attraction between the positively charged group and the anionic redox couple (Figure 49a). This decreased distance between the redox couple and the surface increased the likelihood of electron transfer resulting in decreased charge-transfer resistance values. At higher pH values, the carboxylic acid portion of the monolayer is deprotonated resulting in electrostatic repulsion between the carboxylate group and the anionic redox probe (Figure 49b). The increased distance between the redox probe and the monolayer decreased the electron transfer rate producing an increase in charge-transfer resistance values.

Charge-transfer resistance values obtained with LEVM fitting software free for download and were plotted against solution pH (Figure 50) and the surface pK_a value for cysteine monolayers was determined to be 4.8$\pm$0.3, which is close to the reported isoelectric point of cysteine monolayers assembled on gold (5.06)[104].

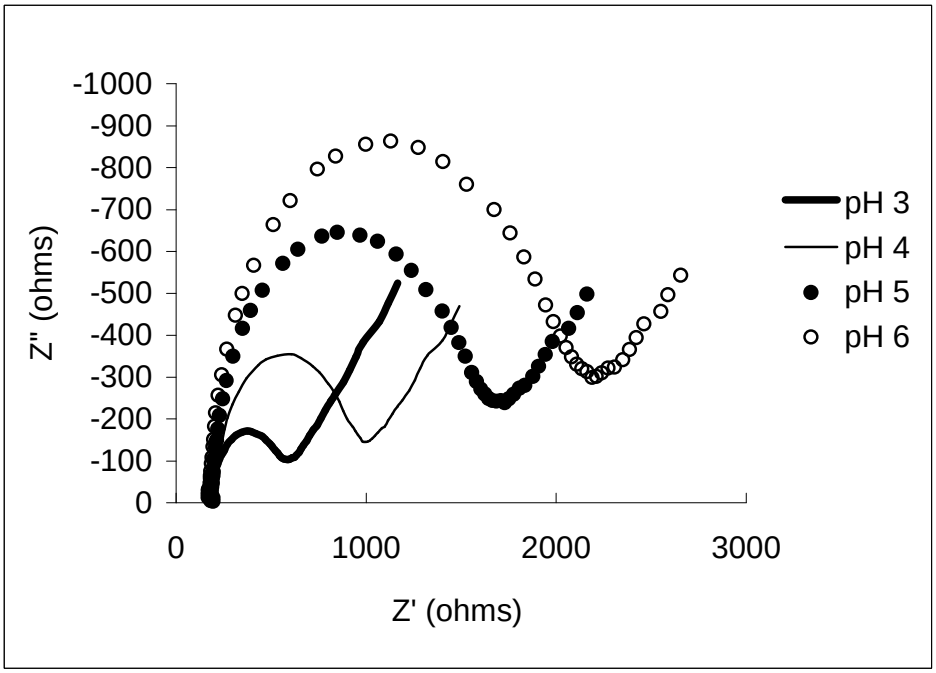

Figure 48: Impedance measurements of cysteine modified electrodes in phosphate buffer solutions with varying pH values. Impedance measurements were conducted in 0.005 mol·L^{-1}[Fe(CN)$_6$]$^{3-/4-}$ containing 0.1 mol·L^{-1} KCl at a potential of 0.2 V vs Ag/AgCl.

Table 6: Charge-transfer resistances for cysteine monolayers in varying solution pH values.

pH	R_{CT} (Ω)
3	305±131
4	609±240
5	1414±135
6	1941±134
7	2339±145

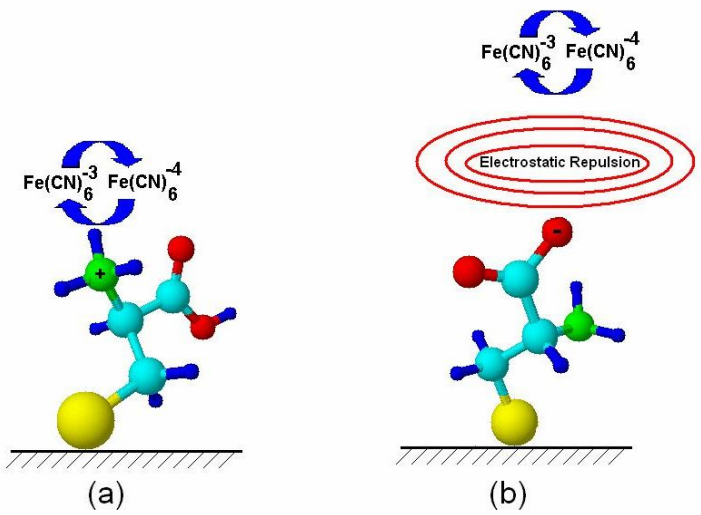

Figure 49: Schematic representing the likely electrostatic interaction between anionic redox probe and protonated amine groups (a) and deprotonated carboxylic acid groups (b) of cysteine monolayers.

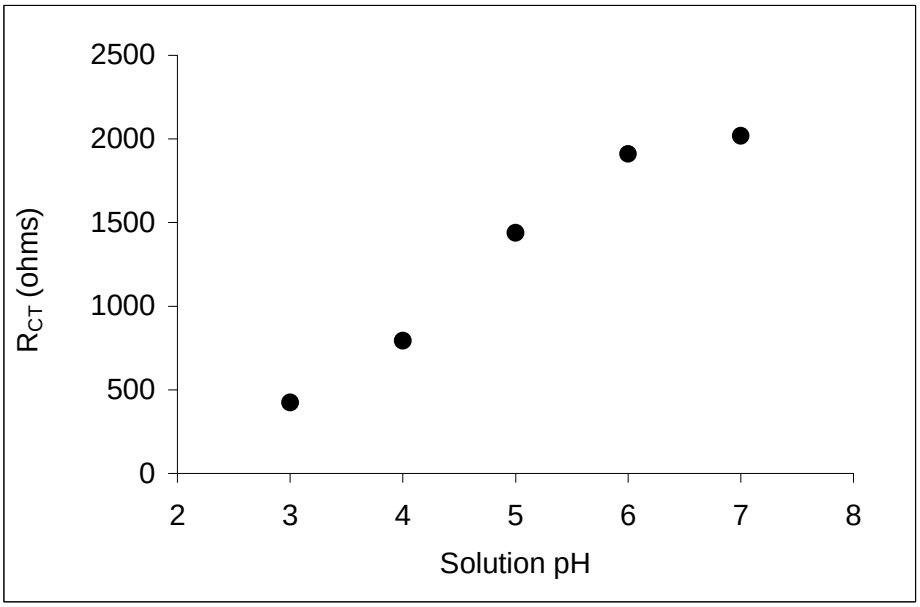

Figure 50: Electrochemical impedance titration of cysteine monolayers assembled on gold. Impedance measurements were conducted in 0.005 mol·L-1$[Fe(CN)_6]^{3-/4-}$ containing 0.1 mol·L^{-1} KCl at a potential of 0.2 V vs Ag/AgCl.

Impedance titrations of cysteine monolayers were also conducted using a cationic redox probe, hexamine ruthenium chloride ($[Ru(NH_3)_6]^{3+}$). Impedance titrations conducted using this probe produced pK_a values that showed a significant positive shift (6.1±0.6) as shown in Figure 51. The titration curve shows reversed behavior from impedance titrations performed

with$[Fe(CN)_6]^{3-/4-}$. This is due to the differences in electrostatic interactions between the cationic redox probe and the surface groups of the cysteine monolayer. In solutions with pH values less than 5, the amine groups are protonated and electrostatic repulsion exists between the amine groups and the cationic redox probe (Figure 52a). The increased distance between the redox probe and the modified electrode decreased the extent of electron transfer resulting in an increase in charge-transfer resistance values. At pH values in excess of 5, the carboxylic acid groups are deprotonated and an electrostatic attraction exists between the carboxylate surface and the cationic redox probe resulting in decreased distance between the probe and the monolayer surface. As a result, electron transfer is increased and the charge-transfer resistance decreases (Figure 52b).

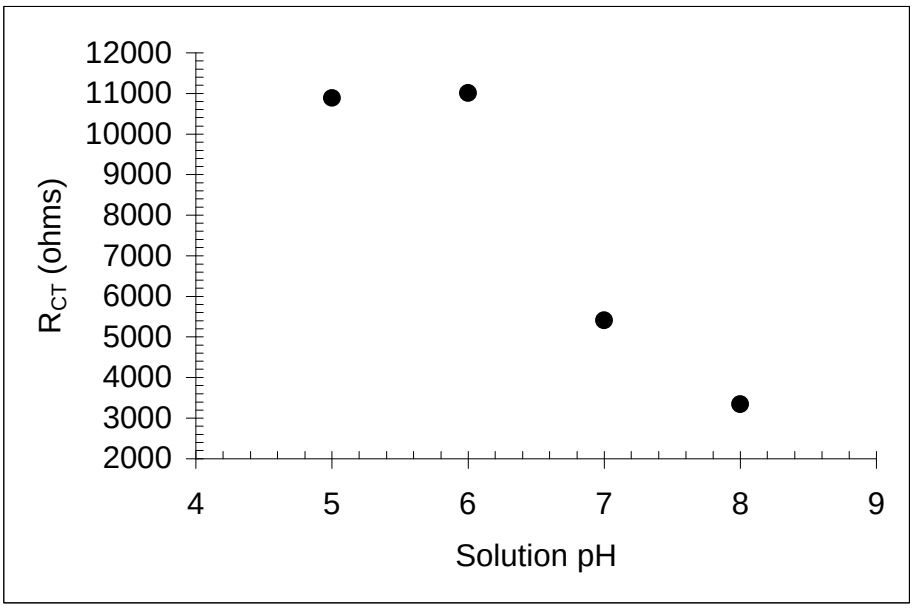

Figure 51: Electrochemical impedance titration of cysteine monolayers assembled on gold. Impedance measurements were conducted in 0.005 mol·L^{-1} $[Ru(NH_3)_6]^{3+}$ containing 0.1 mol·L^{-1} KCl at a potential of 0.2 V vs Ag/AgCl.

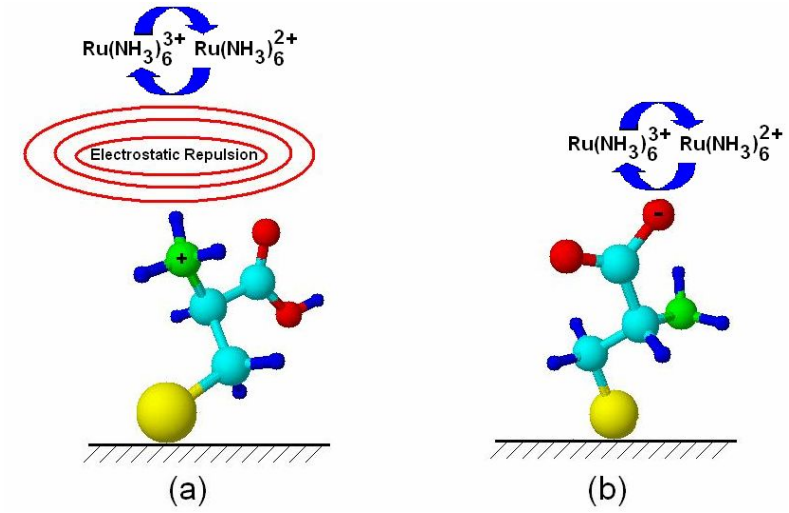

Figure 52: Schematic representing the likely electrostatic interaction between a cationic redox probe and a protonated amine group (a) and a deprotonated carboxylic acid group (b) of cysteine monolayers.

When conducting impedance titrations using different redox probes, different formal potentials are required; those potentials are 0.2 V vs Ag/AgCl for$[Fe(CN_6)]^{3-/4-}$ and -0.3 V vs Ag/AgCl for $[Ru(NH_3)_6]^{3+}$. The difference in the pK_a values is much more pronounced than the difference observed for 3-MPA and 11-MUA monolayers; it is believed that the significant change is due to the presence of amine and carboxylic acid groups in cysteine monolayers. This provided an early indication that the terminal functional groups have a response to applied potential.

4.3.2 PZC determination

Since the objectives of this dissertation research include using applied potential to modulate the interfacial pH of functionalized monolayers in order to drive self assembly, it was once again necessary to determine the PZC, this time of cysteine monolayers. Impedance measurements were taken at various potentials in the absence of a redox probe to ensure that the impedance measurements were a direct result of the behavior of the double-layer adjacent to the terminal region of the monolayer as it responds to applied potential. Determination of the double-layer capacitance values for the PZC was achieved by plotting log of the total impedance (Z) vs log frequency. Figure 53 is an example of the Log Z vs Log F plots used in the double-

layer capacitance determination. The y-intercepts of Log Z vs Log F plots, equivalent to $\frac{1}{C_{DL}}$, were plotted against potential in order to determine the PZC of cysteine monolayers, denoted by the minimum in Figure 54. The PZC of cysteine was determined to be approximately -0.1 V.

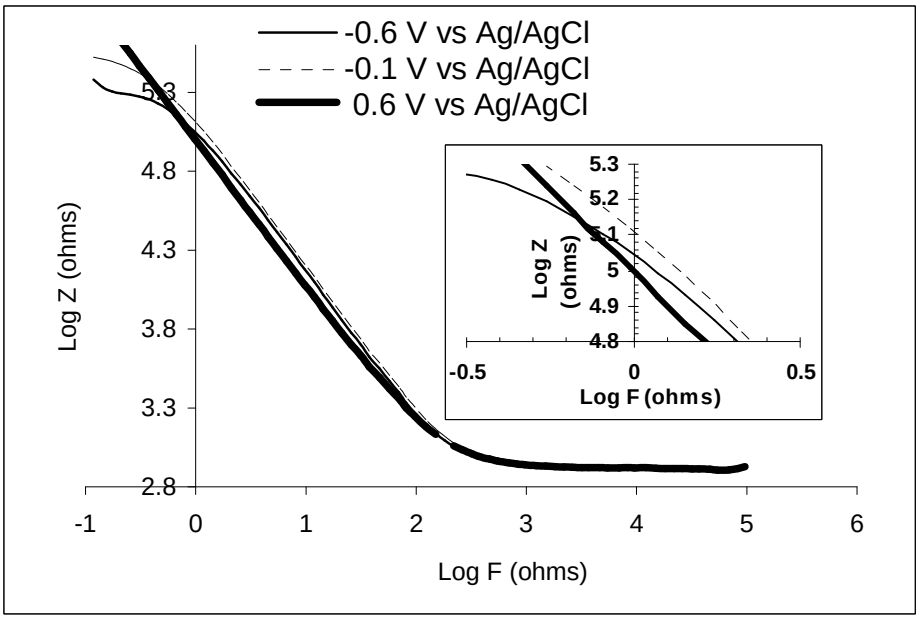

Figure 53: Double-layer capacitance determination of cysteine at -0.4 V, -0.1 V, and 0.4 V. Impedance measurements were conducted in 0.05 mol·L^{-1} pH 5 phosphate buffer solution from -0.6 V to 0.6 V vs Ag/AgCl.

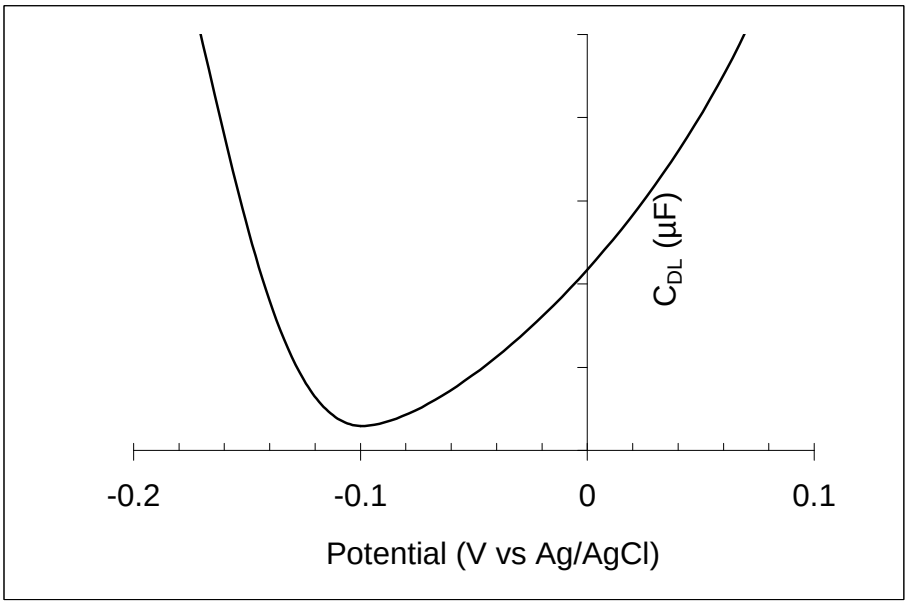

Figure 54: Potential of zero charge determination for cysteine.

4.3.3 pH Driven Deposition

After determining pK_a and PZC values for cysteine, impedance measurements were used to confirm the absence or presence of polyelectrolytes deposited onto the surface of cysteine monolayers in reponse to applied potential. The charge-transfer resistance parameter of impedance data was used to confirm the deposition of polyelectrolytes. Charge-transfer resistance is an ideal parameter to use to confirm polyelectrolyte deposition because it provides a measure of the extent of the electrostatic interaction between the monolayer surface and the redox probe in solution. Cysteine modified electrodes were exposed to 0.1 $mol \cdot L^{-1}$ NaOH and 0.1 $mol \cdot L^{-1}$ HCl solutions containing 1.08×10^{-6} $mol \cdot L^{-1}$ PDDA for the purpose of examining the effect impedance data in solutions were ionic self assembly is promoted and inhibited. Similar impedance experiments were conducted that involved conducting impedance analyses on cysteine modified electrodes before and after immersion of cysteine modified electrodes in 0.1 $mol \cdot L^{-1}$ HCl and 0.1 $mol \cdot L^{-1}$ NaOH solutions containing 1.3×10^{-3} $mol \cdot L^{-1}$ PSS.

In Figure 55, diameters of the Nyquist plot for cysteine monolayers exposed to 0.1 $mol \cdot L^{-1}$ NaOH solutions containing dilute PDDA show a dramatic decrease. Charge-transfer resistance values listed in Table 7 also show a drastic decrease. This is a direct result of deprotonation of the carboxylic acid groups which drives the ionic self assembly of PDDA (Figure 56a). The positive charge of the PDDA layer attracts the anionic redox probe decreasing the distance between the redox probe and the surface. Also illustrated in Figure 55, there is evidence of a significant increase in Nyquist semicircle diameter when cysteine monolayers are exposed to PSS solutions made from 0.1 $mol \cdot L^{-1}$ HCl. The increase in Nyquist plot diameter in this case is a result of the protonation of the amine group encouraging ionic self assembly of anionic PSS (Figure 56b). Electrostatic repulsion between the deposited PSS layer and the anionic redox probe increased the distance between the electrode and the redox probe. As a result, electron transfer is decreased producing an increase in charge-transfer resistance as shown in Table 8.

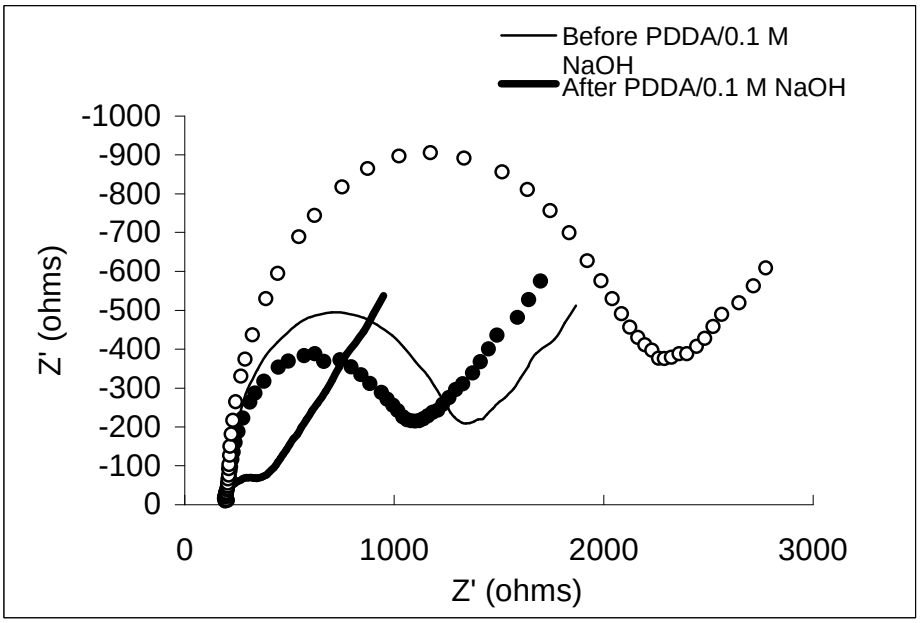

Figure 55: Nyquist plots of cysteine monolayers before and after PDDA and PSS in 0.1 mol·L^{-1} NaOH and 0.1 mol·L^{-1} HCl respectively. Impedance measurements were conducted in 0.005 mol·L^{-1}[Fe(CN)$_6$]$^{3-/4-}$ containing 0.1 mol·L^{-1} KCl at a potential of 0.2 V vs Ag/AgCl.

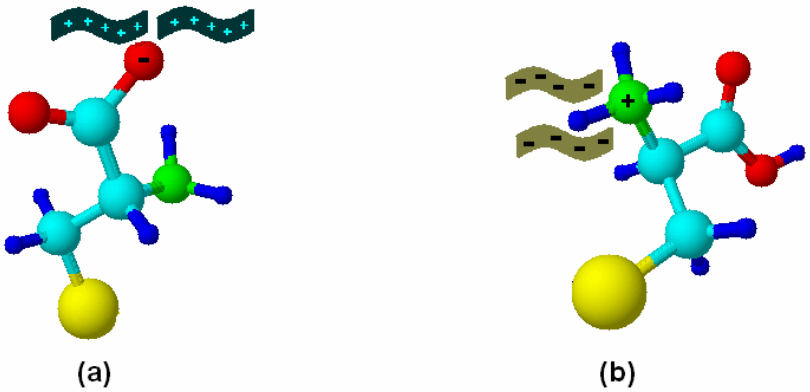

Figure 56: Ionic self assembly of PDDA in 0.1 mol·L^{-1} NaOH (a) and ionic self assembly of PSS in 0.1 mol·L^{-1} HCl (b).

Table 7: Charge-transfer resistances before and after solution adsorption of PDDA onto cysteine monolayers in 0.1 mol·L^{-1} NaOH.

	0.1 mol·L^{-1} NaOH (Ω)
Before PDDA Exposure	1200±15
After PDDA Exposure	36]3±185
ΔR	837

Table 8: Charge-transfer resistances before and after solution adsorption of PSS onto cysteine monolayers in 0.1 mol·L^{-1} HCl.

	0.1 mol·L^{-1} HCl (Ω)
Before PSS Exposure	1560±656
After PSS Exposure	2690±696
ΔR	1130

In Figure 57, Nyquist plots are shown that present impedance data for cysteine monolayers immersed in solutions where ionic self assembly of PDDA and PSS is inhibited. In this figure, there is minimal change in Nyquist plot diameter when modified electrodes are exposed to PDDA in 0.1 mol·L^{-1} HCl; there is also minimal change in charge-transfer resistance values as seen in Table 9. The small change in charge-transfer resistance is a response to the lack of ionic self assembly of PDDA in the acid solution (Figure 58a). While in the acid solution, the carboxylic acid portion of the cysteine monolayers is neutral; therefore, no ionic self assembly of PDDA is encouraged. The same result is witnessed with the Nyquist semicircle diameters for cysteine monolayers exposed to 0.1 mol·L^{-1} NaOH solutions containing dilute PSS. Also seen in Figure 57, is minimal change in the Nyquist semicircle diameter for cysteine monolayers exposed to 0.1 mol·L^{-1} NaOH solutions containing dilute PSS. This is also evident in the charge-transfer resistances as shown in Table 10. This minimal change is due to the neutrality of the amine group in alkaline solutions (Figure 58b). The lack of sufficient positive charge on the cysteine monolayers discourages the ionic self assembly of PSS to the cysteine surface. For this reason, there is little change between the charge-transfer resistances of cysteine monolayers before and after exposure to PSS/0.1 mol·L^{-1} NaOH solutions.

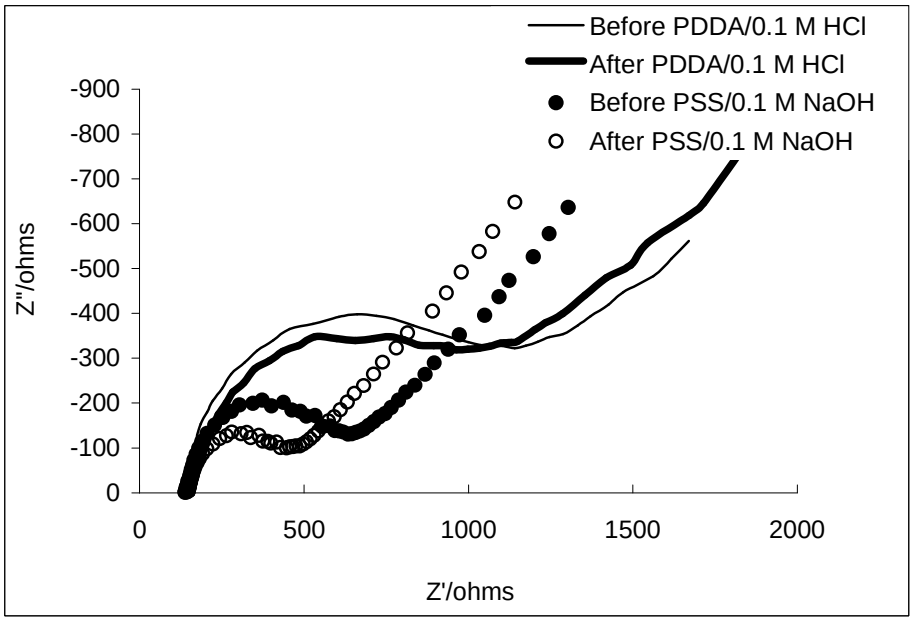

Figure 57: Nyquist plots of cysteine monolayers before and after PDDA and PSS in 0.1 mol·L^{-1} HCl and 0.1 mol·L^{-1} NaOH respectively. Impedance measurements were conducted in 0.005 mol·L-1[Fe(CN)$_6$]$^{3-/4-}$ containing 0.1 mol·L^{-1} KCl at a potential of 0.2 V vs Ag/AgCl.

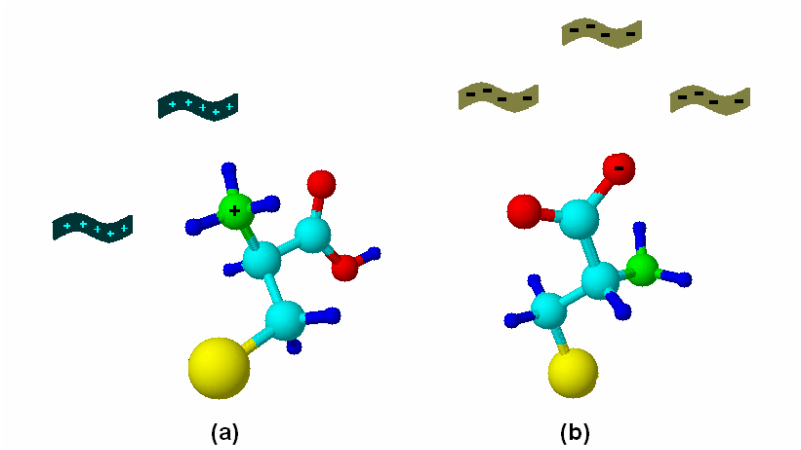

Figure 58: Inhibition of the ionic self assembly of PDDA in 0.1 mol·L^{-1} HCl (a) and ionic self assembly of PSS in 0.1 mol·L^{-1} NaOH (b).

Table 9: Charge-transfer resistances before and after solution adsorption of PDDA onto cysteine monolayers in 0.1 mol·L^{-1} HCl.

	0.1 mol·L^{-1} HCl (Ω)
Before PDDA Exposure	900±40
After PDDA Exposure	820±60
ΔR	80

Table 10: Charge-transfer resistances before and after solution adsorption of PSS onto cysteine monolayers in 0.1 mol·L^{-1} NaOH.

	0.1 mol·L^{-1} NaOH (Ω)
Before PSS Exposure	703±205
After PSS Exposure	557±221
ΔR	146

An additional diagnostic tool used to confirm deposition of polyelectrolytes was the quartz crystal microbalance (QCM). Cysteine modified quartz plates were immersed in cationic and anionic polyelectrolyte solutions where ionic self assembly was promoted and inhibited. Solution driven PDDA deposition onto cysteine monolayers was examined using QCM by immersing cysteine modified QCM plates in 0.1 mol·L^{-1} NaOH containing 1.08×10^{-6} mol·L^{-1} PDDA for approximately one minute. The average frequency changes and corresponding masses in response to solution driven deposition of PDDA onto cysteine modified quartz plates are listed in Table 11. It is evident from this data that a significant amount of PDDA is deposited onto cysteine monolayers as expected as a result of the deprotonation of the carboxylic acid groups. The resulting carboxylate groups to served as an anionic template for the deposition of the cationic PDDA polyelectrolyte.

Similar experiments were conducted with cysteine modified plates immersed in 1×10^{-3} mol·L^{-1} PSS/0.1 mol·L^{-1}HCl. Average frequency changes and resulting mass determinations for cysteine monolayers exposed to PSS in acidic solutions are also listed in Table 11. This data reveals that a significant amount of PSS is deposited to the surface to cysteine monolayers in acidic solutions. This is expected because the amine group is protonated, providing an cationic template for the deposition of PSS.

Table 11: ΔF and mass approximations for solution adsorbed PDDA and PSS onto cysteine monolayers.

	ΔHz (F)	Mass (ng)
PDDA/0.1 mol·L^{-1} NaOH	15±10	418±115
PSS/0.1 mol·L^{-1} HCl	30±9	477±166

In order to examine QCM conditions where ionic self assembly is inhibited, cysteine modified QCM plates were immersed in 0.1 mol·L^{-1} HCl containing 1.08×10^{-6} PDDA mol·L^{-1} for approximately one minute. The average frequency changes and corresponding masses for cysteine modified electrodes exposed to PDDA in acidic solutions are listed in Table 12. It is evident from this data that there is a significantly lower amount of PDDA deposited when compared to PDDA deposition in 0.1 mol·L^{-1} NaOH. In acidic solutions, the carboxylic acid

groups of cysteine monolayers are neutral providing no anionic surface to drive ionic self assembly of a cationic polyelectrolyte.

A similar test was conducted on cysteine monolayers exposed to 0.1 mol·L^{-1} NaOH containing 1×10^{-3} mol·L^{-1} PSS. Average frequency changes and resulting mass determinations for cysteine monolayers exposed to PSS in basic solutions are also listed in Table 12. In this case, a smaller amount of PSS is deposited on the surface compared to the mass of PSS deposited in 0.1 mol·L^{-1} HCl. In basic solutions, the amine groups are neutral providing no cationic template for negatively charged PSS deposition.

Table 12: ΔF and mass approximations for the inhibition of solution adsorbed PDDA and PSS onto cysteine monolayers.

	ΔHz (F)	Mass (ng)
PDDA/0.1 mol·L^{-1} HCl	1	9
PSS/0.1 mol·L^{-1} NaOH	6±1	70±8

The results obtained from the impedance and QCM analysis of solution driven deposition of polyelectrolytes to cysteine monolayers serve as a prediction of the expected trends associated with impedance and QCM analyses of cysteine modified plates immersed in polyelectrolyte solutions while energized with potentials positive and negative of the of the PZC.

4.4 Applied potential deposition

In this section, impedance and QCM experiments involving the potential-driven deposition and inhibition of polyelectrolytes onto cysteine monolayers using applied potential are described. Cysteine monolayers were used to see if potential could be used to deposit both cationic and anionic polyelectrolytes onto cysteine monolayers. Figure 59 illustrates Nyquist plots for cysteine modified electrodes before and after application of potential positive of the PZC while exposed to PDDA and PSS in phosphate buffer solutions. The results were opposite of the 3-MPA and 11-MUA applied potential experiments. At potentials positive of the PZC, the Nyquist plots representing the exposure of cysteine monolayers to phosphate buffer solutions containing PDDA show minimal change in Nyquist semicircle diameter. From this result, the assumption can be made that there is no significant deposition of PDDA.

This is in stark contrast to the applied potential impedance data obtained with 3-MPA and 11-MUA monolayers. For those carboxylic acid terminated surfaces, application of potentials positive of the PZC resulted in a change in the local pH at the monolayers promoting ionic self assembly, noted with a decrease in Nyquist semicircle diameter. With the cysteine monolayers, application of potentials positive of the PZC results in a small change in the Nyquist semicircle diameter when exposed to PDDA. At the same potential, there is a substantial increase in the Nyquist semicircle diameter for cysteine modified electrodes exposed to PSS. The charge-transfer resistances for cysteine modified electrodes exposed to PDDA and PSS at potentials positive of the PZC are listed in Table 13. These charge-transfer resistance values show minimal change in when cysteine modified electrodes are exposed to PDDA at potentials positive of the PZC; under the same potential, cysteine modified electrodes exposed to PSS solutions yield charge-transfer resistances that show a significant increase. These values suggest that ionic self assembly of PSS is encouraged at potentials more positive than the PZC and ionic self assembly of PDDA is not. The behavior of the impedance data suggests that some other mechanism is operating other than amine group protonation or carboxylic acid group deprotonation.

Since cysteine exists as a zwitterion at the pH values used in the applied potential experiments (pH 5)[101, 102] it is believed that application of potentials positive of the PZC introduces excess positive charges at the substrate that attract the carboxylate groups towards the surface (Figure 60). Applications of potentials negative of the PZC are believed to attract the protonated amine groups towards the surface. Reductive desorption measurements performed on cysteine monolayers provides evidence that the stability of cysteine monolayers may establish conditions favorable for the tilting of the immobilized molecules in response to potential. Sato and Mizutani report that the stability of the monolayer is directly related to the desorption potential[106]. It is further asserted that a less negative reduction potential is indicative of a partially formed monolayer[89]. Peak potentials listed on the reductive voltammograms of cysteine and 3-MPA (Figure 29) show close to a 200 millivolt difference in the potential required for

desorption. Despite both thiols having the same carbon chain length, the reduction potential for cysteine is much more positive. The positive reduction potential of cysteine provides evidence that cysteine monolayers are partially formed, and are less stable which may provide some freedom of movement for the immobilized cysteine chains in response to applied potential.

In addition to reduction potential, the charge, *Q*, associated with the reductive desorption mechanism (Figure 17) is used to determine the surface coverage (Γ) of alkanethiol monolayers using Equation 4:

$$\Gamma = \frac{Q}{nFA} \quad (4)$$

Where *n* represents the number of electrons transferred during reductive desorption, *F* is Faraday's constant, and *A* is the area of the electrode. Literature sources assert that reductive desorption studies of well formed monolayers have a coverage of $7.0\text{-}7.6 \times 10^{-10}$ mol·cm^{-2}.[96,89] Monolayers with this coverage are composed of immobilized thiol chains with restricted movement because the molecules are close packed and the chains are fully extended[89]. Using similar reductive desorption measurements with cysteine monolayers yields a coverage estimate of $5.8 \pm 0.9 \times 10^{-10}$ mol·cm^{2}. The low surface coverage for cysteine monolayers provides evidence that there is low packing density.

Therefore it is reasonable to suspect that potentials applied to cysteine modified electrodes can encourage tilting of the terminal groups in response to the accumulation of charge at the electrode. This is possible due to the inefficient packing of cysteine monolayers which allows the immobilized cysteine chains greater freedom of movement.

There are also literature precedents that support the claim that potential induced reorientation occurs at potentials relative to the PZC. Brolo and coworkers report SERS data that demonstrate the potential induced reorientation of L-cysteine monolayers assembled on gold[105]. They report the appearance of carboxylate bands at potentials positive of -0.650 mV resulting from the attraction of chloride counterions to the surface which attract protonated amine groups

to the surface causing the carboxylate groups to extend out. At potentials negative of -0.650 mV, the chloride ions are expelled from the surface resulting in the reorientation of the amine group where it points away from the surface. A more explicit study of the potential dependent orientation of cysteine monolayers is reported by Zhang et al.[107] These authors report that scanning tunneling microscopy (STM) images of homocysteine monolayers assembled on gold at potentials near the PZC show large, highly ordered domains that disappear at potentials positive and negative of the PZC. The authors attribute this to the tilting of the carboxylate and protonated amine groups in response to the electric field produced from applied potential. This allows ionic self assembly of anionic polyelectrolytes to occur at the charged amine groups that extend away from the substrate. The charge-transfer resistance values for cysteine monolayers exposed to PSS results in electrostatic repulsion between the PSS layer and the anionic redox probe in solution. The increased distance between the surface and the redox probe decreases electron transfer resulting in higher charge-transfer resistance values.

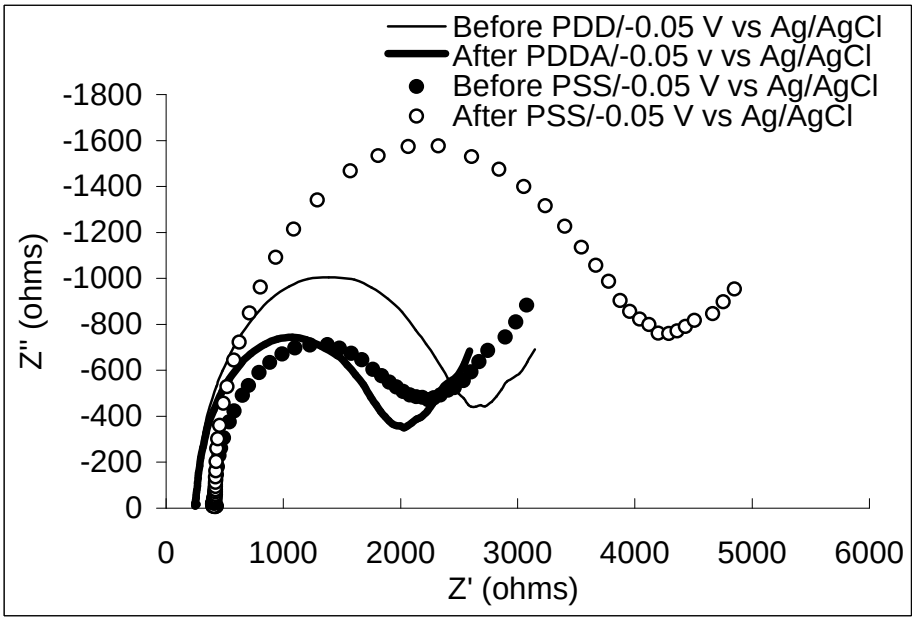

Figure 59: Nyquist plots of cysteine monolayers before and after PDDA and PSS while exposed to -0.5 V vs Ag/AgCl (E> PZC). Impedance measurements were conducted in 0.005 mol·L^{-1}[Fe(CN)$_6$]$^{3-/4-}$ containing 0.1 mol·L^{-1} KCl at a potential of 0.2 V vs Ag/AgCl.

Table 13: Charge-transfer resistance values for cysteine monolayers exposed to PDDA and PSS at -0.05 V vs Ag/AgCl.

	PDDA (Ω)	PSS (Ω)
Before Polyelectrolyte Exposure	1530±686	1760
After Polyelectrolyte Exposure	1390+736	3560
ΔR	140	1800

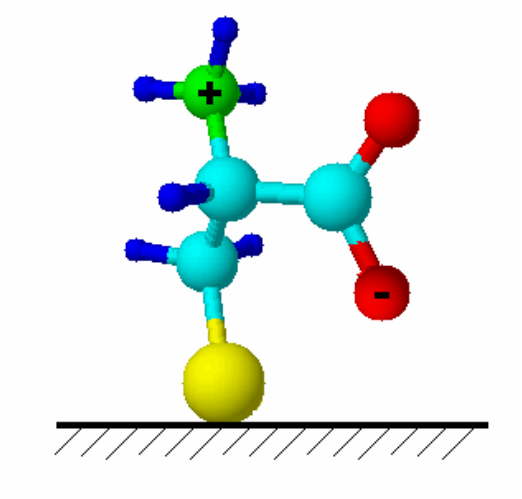

Figure 60: Confirmation of cysteine under the influence of -0.05 V vs Ag/AgCl (E > PZC).

Figure 61 shows Nyquist plots for cysteine modified electrodes before and after application of potential negative of the PZC (-0.40 V vs Ag/AgCl) while exposed to PDDA and PSS in phosphate buffer solutions. At this potential, the Nyquist semicircle diameters for cysteine monolayers exposed to PDDA show a significant decrease while Nyquist semicircle diameters for cysteine monolayers exposed to PSS in phosphate buffer solutions at this potential show minimal change. These trends are also apparent when comparing charge-transfer resistances of modified electrodes exposed to these polyelectrolytes at this potential (Table 14). The charge-transfer resistance values show a 1,100 ohm decrease in charge-transfer resistance for modified electrodes immersed in phosphate buffer solutions containing PDDA at -0.40 V vs Ag/AgCl. For modified electrodes immersed in phosphate buffer solutions containing PSS a few hundred ohm change in charge-transfer resistance is observed. This behavior contradicted what was expected for ionic self assembly at potentials negative of the PZC. At potentials negative of the PZC, it was expected for cations to accumulate at the surface to protonate the amine groups and drive the ionic self assembly of PSS. However, the charge-transfer resistance values listed

in Table 12 clearly show minimal change in charge-transfer resistances for cysteine modified electrodes exposed to PSS at potentials negative of the PZC.

The behavior of the impedance data at potentials negative of the PZC also suggests that a conformational change occurs. Application of potentials more negative than the PZC introduces excess negative charges that attract the protonated amine groups toward the surface while repelling the negatively charged carboxylate groups (Figure 62). This promotes ionic self assembly of cationic polyelectrolytes to carboxylate groups that are extending out. The charge-transfer resistance values for cysteine monolayers exposed to PDDA at this potential support this claim. Attachment of PDDA leads to electrostatic attraction between the PDDA layer and the anionic redox probe in solution. This decreased distance between the redox probe and the surface increases electron transfer resulting in lower charge-transfer resistance values.

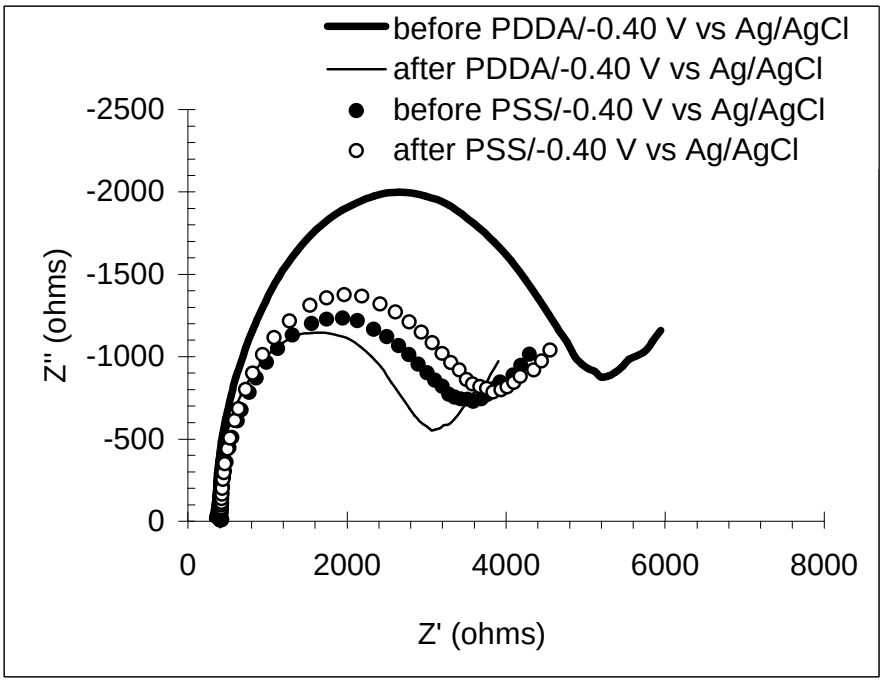

Figure 61: Nyquist plots of cysteine monolayers before and after PDDA and PSS in at -0.40V (E< PZC). Impedance measurements were conducted in 0.005 mol·L^{-1}[Fe(CN)$_6$]$^{3-/4-}$ containing 0.1 mol·L^{-1} KCl at a potential of 0.2 V vs Ag/AgCl.

Table 14: Charge-transfer resistance values for cysteine monolayers exposed to PDDA and PSS at -0.40 V vs Ag/AgCl.

	PDDA (Ω)	PSS (Ω)
Before Polyelectrolyte Exposure	4300±810	3030±142
After Polyelectrolyte Exposure	3200±470	3360±192
ΔR	1,100	330

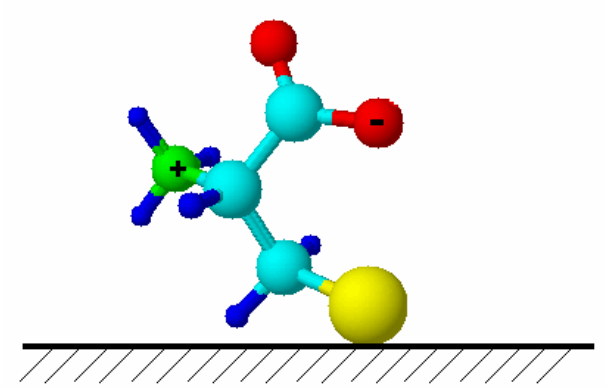

Figure 62: Confirmation of cysteine under the influence of -0.40 V vs Ag/AgCl (E < PZC).

QCM measurements were also used to quantify the extent of polyelectrolyte deposition to the surface of cysteine monolayers under the influence of applied potential. Average frequency changes and corresponding masses for cysteine modified QCM plates exposed to PDDA and PSS at potential more positive than the PZC (-0.05 V vs Ag/AgCl) are listed in Table 15. This data shows trends that are consistent with the impedance analysis of the applied potential deposition of polyelectrolytes at this potential. However, as shown in Table 16, at potential more negative than the PZC (-0.40 V vs Ag/AgCl), more PDDA is deposited onto the surface than PSS. Like the impedance results, this QCM data suggests that application of potentials to cysteine modified electrodes results in a change in the conformation of the terminal groups of cysteine monolayers. Cysteine exists as a zwitterion at the pH values used in the applied potential experiments, which means that both surface groups are charged. The results of the impedance and QCM analyses of applied potential deposition suggests that potentials more positive than the PZC result in the reorientation of the terminal region of the cysteine monolayer in a way that extends the protonated amine group away from the electrode due to the excess positive charge. The greater mass of PSS deposited at this potential supports the fact that ionic self assembly of anionic polyelectrolytes is encouraged. At potentials more negative than the PZC, the QCM data suggests that the carboxylate group points away from the surface due to excess negative charges. The extended carboxylate group encourages the deposition of cationic polyelectrolytes, as is evident from the greater mass of PDDA that is deposited at this potential

Table 15: ΔF mass approximations of polyelectrolytes deposited at -0.05 V vs Ag/AgCl.

	ΔHz (F)	Mass (ng)
PDDA	1.4±0.6	20±6
PSS	5.3±0.4	61±5

Table 16: ΔF and mass approximations of polyelectrolytes deposited at -0.40 V vs Ag/AgCl.

	ΔHz (F)	Mass (ng)
PDDA	4.73±.6	82±18
PSS	0.9±0.5	16±4

4.5 Summary

The applied potential experiments for cysteine monolayers produced results that were contrary to what was observed with 3-MPA and 11-MUA monolayers. In the case of 3-MPA and 11-MUA monolayers, application of potentials more positive than the PZC promoted the accumulation of anionic counterions that encouraged carboxylic acid group deprotonation producing an anionic surface for the ionic self assembly of cationic PDDA; this was confirmed with an 1,160 Ω decrease in charge-transfer resistance and an increase in PDDA mass deposited at potentials positive of the PZC. Application of -0.05 V vs Ag/AgCl, a potential positive of the PZC, to cysteine modified electrodes resulted in an 1,800 Ω increase in charge-transfer resistance after exposure to PSS, a response believed to be due to electrostatic repulsion between the PSS layer and the anionic redox probe. This increased distance between the redox probe and the monolayer resulted in a decrease in electron transfer which led to an increase in charge-transfer resistance. QCM analyses mirrored these results; a greater mass estimate for PSS was obtained at this potential than for PDDA. At a potential negative of the PZC (-0.40 V vs Ag/AgCl), a 1,100 Ω decrease in charge-transfer resistance values was observed after the modified electrodes were exposed to PDDA solutions. This is a result of the deposition of PDDA at this potential and subsequent electrostatic attraction between the cationic polyelectrolyte and the anionic redox probe. The decreased distance resulted in increased electron transfer and a decrease in charge-transfer resistance. Similarly, QCM measurements show more PDDA deposited on the surface of cysteine modified quartz plates at this potential than PSS.

The behavior of the impedance and QCM data can be attributed to the reorientation of the terminal carboxylate and protonated amine groups in response to applied potential. At a

potential more positive than the PZC (-0.05 V vs Ag/AgCl), the excess positive charge repels the protonated amine group promoting ionic self assembly of anionic polyelectrolytes. At potentials negative of the PZC (-0.40 V vs Ag/AgCl), the carboxylate groups are pointed away from the electrode surface in response to the excess negative charges applied to the electrode. The extension of the carboxylate group at this potential encourages ionic self assembly of cationic polyelectrolytes.

Chapter 5. Imaging the Surface Charge of 3-MPA and 11-MUA Monolayers Assembled on Gold Using Scanning Electrochemical Microscopy

5.1 Introduction

Previous chapters describe the use of impedance and QCM measurements to verify the potential-driven deposition of polyelectrolytes. This was accomplished by monitoring either increases or decreases in charge-transfer resistance in response to electrostatic interactions between redox probes in solution and polyelectrolyte layers. QCM measurements were used to confirm polyelectrolyte deposition via applied potential by monitoring mass increases of modified electrodes after being energized with potentials relative to the PZC while immersed in phosphate buffer solutions containing polyelectrolytes. Impedance and QCM measurements demonstrated that ionic self assembly can be controlled using applied potential, which was the first major objective of this research. The second objective involves controlling spatial deposition of polyelectrolytes. Prior to attempts at site-directed polyelectrolyte depostion, it was first necessary to determine if site selective surface group ionization could take place. This involved monitoring the charge of functionalized monolayers under the effect of applied potential using scanning electrochemical microscopy (SECM). It was believed that SECM would allow a direct measurement of the surface charge of a specific region of a functionalized monolayer subjected to potentials positive or negative of the PZC.

There are several reports that describe the use of scanning electrochemical microscopy (SECM) to observe the electrostatic interactions between charged surfaces and redox probes. In these reports, SECM is used to monitor feedback currents arising from interactions between the terminal ionizable groups and redox probes. Based on the nature of the electrostatic interaction (repulsive vs attraction), the feedback current generated at the SECM tip held tens of micrometers from the surface either increases or decreases. Kurulugama and coworkers report using electrostatic interactions between neurons and the hexamine ruthenium (III) chloride redox probe to image neurons with SECM[108]. Both Turcu[91] and Palchetti[90] report the use of SECM to image hybridized DNA strands by monitoring the electrostatic repulsion between the negatively

charged redox probe, potassium ferrocyanide, and phosphate groups along the backbone of the DNA sample. Ye and coworkers also report the use of SECM to study the surface charge of 4-aminobenzoic acid on a glassy carbon electrode[92]. They show that using $[Ru(NH_3)_6]^{3+}$ and$[Fe(CN)_6]^{3-}$ as a redox probes, they were able to differentiate between the charge state of the protonated and deprotonated forms of carboxylic acid terminated monolayers. Boldt et al.[93] report the using SECM to generate approach curves for SECM tips approaching the surface of 11-mercaptoundecanoic acid in solutions above and below the surface pK_a. Their results show that$[Fe(CN)_6]^{4-}$produces tip current that increases in pH 3 phosphate buffer solution due to the lack of electrostatic interactions between the neutral surface and the redox probe. In pH 6 phosphate buffer solution, tip current shows a decrease due to the electrostatic repulsion between deprotonated surface groups and the anionic redox probe. The aforementioned literature sources report findings that involve monitoring electrostatic interactions between redox probes and charged surfaces. These reports provide evidence that SECM can be used for monitoring of the surface charge of functionalized monolayers under the influence of applied potential. This chapter will report the use of SECM to monitor the surface charge of 3-mercaptopropionic acid and 11-mercaptoundecanoic acid under the influence of applied potential.

5.2 Experimental

Monolayers of 3-MPA and 11-MUA were prepared as described in Section 2.2.1. The modified electrodes were then placed in the SECM cell as illustrated in Figure 22. The solution used for the SECM analysis was 0.005 $mol \cdot L^{-1}$ hexaammine ruthenium chloride ($[Ru(NH_3)_6]Cl_3$) solutions prepared using commercially available 0.05 $mol \cdot L^{-1}$ pH 5 and pH 8 phosphate buffer solutions from VWR scientific. Approximately 20 mL of pH 5 or pH 8 phosphate buffer solutions containing 0.005 $mol \cdot L^{-1}$ $[Ru(NH_3)_6]Cl_3$ were placed in the SECM cell along with the Ag/AgCl reference electrode and SECM tip as shown in Figure 22. An EI-400 FCV model bipotentiostat manufactured by Cypress Systems (Lawrence, KS) was used to apply the appropriate potentials to the SECM tip and the modified gold disk electrode.

While in the 0.05 mol·L^{-1} pH 5 phosphate buffer solution containing 0.005 mol·L^{-1} $[Ru(NH_3)_6]^{3+}$, a potential of -0.500 V vs Ag/AgCl was applied to the SECM tip to facilitate reduction of the $[Ru(NH_3)_6]^{3+}$ redox probe. At the start of the imaging process, the modified electrode was energized with a potential near the PZC, -0.15 V vs Ag/AgCl. Control of the SECM tip over the modified electrode surface was controlled with Z600 actuators from Thorlabs, Inc. The actuators were controlled with a locally written Visual BASIC program. The program was also used to conduct a 30 µm × 30 µm scan the over the functionalized electrode while the SECM tip was maintained at a constant height above the substrate surface (~10 µm). During this scan, the bipotentiostat was set to record the current produced by the reduction of the redox probe directly under the SECM tip; these current measurements were transferred to a PC where the current values were stored in an Excel spreadsheet. Halfway during the scan, the potential of the modified electrode was stepped to a potential more positive than the PZC (-0.05 V vs Ag/AgCl) for approximately 15 seconds and stepped back down to a potential near the PZC (-0.15 V vs Ag/AgCl). After the 30 µm × 30 µm scan was complete, the SECM tip was moved to its original position. A second 30 µm × 30 µm scan commenced; halfway through the scan the potential was stepped to a value negative of the PZC (-0.250 V vs Ag/AgCl) for approximately 15 seconds and stepped back to a potential near the PZC. The experiments were repeated using a 5 mM $[Ru(NH_3)_6]^{3+}$ solution prepared with pH 8 phosphate buffer solution.

5.3 Surface Charge Imaging at E > PZC and E < PZC

In Figures 63a and 63b, there is a conspicuous hill in the middle of the image believed to be produced as a result of stepping the potential to values positive of the PZC. The appearance of the hill is evidence of the deprotonation of the carboxylic acid groups in response to stepping the potential of the modified electrode to values positive of the PZC. The current profiles illustrated in Figures 64a and 64b also show an increase in current during the potential step. This behavior is expected due to surface group deprotonation directly under the SECM tip. This encourages electrostatic attraction between the deprotonated acid groups and the cationic redox probe in

solution. The increased concentration of the redox probe underneath the SECM tip results in increased electron transfer resulting in a current increase that generated the hills in the SECM images. During the potential steps to values more positive than the PZC, and back to values near the PZC, the change in current is gradual in both cases. There is no instantaneous increase or decrease in current following the potential steps. This suggests there are two possible electrostatic migration processes that are taking place. Stepping potentials more positive than the PZC results in the accumulation of phosphate anions in solution that take time to migrate to the region directly below the SECM tip where they initiate carboxylic acid group deprotonation. The second process involves migration of the cationic redox probe from the bulk to the deprotonated acid groups directly below the SECM tip. The gradual decrease in the potential step to a value positive of the PZC and the gradual decrease in current following a potential step back to a value near the PZC provides evidence that the change in current is governed by diffusional effects.

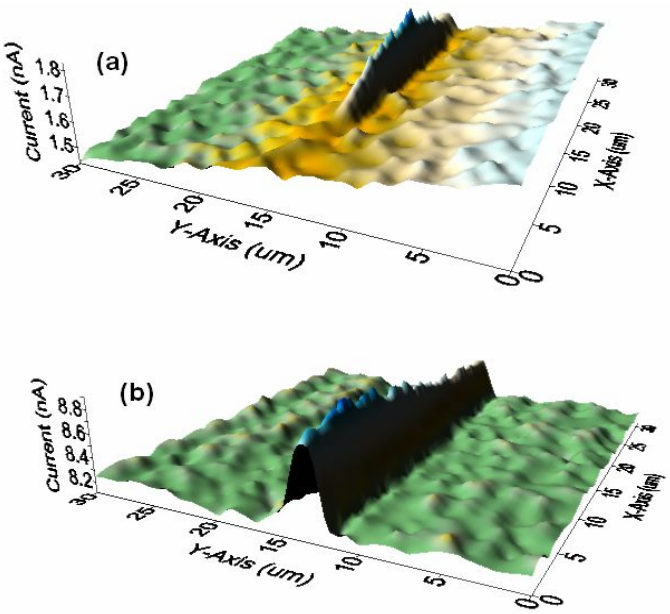

Figure 63: 3-D surface maps for 3-MPA (a) and 11-MUA (b) monolayers exposed to -0.05 V (E > PZC) halfway through the SECM scans. Images were conducted in 0.005 mol·L^{-1} $[Ru(NH_3)_6]^{3+}$ prepared with pH 5 phosphate buffer solution.

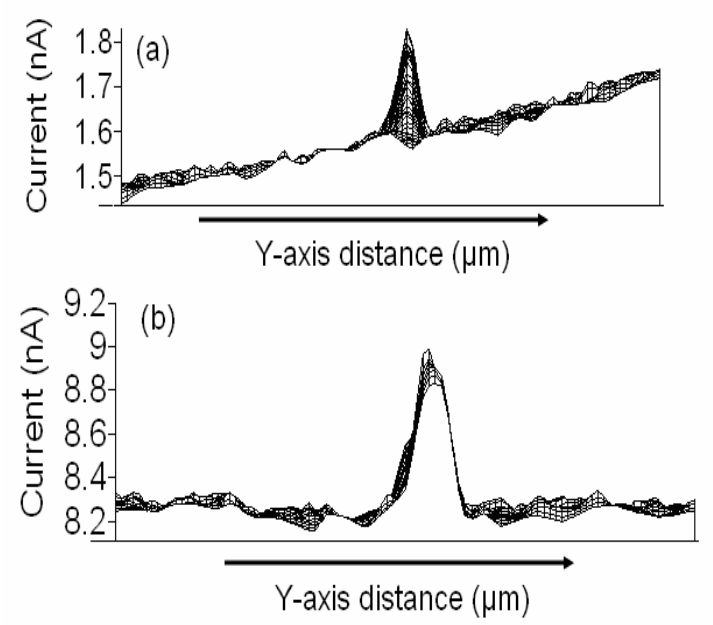

Figure 64: Current profiles of 3-MPA (a) and 11-MUA (b) after potential is stepped to -0.05 V vs Ag/AgCl (E > PZC). Images were conducted in 0.005 mol·L-1 $[Ru(NH_3)_6]^{3+}$ prepared with pH 5 phosphate buffer solution.

Similar experiments were conducted with a potential step to values negative of the PZC. Figures 65a and 65b illustrate that application of potentials negative of the PZC results in the appearance of an inverted hill in the SECM images for 3-MPA and 11-MUA respectively. Current profiles for 3-MPA (Figure 66a) and 11-MUA (Figure 66b) show current decreases at this potential step. This is behavior is attributed to the accumulation of cations directly under the SECM tip. This neutralizes any slight dissociation produced by carboxylic acid groups, minimizing electrostatic attraction between the surface of the monolayer directly underneath the SECM tip and the cationic redox probe, this decreased redox probe concentration produced lower current. These images also show that there is no instantaneous increase or decrease in current following the potential steps suggesting that ion migration in response to an electric field occurs at this potential step also. Stepping potentials more negative than the PZC results in the accumulation of cations that take time to migrate to the region directly below the SECM tip where they protonate the carboxylic acid groups to produce a neutral surface. The neutral surface allows the redox probe to freely diffuse between the space below the SECM tip and the bulk due to the lack of electrostatic interactions; this results in a decrease in current.

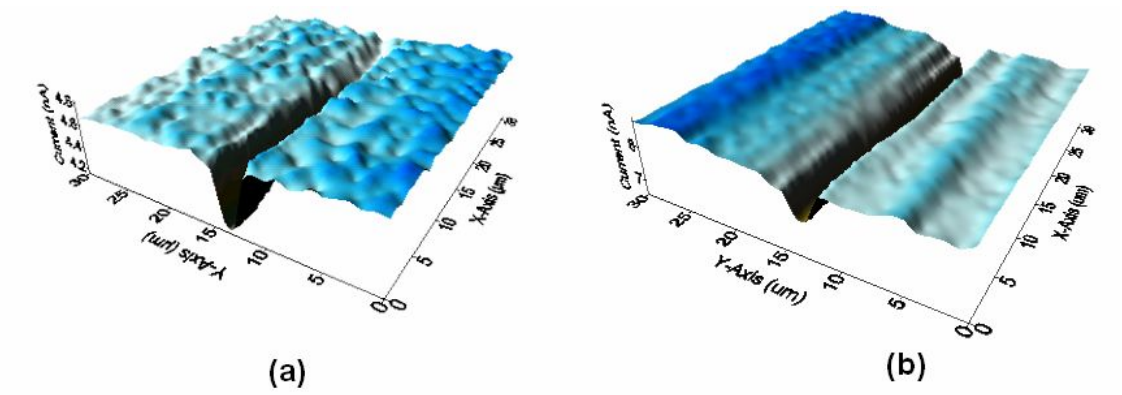

Figure 65: 3-D surface maps for 3-MPA (a) and 11-MUA (b) monolayers exposed to -0.17 V vs Ag/AgCl (E < PZC) halfway through the SECM scan. Images were conducted in 0.005 mol·L^{-1} $[Ru(NH_3)_6]^{3+}$ prepared with pH 5 phosphate buffer solution.

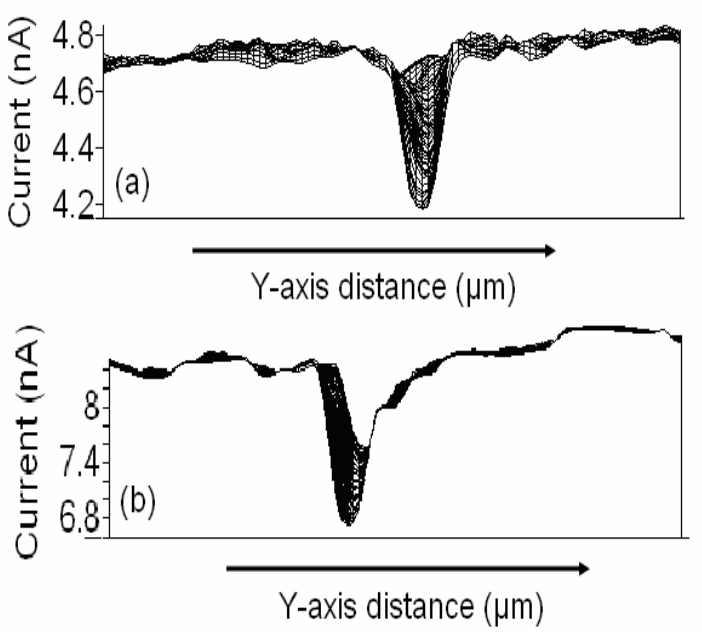

Figure 66: Current profiles of MPA (a) and 11-MUA (b) after potential is stepped to -0.17 V vs Ag/AgCl (E < PZC). Images were conducted in 0.005 mol·L^{-1} $[Ru(NH_3)_6]^{3+}$ prepared with pH 5 phosphate buffer solution.

Imaging of 3-MPA and 11-MUA monolayers under the influence of applied potential was also repeated in pH 8 phosphate buffer solution. At this pH, the surface confined carboxylic acid groups are deprotonated; therefore, application of potentials positive of the PZC should result in no change in current during SECM imaging. While immersed in pH 8 phosphate buffer solution containing 0.005 mol·L^{-1} $[Ru(NH_3)_6]^{3+}$, modified electrodes for 3-MPA (Figure 67a) and 11-MUA (Figure 67b) produced no hill during SECM imaging when the potential was stepped to a potential more positive than the PZC. Current profiles for 3-MPA (Figure 68a) and 11-MUA

(Figure 68b) show minimal change in current when potential of the modified electrodes are stepped to potentials positive of the PZC.

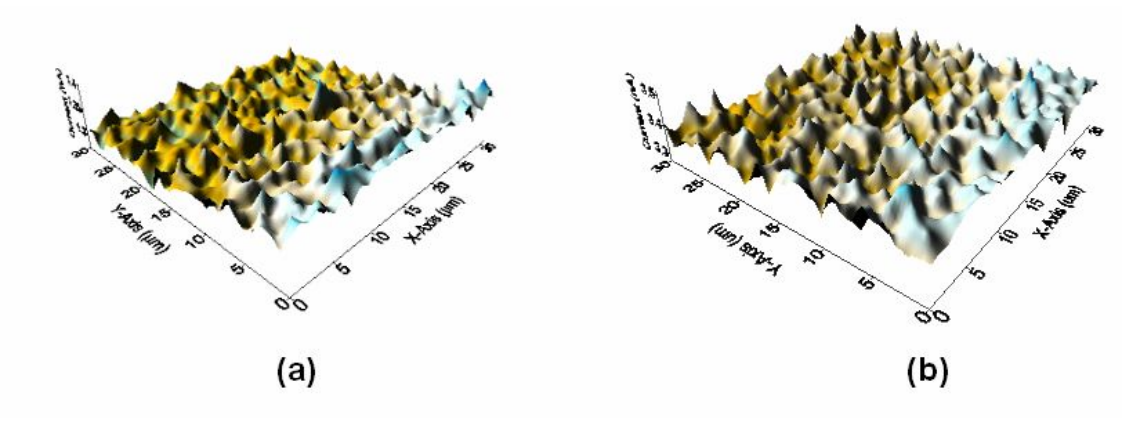

Figure 67: 3-D surface maps for 3-MPA (a) and 11-MUA (b) monolayers exposed to -0.05 V vs Ag/AgCl (E > PZC). Images were conducted in 0.005 mol·L^{-1} $[Ru(NH_3)_6]^{3+}$ prepared with pH 8 phosphate buffer solution.

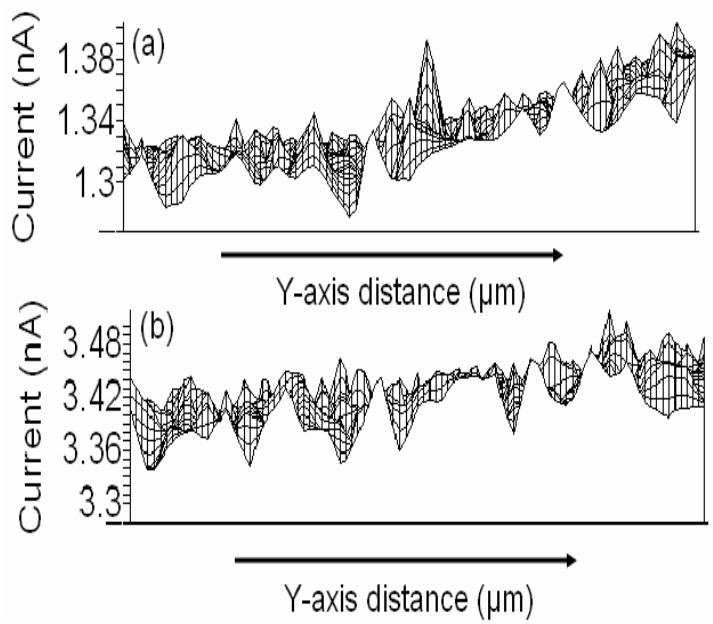

Figure 68: Current profile of MPA (a) and 11-MUA (b) after potential is stepped to -0.17 V vs Ag/AgCl (E < PZC). Images were conducted in 0.005 mol·L^{-1} $[Ru(NH_3)_6]^{3+}$ prepared with pH 5 phosphate buffer solution.

A second SECM scan was conducted on 3-MPA and 11-MUA monolayers in pH 8 phosphate buffer solution containing 0.005 mol·L^{-1} $[Ru(NH_3)_6]^{3+}$ where the potential was stepped to a value negative of the PZC (-0.250 V vs Ag/AgCl). Figure 69a (3-MPA) and Figure 69b (11-MUA) show the appearance of an inverted hill when the potential of the modified electrode is stepped to a potential negative of the PZC halfway through the SECM scan. Current

profiles for 3-MPA (Figure 70a) and 11-MUA (Figure 70b) also show a gradual decrease in current when potential is stepped negative of the PZC. This behavior is attributed to the accumulation of cations to the interface which protonate the carboxylate groups making them neutral. This decreases the electrostatic interaction between the surface and the redox probe in solution; as a result, there is lower concentration of redox probe directly under the tip. The decreased concentration of redox probe directly under the tip encourages a situation where electron transfer is diminished; the end result is a decrease in current registered by the SECM tip.

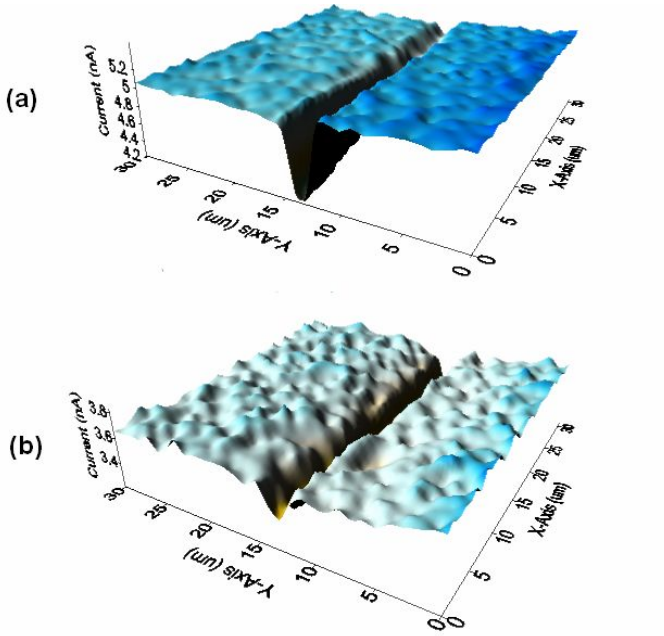

Figure 69: 3-D surface maps for 3-MPA (a) and 11-MUA (b) monolayers exposed to -0.250 V vs Ag/AgCl (E < PZC) . Images were conducted in 0.005 mol·L^{-1} $[Ru(NH_3)_6]^{3+}$ prepared with pH 8 phosphate buffer solution.

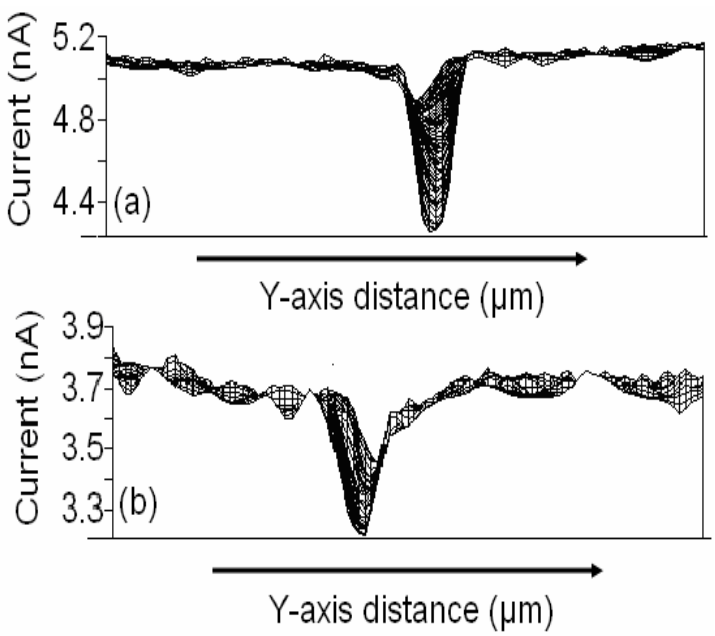

Figure 70: Current profile of 3-MPA (a) and 11-MUA (b) monolayers exposed to -0.250 V vs Ag/AgCl and -0.17 V vs Ag/AgCl respectively. Images were conducted in 0.005 mol·L^{-1} $[Ru(NH_3)_6]^{3+}$ prepared with pH 8 phosphate buffer solution.

5.4 Summary

Unlike the impedance and QCM measurements of potential-driven deposition of polyelectrolytes, scanning electrochemical microscopy allows a direct measurement of the effect that applied potentials, positive and negative of the PZC, have on the surface charge of carboxylic acid terminated monolayers. Substantial changes in charge-transfer resistance served as confirmation of the deposition of polyelectrolytes based on electrostatic interactions between the deposited surface and the redox probe in solution. QCM measurements provided indirect confirmation of potential-driven polylelectrolyte deposition from the increase in mass of modified plates energized with certain potentials while immersed in polyelectrolyte/phosphate buffer solutions. Imaging using scanning electrochemical microscopy allows direct observation of the effects of applied potential on the surface charge of functionalized monolayers due to the presence or absence of electrostatic interactions between the terminal carboxylic acid groups and the cationic redox probe, $[Ru(NH_3)_6]^{3+}$.

While in phosphate buffer solutions with pH values below their surface pK_a values, the majority of the terminal acid groups are fully protonated, yielding a surface that is neutral.

Application of potentials more positive than the potential of zero charge results in the accumulation of phosphate anions that act as conjugate bases resulting in the deprotonation of acid groups directly below the SECM tip. The deprotonation of the acid groups encourages electrostatic attraction between the resulting carboxylate groups and the cationic redox probe in solution. The increased concentration of the redox probe underneath the SECM tip increases electron transfer producing an increase the current registered by the SECM tip. The converse is true when the potential of 3-MPA and 11-MUA monolayers are stepped to potentials below the PZC. The excess negative charges discourage the accumulation of phosphate anions to the surface and promote the attraction of cations to the region of the monolayer directly below the SECM tip. This ensures the the neutrality of the carboxylic acid groups. The lack of electrostatic interaction between the monolayer surface directly underneath the SECM tip and the cationic redox probe leads to a decrease in the concentration of the redox probe at the surface. This decreased concentration results in minimized electron transfer producing lower current detected by the SECM tip. The suggested behavior of the current directly underneath the redox probe at potentials positive and negative of the PZC, in response to the potential-driven control of surface charge, is justified with Equation 5. Where the current, i, is directly proportional to the product of the moles of electrons transferred (n), Faraday's constant (F), the diffusion coefficient of the redox probe (D), the concentration of redox probe in solution (C), and the area of the electrode surface (a)[11].

$$i = 4nFDCa \quad (5)$$

This equation describes steady state current that exists underneath the SECM tip. Under steady state conditions, the limiting current is under the control of diffusion controlled mass transfer from the bulk solution to the region directly underneath the SECM tip[85]. Therefore the increase and decrease of the concentration of the redox probe in response to electrostatic interactions induced by potential-driven manipulation of surface charge leads to significant

changes in current that are apparent by the presence of upright or inverted hills in the SECM image.

Similar experiments conducted in pH 8 phosphate buffer solutions containing 0.005 mol·L^{-1} $[Ru(NH_3)_6]^{3+}$ provide further evidence of the influence of potential on the surface charge of carboxylic acid terminated monolayers. The absence of a hill image in the SECM images of 3-MPA and 11-MUA monolayers when potential is stepped to values positive of the PZC while immersed in pH 8 phosphate buffer solutions is due to the deprotonation of the terminal acid groups. Stepping the potential positive of the PZC has no effect on carboxylic acid terminated surfaces that are already deprotonated. Therefore, the SECM images contains random current fluctuations the occur due to uninhibited diffusion of the redox probe. However, stepping the potential of modified electrodes immersed in alkaline buffer solution to potentials negative of the PZC results in the appearance of an inverted hill in response to a drop in current due to the decreased concentration of the cationic redox probe directly underneath the SECM tip. When potential is stepped to a value negative of the PZC, cations are attracted to the surface and promote the protonation of the surface groups minimizing the electrostatic interaction between the surface and the redox probe. The result is a decrease in current which leads to the appearance of the inverted hill in the SECM image.

The current profiles of each SECM experiment illustrate that the current behaves in the similar manner each time at the onset of the potential step. While in pH 5 phosphate buffer solutions, there is no instantaneous increase or decrease in current. This is expected behavior because the counterions in solution have to migrate from the bulk to the region of the monolayer directly underneath the SECM tip in response to the potential-driven deprotonation of surface groups. In addition, the cationic redox probe has to migrate to the area directly underneath the SECM tip due to the deprotonated carboxylic acid groups.

The results of the SECM characterization of the potential-driven modulation of surface charge provide further evidence that the potential-driven ionic self assembly of polyelectrolytes

observed with impedance and QCM measurements is likely due to the change in the interfacial pH of the monolayers in response to the application of potentials positive of the PZC. In addition, these SECM images provided evidence that the local pH of a specified region of a functionalized monolayer can be altered making it possible for the site-directed deposition of polyelectrolytes.

Chapter 6. Site-Selective Deposition of Polyelectrolytes Using Scanning Electrochemical Microscopy

6.1 Introduction

Previously, it was shown that scanning electrochemical microscopy could be used to monitor the surface charge of 3-MPA and 11-MUA monolayers under the influence of potentials positive and negative of the PZC. The results from these experiments provided evidence that potential induced modulation of interfacial pH directly under the SECM tip is possible. This laid the framework for the second objective of the dissertation research, site-directed deposition of polyelectrolytes. There are reports that describe microfabrication of monolayer surfaces using scanning probe microscopy (SPM) techniques. Some of the earliest attempts at microfabcrication of monolayer surfaces involves site selective desorption using SECM[85, 88]. Wittstock and coworkers report the desorption of holes in dodecylthiolate monolayers and the formation of a simple "L" pattern desorbed in the monolayer using SECM[88]. Roach also reports the used of SECM to desorb patterns in decanethiol monolayers[85]. Site-selective reductive desorption involves application of a negative overpotential to the modified substrate while using the SECM tip to localize the electric field to facilitate thiol desorption (Figure 17) in a specific region of the monolayer.

In addition to surface patterning via electrochemical desorption, SECM has been used to pattern interfaces by depositing conductive polymers on substrates. Polyaniline, polypyrrole, and polythiopene are the most commonly used polymers for this process because they are easily polymerized with applied potential. Kranz et al. report successful fabrication of polypyrrole towers on gold electrodes using SECM[83]. They report that these microscale 3-D polymer structures can be used as templates for the immobilization of elements with biological recognition capabilities. Wuu et al.[82] report the use of a thin Nafion film containing protonated aniline sandwiched between the SECM tip and a metallic substrate. A constant current was applied to the tip and the substrate in order to promote proton exchange and initiate polymerization at the electrode surface. Marck and coworkers report the use of SECM to deposit

polythiopene micropatters in an aqueous solution[81]. The aforementioned SECM driven polymer depositions[81-83] are all examples of microfabrication in the "direct mode"; in this mode, the SECM tip acts as a microscale auxiliary electrode for the purpose of confining the current to a small area on a substrate[53].

An alternative method of SECM patterning involves the "microreagent mode". In this mode, the SECM tip electrically generates species used in the patterning process[53]. This technique typically involves creating a pH gradient by the reduction of hydrogen ions. Shohat and Mandler[87] report successful deposition of nickel hydroxide structures on the surface of platinum electrodes using SECM in microreagent mode. They were able to consume protons in the small space between the SECM tip and the platinum surface to increase the pH at the surface; the platinum also acted as a catalyst for the reaction. The incorporation of nickel sulfate in the reaction vessel led to the formation of nickel hydroxide due to the local increase in pH resulting from hydrogen ion consumption. Zhou and Wipf describe the use of SECM in the microreagent mode to deposit polyaniline on gold, platinum, and carbon electrodes[53]. Positioning the SECM tip close to the electrode surface and applying the appropriate potential facilitated the reduction of protons and led to an increase in local pH resulting in the formation of polyaniline features[53]. Potential induced change in local pH for the purpose of polymer deposition as previously described[53, 81, 87] is the basis behind the work presented in this chapter.

6.2 Experimental

Monolayers of 3-MPA, 11-MUA, and cysteine were prepared as described in Section 2.6.1. The modified electrodes were then placed in the SECM cell as illustrated in Figure 22. Phosphate buffer solutions (0.05 mol·L^{-1}), commercially available from VWR scientific, with a pH of 5 were used in the site-selective deposition experiments. Two types of solutions were used for imaging purposes; 0.005 mol·L^{-1} $[Ru(NH_3)_6]^{3+}$ and 0.005 mol·L^{-1}$[Fe(CN)_6]^{4-}$ both prepared with 0.05 mol·L^{-1} pH 5 phosphate buffer solutions. Hexaamine ruthenium (III) chloride ($[Ru(NH_3)_6]Cl_3$) and potassium ferrocyanide ($K_4Fe(CN_6)$) were purchased from Aldrich and

Fisher respectively and used without further purification. After the modified electrode was placed in the SECM cell, the cell was filled with approximately 20 mL of 0.05 mol·L^{-1} pH 5 phosphate buffer solution containing 1.08×10^{-6} mol·L^{-1} PDDA. Only three electrodes were used in the SECM deposition experiments, the Ag/AgCl reference electrode, the modified gold disk working electrode, and the SECM tip, which in this case, was used as the auxiliary electrode. The potential of the modified working electrode was controlled using an EI-400 FCV bipotentiostat manufactured by Cypress Systems (Lawrence, KS).

Initial applied potential deposition experiments attempted to produce simple geometric patterns such as squares. This involved placing the modified electrode in the SECM cell and filling the cell with 1.08×10^{-6} mol·L^{-1} PDDA in 0.05 mol·L^{-1} pH 5 phosphate buffer solution. The SECM tip was then brought close to the electrode surface using a locally written Visual BASIC program until the current overload LED on the biopotentiostat was activated, indicating that the SECM tip was too close to the surface. The tip was vertically moved away from the surface in 0.5 µm increments in until the LED was extinguished. The SECM tip was laterally moved in 75 µm increments to produce a 300 µm × 300 µm square as shown in Figure 71. After each incremental move, the potential of the modified working electrode was stepped to a potential positive of the PZC (~-0.05 V vs Ag/AgCl) and held for approximately 5 seconds and stepped back to a potential more negative of the PZC.

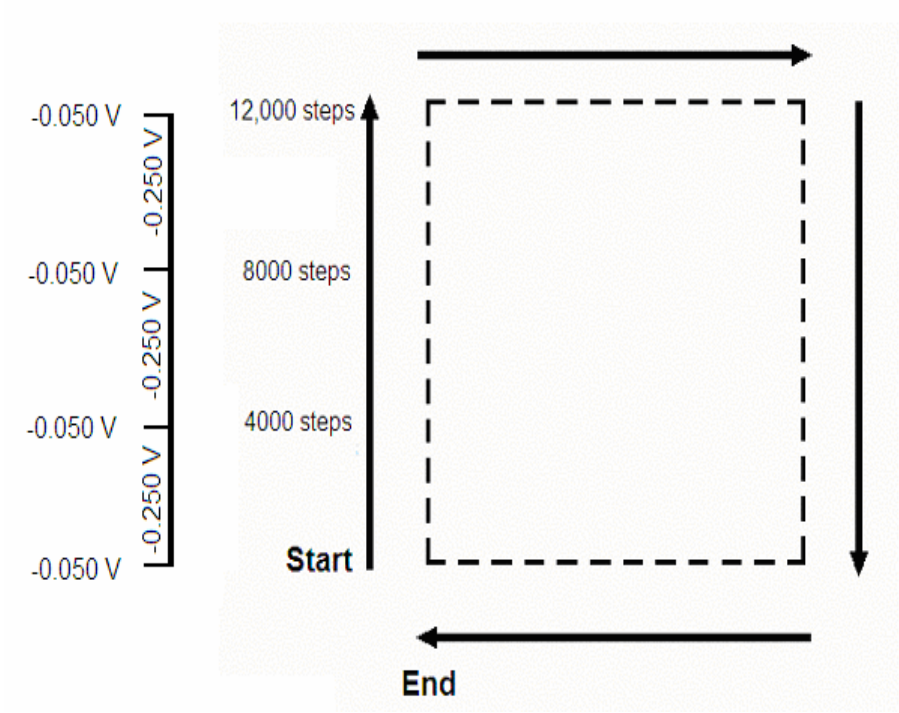

Figure 71: SECM polyelectrolyte deposition scheme.

An additional deposition experiment involved making polyelectrolyte spots on the monolayer surface (Figure 72). Once again, this involved bringing the SECM tip close to the electrode surface until the LED overload indicator light was activated. The tip was moved away from the surface vertically in ~0.5 µm steps until the overload LED was extinguished. The potential of the working electrode was then stepped to a potential more positive than the PZC (~-0.05 V vs Ag/AgCl) and held for 1-3 minutes. When cysteine monolayers were used, the potential was stepped to -0.40 V vs Ag/AgCl. After holding the potential positive of the PZC (E< PZC for cysteine), the potential was stepped to a potential much negative than the PZC (-0.250 V vs Ag/AgCl) and the SECM tip was moved vertically several microns away from the electrode surface (~75 µm). For cysteine experiments, the potential was stepped to -0.10 V vs Ag/AgCl after polyelectrolyte deposition.

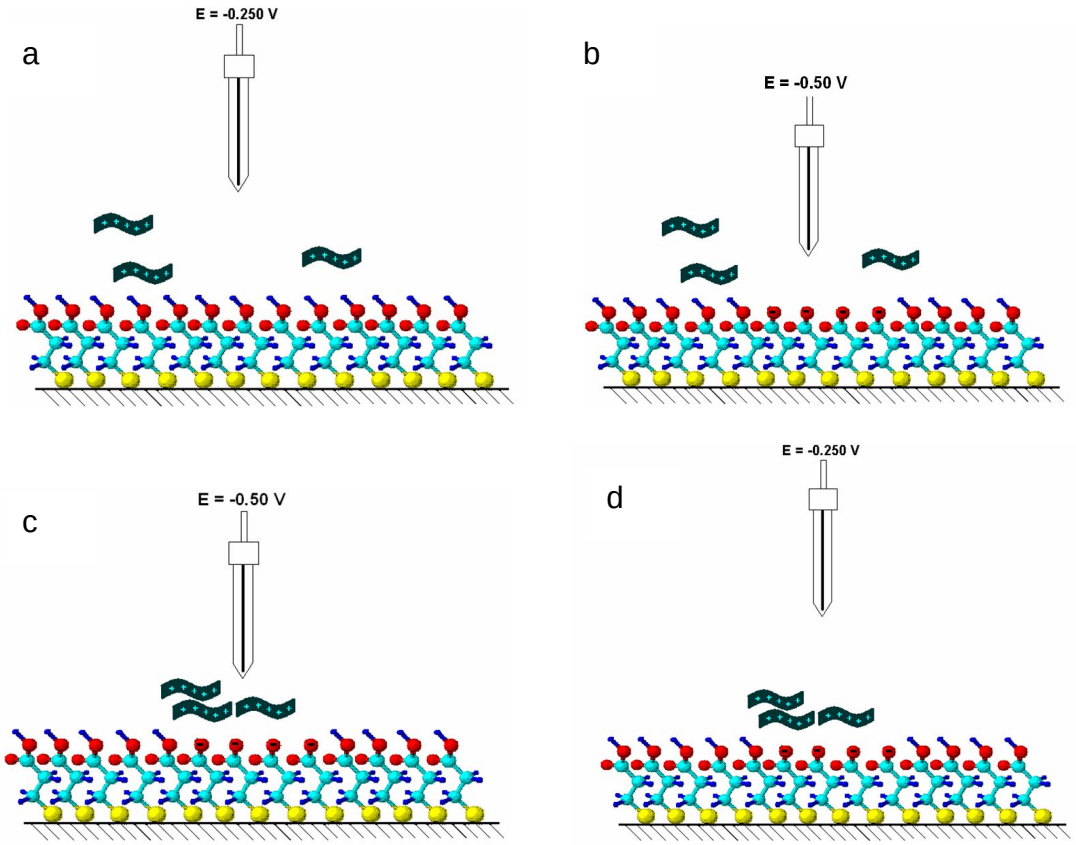

Figure 72: Deposition of a single polyelectrolyte spot onto a functionalized monolayer starts with the SECM tip ~100 µm away from the electrode surface (a). The tip is brought closer to the surface where it is 10 µm away from the monolayer surface and potential. Deposition was conducted in 0.05 mol·L^{-1} pH 5 phosphate buffer solution containing 1.08 × 10^{-6} mol·L^{-1} PDDA.

After the square and spot deposition experiments, the dilute PDDA solution was removed from the SECM cell, it was rinsed with de-ionized water, and the solutions were removed from the cell. After rinsing the cell, approximately 20 mL of 0.005 mol·L^{-1} $[Ru(NH_3)_6]^{3+}$ or 0.005 mol·L^{-1}$[Fe(CN)_6]^{-4}$ in 0.05 mol·L^{-1} pH 5 phosphate buffer solution was added to the cell. The SECM tip was then connected as the second working electrode biased at a potential of -0.500 V vs Ag/AgCl for the reduction of the $[Ru(NH_3)_6]^{3+}$ when the cationic redox probe was used. When the$[Fe(CN)_6]^{-4}$ redox probe was used, the SECM tip was biased at a potential of +0.600 V vs Ag/AgCl for the oxidation of the anionic redox probe. A thin platinum wire embedded in the glass SECM cell was used as the auxiliary electrode during imaging. A locally written Visual BASIC program was used to conduct 800 µm × 800 µm scans for the square and a 300 µm × 300 µm scans for the polyelectrolyte spots. Both SECM imaging experiments were conducted in 2 µm step increments.

Prior to scanning electron microscopy (SEM) imaging, 2 cm × 1 cm gold slides were cleaned by immersing the gold slides in pirhana solution (25% hydrogen peroxide/75% concentrated sulfuric acid) for approximately 20 minutes. After cleaning, the gold slides were rinsed with de-ionized water, dried with a stream of nitrogen, and placed an ethanol solution containing 0.005 $mol \cdot L^{-1}$ 3-MPA or 11-MUA for approximately 24 hours. Hexane was used for cysteine monolayer immobilization. Following thiol immobilization, the modified plates were rinsed with ethanol, deionized water, and dried with a stream of nitrogen. The SECM cell was set up as shown in Figure 22 without solution. A 1 cm × 1 cm strip of double sided foam tape was placed on top of the working electrode and the modified gold plate was secured using the tape. A small circle was drawn on the surface of the modified plate with a felt tip pen for the purpose of locating the PDDA spot during SEM imaging. A small platinum wire was shaped to allow one end to rest over the edge of the SECM cell and the other end to rest on the modified gold plate. This wire was connected to the bipotentiostat for the application of potential to the modified plate. The SECM cell was then filled with 0.05 $mol \cdot L^{-1}$ pH 5 phosphate buffer solution containing 1.08×10^{-6} $mol \cdot L^{-1}$ PDDA. The motor mover program was used to position the SECM tip within the circle drawn on the modified gold plate. The polyelectrolyte spot deposition procedure outlined in Figure 72 was followed. Immediately after polyelectrolyte deposition, the modified plate was removed from the cell, rinsed with deionized water, and dried with a stream of nitrogen. Scanning electron microscopy images of the polyelectrolyte spots deposited on the modified plates were obtained using a Zeiss EVO 40 XVP SEM available in the Virginia-Maryland Regional School of Veterinary Medicine.

6.3 Results and Discussion

SECM was used to generate a local change in interfacial pH on a specific region of a functionalized monolayer. This was accomplished by using the SECM tip as an auxiliary electrode, and moving the tip close to the surface of a functionalized monolayer. While close to

the monolayer surface and biased at a potential positive of the PZC, the SECM tip was moved in order to deposit a polyelectrolyte pattern in the shape of a square. The resulting SECM image of the polyelectrolyte pattern is shown in Figure 73. There is clear evidence of an artificially produced pattern. However, the current at the sides of the square increased. This was contrary to what was expected; it was believed that current would decrease at deposited PDDA domains as a result of electrostatic repulsion between the cationic redox probe and the cationic polyelectrolyte. The current profile shown in Figure 74 also provides further evidence that the unexpected current increase over the sides of the patterned square may not be a result of deposited PDDA. Further analysis of the patterned square involved conducing scanning electron microscopy (SEM) imaging of the pattern. In the SEM image (Figure 75), there is clear evidence of scratching of the substrate.

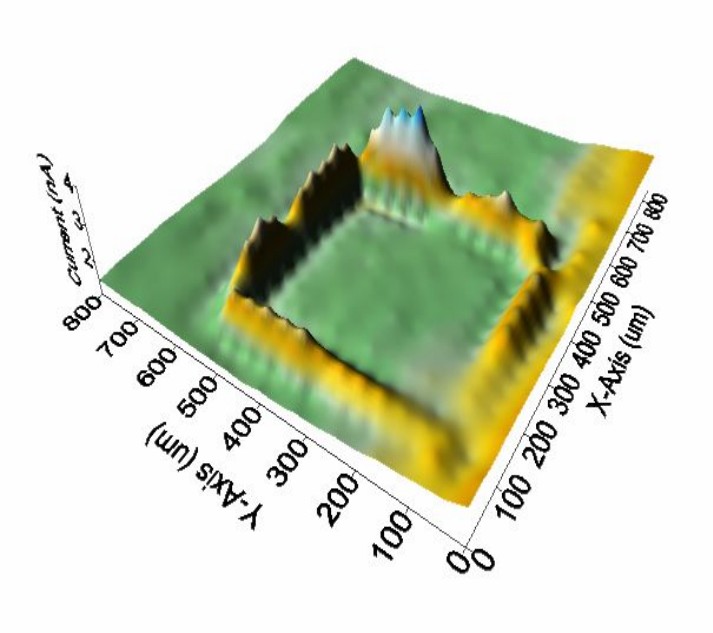

Figure 73: SECM image of patterned 11-MUA monolayer. Image was conducted in 0.005 mol·L^{-1} $[Ru(NH_3)_6]^{3+}$ prepared with 0.05 mol·L^{-1} pH 5 phosphate buffer solution.

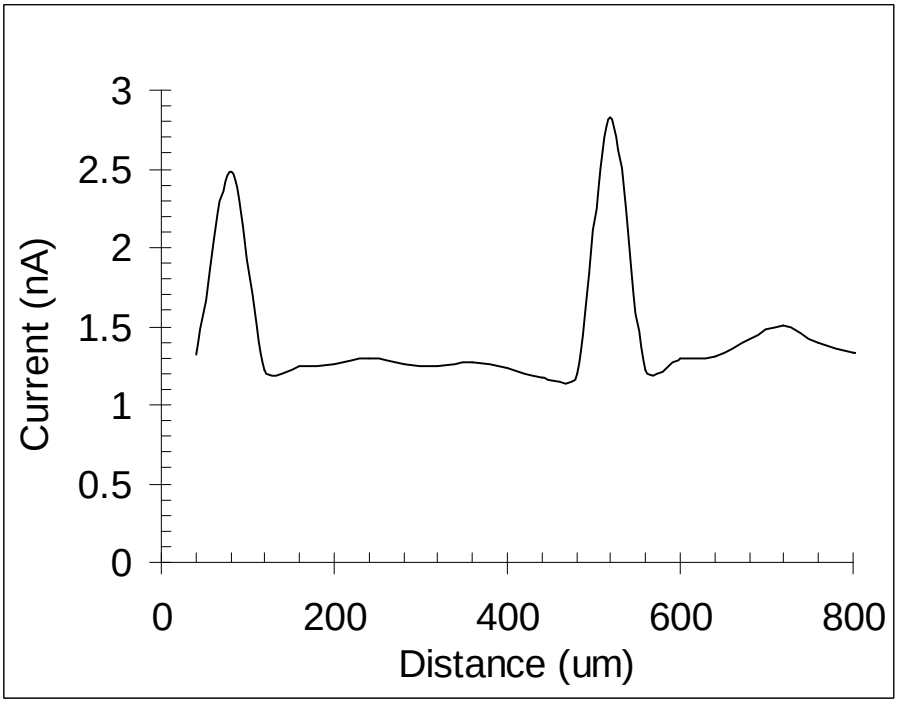

Figure 74: Cross sectional current profile of patterned 11-MUA monolayer.

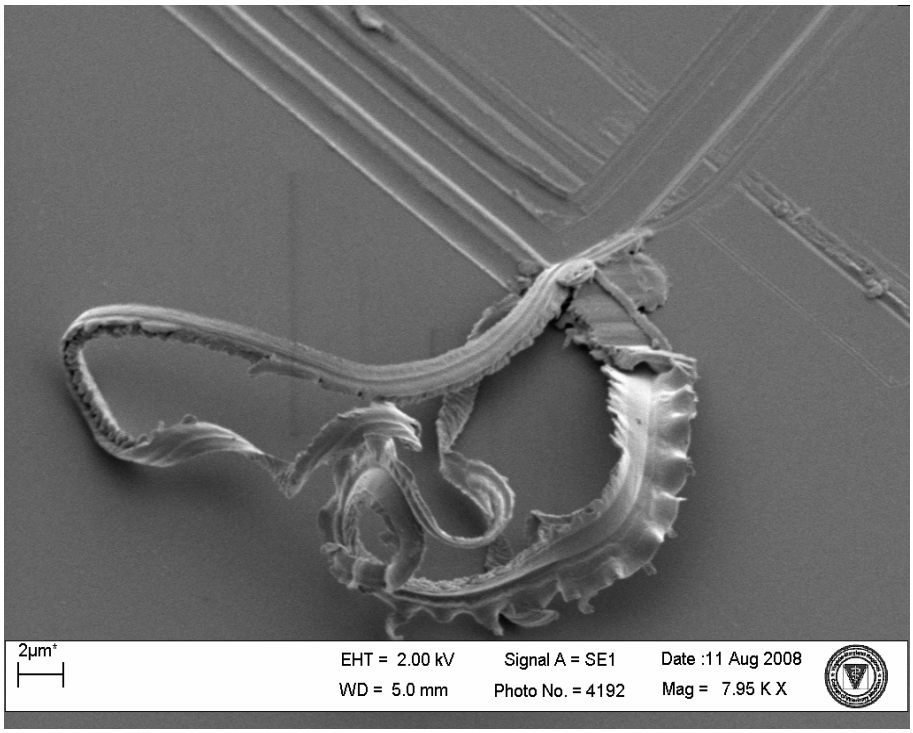

Figure 75: SEM image of an attempt at PDDA patterning on the surface of 11-MUA monolayer.

Since it was apparent that the SECM tip was scraping the monolayer as well as scraping the gold itself, a new approach at polyelectrolyte deposition was attempted. In this attempt, while the modified electrode was immersed in 0.05 mol·L^{-1} pH 5 phosphate buffer solution containing 1.08×10^{-6} mol·L^{-1} PDDA, the SECM tip was brought close to the surface with no

lateral movement. The potential of the modified electrode was stepped positive of the PZC for a few minutes in order to deposit a single polyelectrolyte spot; potential was then ramped to a value negative of the PZC and raised 75 µm above the modified electrode. After the dilute PDDA solution was removed from the SECM cell and replaced with 0.005 mol·L^{-1} [$[Ru(NH_3)_6]^{3+}$ or 0.005 mol·L^{-1} $[Fe(CN)_6]^{-4}$ made with 0.05 mol·L^{-1} pH 5 phosphate buffer solution, the polyelectrolyte spot was imaged. SECM images of polyelectrolyte spots on cysteine monolayers imaged with $[Ru(NH_3)_6]^{3+}$ and 11-MUA monolayers imaged with$[Fe(CN)_6]^{-4}$ are shown in Figures 76a and Figure 76b respectively. The cross sectional profile images of PDDA spots on cysteine and 11-MUA shown in Figures 77 and 78 show the expected current behavior of a PDDA spots to anionic and cationic polyelectrolytes. When imaged with a cationic redox probe, the current decreases as expected due to the electrostatic repulsion between the redox probe and the PDDA. When imaged with the anionic redox probe, the current increases when the PDDA in response to the electrostatic attraction between the cationic polyelectrolyte and the anionic redox probe.

In addition to SECM analysis of applied potential deposition of polyelectrolyte spots, scanning electron microscopy (SEM) images of polyelectrolytes were also conducted. The SEM images of a PDDA spot deposited on 3-MPA (Figure 79) shows clear evidence of the deposition of polyelectrolyte spots under the direction of applied potential.

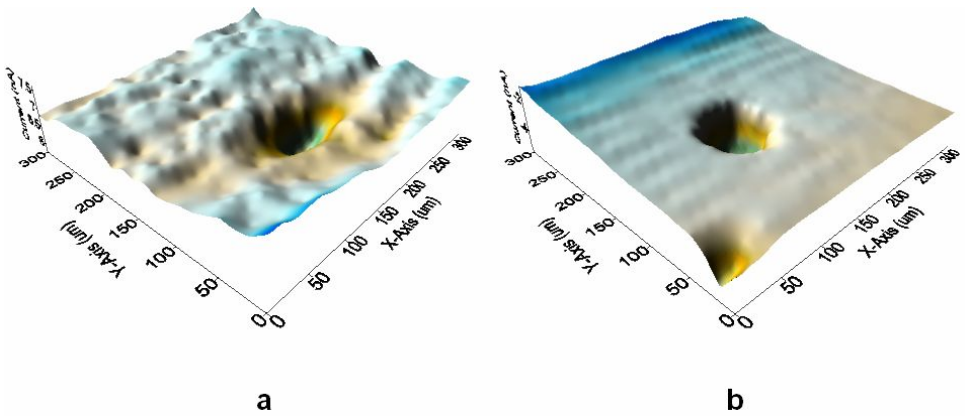

Figure 76: 3-D image surfaces of PDDA spots deposited on cysteine monolayers (a) and 11-MUA monolayers (b). Images for the PDDA spots on cysteine were conducted in 0.005 mol·L^{-1} $[Ru(NH_3)_6]^{3+}$ prepared with 0.05 mol·L^{-1} pH 5 phosphate buffer solution. Images for the PDDA spots on 11-MUA were conducted in 0.005 mol·L^{-1}$[Fe(CN)_6]_3^{-/4-}$ prepared with 0.05 mol·L^{-1} pH 5 phosphate buffer solution.

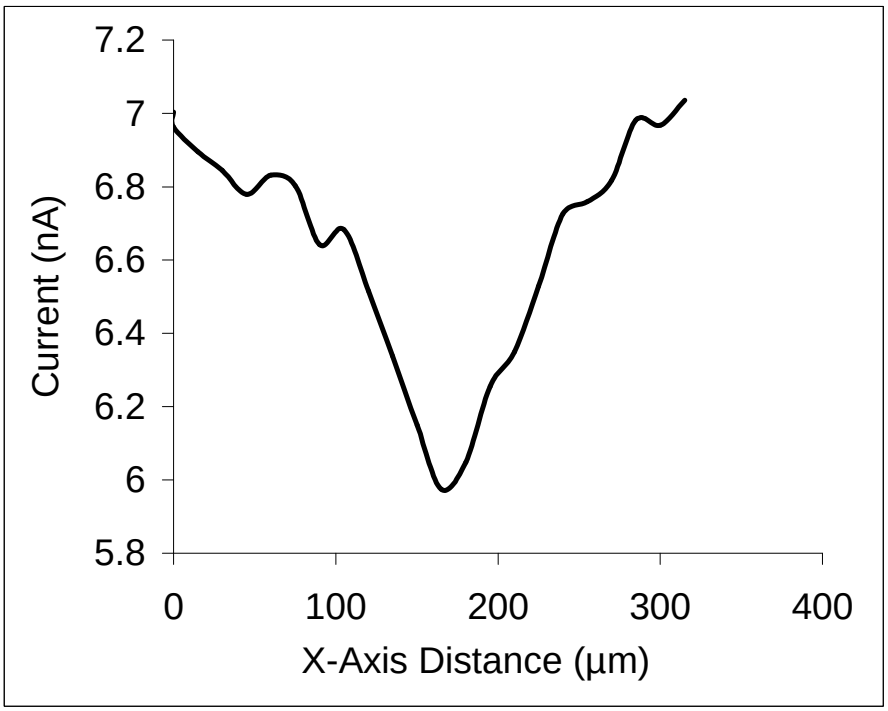

Figure 77: Cross sectional current profile of PDDA spot deposited onto cysteine monolayer.

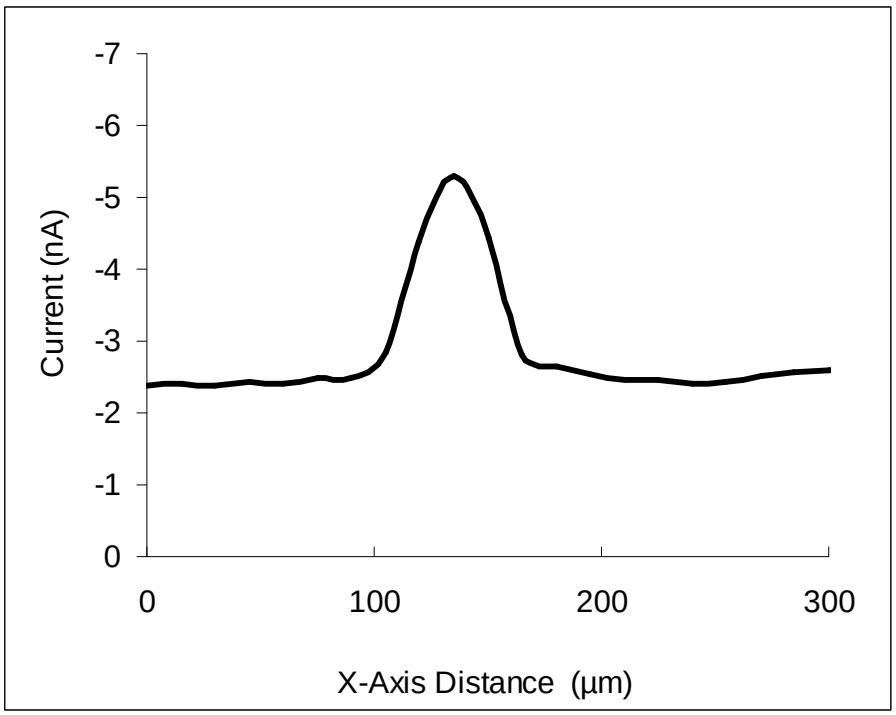

Figure 78: Cross sectional current profile of PDDA spot deposited onto cysteine monolayer.

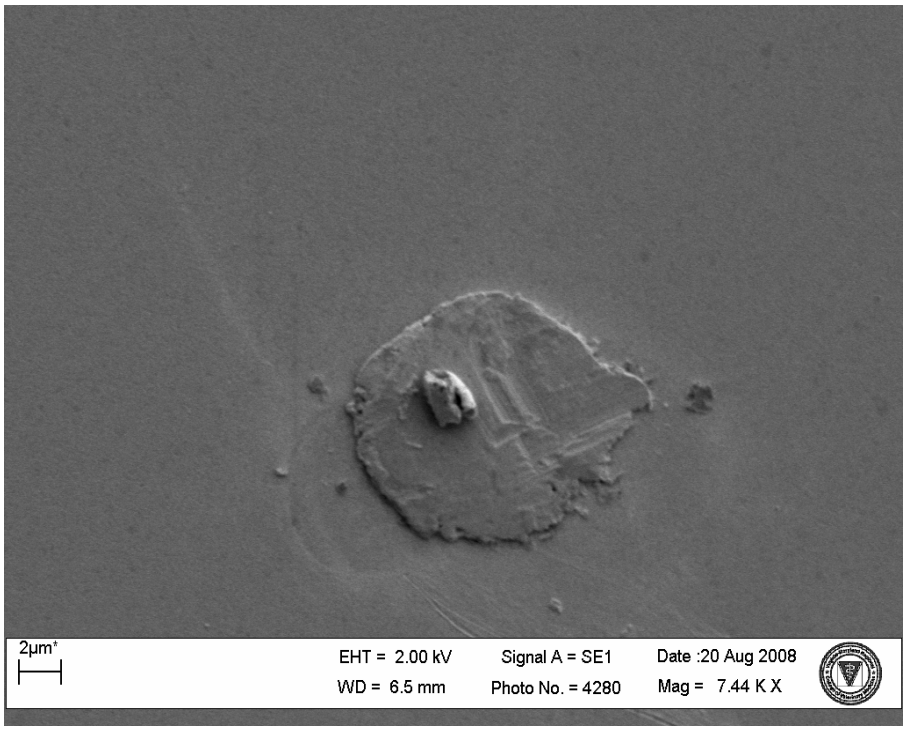

Figure 79: SEM images of PDDA deposited on a 3-MPA monolayer.

6.4 Summary

Impedance and QCM measurements from previous chapters provided indirect evidence of potential-driven deposition of polyelectrolyes. However, observation of the surface charge of acid terminated monolayers at potentials near the PZC and positive of the PZC was possible due to the electrostatic interaction between the surface and the redox probe. This modifies the redox probe concentration directly underneath the SECM tip. As a result, the extent of electron transfer is modulated producing an increase or decrease in current. This suggests that the SECM tip could be used to control the surface charge of a specific region of a functionalized monolayer to drive polyelectrolyte deposition in a particular region.

The SECM tip was used as an auxiliary electrode for the purpose of localizing an electric field on a specific region of a functionalized monolayer in order to drive surface group ionization at a specific point. This promotes the ionic self assembly of a cationic polyelectrolyte. When imaging the cationic polyelectrolyte spot with a cationic redox probe, there is electrostatic repulsion between the cationic redox probe and the polyelectrolyte. The electrostatic repulsion decreases the concentration of the redox probe directly underneath the SECM tip. This

decreased concentration results in a decrease in electron transfer producing lower current detected by the SECM tip. When an anionic redox probe is used to image the PDDA spot, electrostatic attraction exists between the redox probe and the polyelectrolyte spot. This results in an increase in the concentration of the anionic redox probe directly underneath the SECM tip leading to an increase in electron transfer that producing increased current.

The opposite current responses observed during SECM scans of PDDA spots when oppositely charged redox probes are used strongly suggests that polyelectrolyte is deposited during a potential step positive of the PZC. The results presented in this chapter are consistent with the behavior of the impedance and QCM results described in previous chapters; it was shown that applications of potentials positive of the PZC can drive the deposition of an oppositely charged polyelectrolyte to the monolayer surface. The results described in the chapter not only provide evidence than potential can be used to drive ionic self assembly, they also indicate that an SECM tip connected as an auxiliary electrode can act as a “pen” to write spots of polyelectrolytes to the surface of functionalized monolayers biased at potentials positive of the PZC.

Chapter 7. Summary and Future Work

7.1 Summary

The impedance, QCM, and SECM analysis conducted on 3-MPA, cysteine, and 11-MUA monolayers exposed to different potentials relative to the PZC have shown that ionic self assembly of polyelectrolytes can be controlled with applied potential. In addition, SECM experiments provide evidence that the spatial deposition of the polyelectrolytes to modified electrodes energized with potentials positive of the PZC can be controlled with the SECM tip.

The conceptual basis for the research described in this dissertation is based on several reports that describe the manipulation of the interfacial pH of functionalized monolayers using applied potential[29, 30, 34, 35]. One of the novel endeavors associated with this dissertation research involves potential-driven deposition of polyelectrolytes to monolayer surfaces in solutions were no surface group ionization is present and ionic self assembly is inhibited.

The principle means used to confirm the deposition of polyelectrolytes via applied potential was electrochemical impedance measurements. Charge-transfer resistance measurements extrapolated from impedance data using a fitting program free for download provided indirect evidence of polyelectrolyte deposition. Charge-transfer resistance is a measure of the extent of electron transfer between the modified electrode and the redox probe in solution. When the redox probe is in close proximity to the modified electrode, electron transfer is encouraged which translates into a decrease in charge-transfer resistance resulting from the ease at which electrons are moved between the redox probe and the electrode. When the distance between the redox probe and the modified electrode is increased, the extent of electron transfer between the redox probe and the modified electrode decreases, which translates into an increase in charge-transfer resistance. Electrostatic interactions between the modified electrode and charged redox probes in solution can also result in modulation of the charge-transfer resistance. This was the basis for using impedance to confirm the deposition of polyelectrolytes under the influence of applied potential. Prior to each applied potential deposition experiment, impedance analyses of

3-MPA and 11-MUA modified electrodes were conducted while the electrodes were immersed in a solution containing$[Fe(CN)_6]_3^{-/4-}$. After initial impedance measurements, applied potential deposition was attempted in dilute polyelectrolyte solutions with a pH of approximately 5; at this pH, the surface charge of the monolayers was minimal. Sixty-second, potential steps were used to apply potentials near the PZC or positive of the PZC. After the potential ramps, second impedance analyses were conducted on the modified electrodes in the solution containing the anionic redox probe. It was observed that electrodes immersed in PDDA solution energized with potential near the PZC showed little to no change in charge-transfer resistance. It can be inferred from this result that at the PZC, there is no accumulation of anions to the terminal region of the monolayer. This results in no surface acid group deprotonation and no electrostatic attraction between the surface and the polyelectrolyte, evidence of the inhibition, or turning off of ionic self assembly. The electrostatic interaction between the redox probe and the surface of the monolayer was the same before exposure of PDDA, and after exposure to PDDA at the PZC; for this reason, there was minimal change in the charge-transfer resistance. Impedance analysis of the modified electrodes after exposure to potentials positive of the PZC while immersed in dilute PDDA solutions showed a drastic decrease in charge-transfer resistance. This indicates that the electrostatic interaction between the redox probe and the surface of the monolayer after exposure to PDDA at potentials more positive than the PZC is different than the interaction before the potential step. It is believed that application of a potential positive of the PZC results in the accumulation of anions to the surface of the carboxylic acid terminated monolayers. This results in the deprotonation of the teminal acid groups and promotes the attachment of cationic polyelectrolytes via electrostatic attraction. The newly deposited polyelectrolyte layer increases the electrostatic attraction between the monolayer surface and the anionic redox probe. The decrease in distance increases the degree of electron transfer between the redox probe and the electrode; the ease with which electron transfer takes place under these conditions yields an observed decrease in the apparent charge-transfer resistance. These impedance results show that

the minimal change in charge-transfer resistance prior to and after the modified electrodes are energized with potential near the PZC while exposed to dilute PDDA solutions discourages ionic self assembly. The decrease in charge-transfer resistance after exposure of modified electrodes to dilute PDDA solutions while energized with potentials positive of the PZC suggests that ionic self assembly of the polyelectrolyte takes place.

Impedance analyses were also conducted on cysteine modified electrodes to determine if applied potential could be used to deposit both PDDA and PSS to cysteine monolayers. Cysteine was chosen because at pH values near its isoelectric point (5.06[104]) both NH_3^+ and COO^- groups are present. It was believed that potential could be used to control the extent of amine group protonation and carboxylic acid group deprotonation.

It was expected for the impedance behavior of cysteine monolayers exposed to PDDA solutions at potentials positive of the PZC to show a decrease in charge-transfer resistance, behavior similar to what was observed with 3-MPA and 11-MUA monolayers. It was observed that after exposure to dilute PDDA solutions at potentials positive to the PZC, the charge-transfer resistance of cysteine modified electrodes showed little change. However, impedance analyses of cysteine modified electrodes exposed to PSS at this potential showed an increase in charge-transfer resistance. A similar experiment involving a potential step in a direction negative of the PZC showed a decrease in charge-transfer resistance after PDDA exposure and no change in charge-transfer resistance after PSS exposure. This behavior was the opposite of what was expected; it was believed that potentials positive of the PZC would promote anion accumulation that would result in acid group deprotonation encouraging the ionic self assembly of a cationic polyelectrolyte. Alternatively, it was expected for potentials negative of the PZC to drive the accumulation of cations to the interface encouraging the protonation of amine groups that would encourage the ionic self assembly of anionic polyelectrolytes. It appears that application of potentials positive or negative of the PZC has little effect on the protonation or deprotonation of terminal cysteine groups because cysteine is zwitterionic over a wide pH range. Based on the

behavior of the impedance data after exposure of the modified electrodes to polyelectrolytes at potentials relative of the PZC, it is believed that the surface groups are experiencing potential induced rearrangement. There are literature precedents for the potential induced conformational change of cysteine functional groups. Brolo and coworkers report that the protonated amine groups of cysteine monolayers point towards the surface at potentials positive of the PZC due to the coadsorption of chloride anions[105].

Zhang et al. report that the NH_3^+ and COO^- groups are tilting in response to application of potential[107]. They report that immobilized cysteine chains are upright at potentials equal to the PZC, but application of potential negative of the PZC results in the attraction of the NH_3^+ group towards the surface. At potentials positive of the PZC, the excess positive charge encourages in the attraction of the COO^- groups towards the surface[107]. The Zhang manuscript in particular provides further credence to the results obtained from the applied potential-driven deposition of polyelectrolytes onto cysteine monolayers. Potentials positive of the PZC results in the tilting of the COO^- groups towards the surface. This action leaves the NH_3^+ groups exposed as a template for anionic polyelectrolyte deposition. The impedance analysis obtained after exposure of cysteine modified electrodes to PSS at this potential show a significant increase in charge-transfer resistance. This occurs due to deposition of the anionic layer, which repels the$[Fe(CN)_6]^{3-/4-}$ redox probe in solution. This increased distance between the redox probe and the electrode surface decreases the ease of electron transfer, which translates into an increase in charge-transfer resistance. Application of potential negative of the PZC results in the tilting of NH_3^+ group towards the surface. This leaves the COO^- group exposed for cationic polyelectrolyte deposition. It is shown that cationic deposition does occur at this potential because after exposure of the cysteine modified electrode to PDDA at this potential, the charge-transfer resistance decreases. This is due to the decreased distance between the cationic layer and the anionic redox probe resulting from electrostatic attraction. This decreased distance

increases the rate of electron transfer between the redox probe and the electrode, resulting in a decrease in charge-transfer resistance.

In addition to impedance analyses, quartz crystal microbalance measurements also served as a diagnostic tool to confirm polyelectrolyte deposition in response to applied potential. In the case of 3-MPA and 11-MUA, the behavior of the QCM data mirrors the impedance data. Greater accumulations of mass were observed with modified QCM plates exposed to PDDA solutions at potentials positive of the PZC. The QCM data for cysteine experiments also mirrors the impedance results. Greater mass approximations were obtained when cysteine modified QCM plates were exposed to potentials positive of the PZC while immersed in PSS. Conversely, greater accumulations were obtained when cysteine modified QCM plates were immersed in PDDA solutions and energized with potential negative of the PZC.

The main objective of this dissertation research was met as evident from the impedance and QCM results presented in earlier chapters. Data suggests that applications of potentials to modified electrodes relative to the PZC can result in the turning on or turning off of ionic self assembly. A more direct measure of applied potential control over surface group ionization was accomplished using images obtained from scanning electrochemical microscopy. Carboxylic acid terminated monolayers (3-MPA and 11-MUA) exposed to potentials positive of the PZC while immersed in pH 5 phosphate buffer solutions containing 0.005 $mol \cdot L^{-1}$ $[Ru(NH_3)_6]^{3+}$ resulted in the formation of a “hill” in the SECM image. This hill is in response to the increase in current when potential is stepped positive of the PZC. It is believed that accumulation of anions deprotonates the terminal acid groups; the carboxylate groups encourage the accumulation of the cationic redox probe directly underneath the SECM tip. The increased concentration of the redox probe increases electron transfer resulting in the observed increase in current. The opposite effect is observed when potential is stepped negative of the PZC; in this case, an inverted hill appears. When potential is stepped negative of the PZC, the surface groups become neutral directly underneath the SECM tip. This decreases the electrostatic interaction

between the surface and the cationic redox probe in solution. This decreased concentration results in a decrease in electron transfer which produces a decrease in current.

Attempts at site-directed ionic self assembly involve using the SECM tip as an auxiliary electrode to localize the potential applied to modified electrodes. While immersed in pH 5 phosphate buffer solution containing PDDA, there is evidence that application of potential positive of the PZC deprotonates surface confined acid groups and encourages the deposition of cationic polyelectrolytes. Evidence that site-directed applied potential deposition occurs is based on the behavior of the redox probe as it interacts with the polyelectrolyte spot. PDDA spots deposited on cysteine monolayers imaged with a cationic redox probe ($[Ru(NH_3)_6]^{3+}$) show a decrease in current. A cationic redox probe is expected to experience electrostatic repulsion with the positively charged PDDA polyelectrolyte. This electrostatic interaction results in the decrease in concentration of the redox probe in the vicinity of the PDDA spot which results in an apparent decrease in current when the SECM tip passes over the spot during imaging. When PDDA spots are imaged using an anionic redox probe ($[Fe(CN)_6]^{-4}$) once again the current behaved as expected. Anionic redox probes are expected to experience electrostatic attraction with the deposited PDDA spot. This increased electrostatic attraction increases the concentration of the redox probe in the vicinity of the polyelectrolyte spot. This increased concentration increases electron transfer producing an increase in current.

7.2 Future plans

7.2.1 *In-situ* IR analysis of functionalized monolayers exposed to applied potential

A future direction of this project involves an *in-situ* IR analysis of 3-MPA, 11-MUA, and cystiene modified plates exposed to potentials positive and negative of the PZC. An IR analysis of carboxylic acid terminated monolayers energized with potentials positive of the PZC would result in the decrease in the intensities observed at approximately 1730 and 1200 cm^{-1}, intensities that are specific for protonated carboxylic acid groups[39]. A decrease in these intensities would take place at this potential due to the deprotonation of the surface groups in response to the

application of potentials positive of the PZC. The intensity at 1610 cm^{-1} is expected to increase due to the appearance of carboxylate surface groups[39] at these potentials. The opposite effect is expected at potentials equal to and negative of the PZC.

In the case of the cysteine monolayers, an *in-situ* IR analysis of cysteine modified electrodes in response to applied potential would produce a different result. In pH 5 phosphate buffer solutions, cysteine exists as a zwitterion, therefore appearance and disappearance of peaks associated with the carboxylate groups (1610 cm^{-1}) and amine groups (3290 cm^{-1}) in response to applied potential would assist in confirming the assertion that the NH_3^+ groups and the COO^- groups tilt in response to applied potential. At potentials positive of the PZC it is believed that the COO^- surface group would tilt towards the surface extending the NH_3^+ groups away from the surface. As a result, a decrease in the COO^- intensity at 1610 cm^{-1} and an increase in NH_3^+ intensity at 3290 cm^{-1} should be observed. The opposite effect is expected at potentials negative of the PZC.

7.2.2 Applied potential deposition of polyelectrolyte lines and patterns

This dissertation research presents results that strongly suggest that polyelectrolytes can be deposited using applied potential. Incorporating the SECM offers the ability to selectively deposit the polyelectrolyte at specific locations along the surface. An attempt at patterning lines and simple geometric shapes would involve using spots deposited linearly to generate patterns. The deposition procedure would have three main steps: bringing the SECM tip close to the electrode surface, stepping the potential positive of the PZC, and stepping the potential negative of the PZC while the electrode is raised up from the surface. To pattern polyelectrolyte shapes, an additional step would be added to the deposition procedure which involves moving the SECM tip laterally to a new position where the process would be repeated until the desired pattern is produced. To address issues associated with the formation of aggregates or slowly diffusing polyelectrolytes near the SECM tip after deposition, the solution

in the SECM cell would be purged with nitrogen between each deposition cycle to clear the tip of debris.

7.3 General Conclusions

The results presented in this dissertation provide strong evidence that application of potentials positive of the PZC leads to deprotonation of surface confined acid groups. This is possible by manipulating the double-layer in a way that involves the accumulation of excess charge at the outer Helmholtz plane, which induces a change in the surface charge of the surface confined acid groups in the inner Helmholtz plane. Drastic changes in the impedance and QCM data suggests that at certain potentials, polyelectrolytes are deposited at the surface, and at other potentials polyelectrolytes deposition is inhibited. It can be inferred from the data that while in solutions with pH values buffered just below the surface pK_a of the monolayer, application of potentials positive or negative of the PZC can turn of or turn off ionic self assembly, and this process has application to forming patterns along the modified interface.

.

References

1. Jr., R. C.; Lee, T. R., Thiol based self-assembled monolayers: formation and organization *Encyclopedia of Materials: Science and Technology* **2001**.

2. Brito, R.; Tremont, R.; Cabrera, C. R., Electron transfer kinetics across derivatized self-assembled monolayers on platinum: a cyclic voltammetry and electrochemical impedance spectroscopy study. *Journal of Electroanalytical Chemistry* **2004,** 574, 15-22.

3. Petri, M.; Kolb, D. M.; Memmert, U.; Meyer, H., Adsorption of Mercaptopropionic Acid onto Au(111) Part I. Adlayer formation, structure, and electrochemistry. *Electrochimica Acta* **2003,** 49, 175-182.

4. Sawaguchi, T.; Sato, Y.; Mizutani, F., In situ scanning tunneling microscopy observation of self-assembled monolayers of 3-mercaptopropionic acid on Au(111) in perchloric acid solution. *Journal of Electroanalytical Chemistry* **2001,** 507, 256-262.

5. Giz, M. J.; Duong, B.; Tao, N. J., In situ STM study of self-assembled mercaptopropionic acid monolayers for electrochemical detection of dopamine. *Journal of Electroanalytical Chemistry* **1999,** 465, 72-79.

6. Bott, A. W., Mass Transport. *Current Separations* **1996,** 14, 104-109.

7. Smith, C. P.; White, H. S., Voltammetry of Molecular Films Containing Acid-Base Groups. *Langmuir* **1993,** 9, (1), 1-3.

8. White, H. S.; Peterson, J. D.; Cui, Q.; Stevenson, K. J., Voltammetric measurement of interfacial acid-base reactions. *Journal of Physical Chemistry B* **1998,** 102, 2930-2934.

9. Fawcett, W. R.; Fedurco, M.; Kovacova, Z., Double-Layer Effects at Molecular Films Containing Acid-Base Groups. *Langmuir* **1994,** 10, (7), 2403-2408.

10. Wang, J., *Analytical Electrochemistry*. VCH Publishers, Inc.: New York, 1994; p 198.

11. Monk, P., *Fundamentals of Electroanalytical Chemistry*. John Wiley and Sons Limited: 2001.

12. Duffy, D. C.; Ward, R. N.; Davies, P. B.; Bain, C. D., Direct Observation of Counterions Bound to a Charged Surfactant Monolayer by Sum-Frequency Vibrational Spectroscopy. *Journal of the American Chemical Society* **1994,** 116, (3), 1125-1126.

13. Bard, A. J.; Faulkner, L. R., *Electrochemical Methods: Fundamentals and Applications*. 2nd ed.; John Wiley and Sons: New York, 2001.

14. Atkins, P. W., *Physical Chemistry*. Fourth ed.; W. H. Freeman and Company: New York, 1990; p 995.

15. Slowinski, K.; II, R. V. C.; Bilewicz, R.; Majda, M., Evidence for inefficient chain-to-chain coupling in electron tunneling through liquid alkanethiol monolayer films on mercury. *Journal of the Americal Chemical Society* **1996,** 118, 4709-4710.

16. Teppner, R.; Haage, K.; Wantke, D.; Motschmann, H., On the internal structure of an adsorption layer of an ionic soluble surfactant. The-buildup of a stern layer monitored by optical-means. *Journal of Physical Chemistry B* **2000,** 104, (48), 11489-11496.

17. Hu, Y., Effects of an inner Helmholtz layer on the dielectric dispersion of colloidal suspensions. *Langmuir* **1998,** 14, (2), 271-276.

18. Kakiuchi, T.; Iida, M.; Imabayashi, S.-i.; Niki, K., Double-layer capacitance titration of self-assembled monolayers of omega functionalized alkanethiols on Au(111) surface. *Langmuir* **2000,** 16, 5397-5401.

19. Mendes, R. K.; Freire, R. S.; Fonseca, C. P.; Neves, S.; Kubota, L. T., Characterization of self-assembled thiols monolayers on gold surface by electrochemical impedance spectroscopy. *Journal of the Brazillian Chemical Society* **2004,** 15, 849-855.

20. Burgess, I.; Seivewright, B.; Lennox, R. B., Electric Field Protonation/Deprotonation of Self-Assembled Monolayers of Acid Terminated Thiols. *Langmuir* **2006,** 22, 4420-4428.

21. Schweiss, R.; Werner, C.; Knoll, W., Impedance spectroscopy studies of interfacial acid-base reactions of self-assembled monolayers. *Journal of Electroanalytical Chemistry* **2003,** 540, 145-151.

22. Campina, J. M.; Martins, A.; Silva, F., Selective permeation of a liquidline self-assembled monolayer of 11-amino-1-undecanethiol on polycrystalline gold by highly charged electroactive probes. *Journal of Physical Chemistry C* **2007,** 111, 5351-5362.

23. Becka, A. M.; Miller, C. J., Electrochemistry at ω-hydroxy thiol coated electrodes. 4. Comparison of the double layer at ω-hydroxy thiol and alkanethiol monolayer coated Au-electrodes. *Journal of Physical Chemistry* **1993,** 97, (97), 6233-6239.

24. Hamm, U. W.; Kramer, D.; Zhai, R. S.; Kolb, D. M., The pzc of Au(111) and Pt(111) in a perchloric acid solution: an ex situ approach to the immersion technique. *Journal of Electroanalytical Chemistry* **1996,** 414, 85-89.

25. Janek, R. P.; Fawcett, W. R., Impedance spectroscopy of self-assembled monolayers on Au(111): evidence for complex double-layer structure in aqueous NaClO4 at the potential of zero charge. *Journal of PHysical Chemistry B.* **1997,** 101, 8550-8558.

26. Bryant, M. A.; Crooks, R. M., Determination of surface pKa values of surface-confined molecules derivatized with pH-sensitive pendant groups. *Langmuir* **1993,** 9, 385-387.

27. Calvente, J. J.; Marinkovic, N. S.; Kovacova, Z.; Fawcett, W. R., SNIFTIRS studies of the double layer at the metal vertical bar solution interface .1. Single crystal gold electrodes in aqueous perchloric acid. *Journal of Electroanalytical Chemistry* **1997,** 421, (1-2), 49-57.

28. Ramirez, P.; Andreu, R.; Cuestra, A.; Calzado, C. J.; Calvented, J. J., Determination of the potential of zero charge of Au(111) modified with thiol monolayers. *Analytical Chemistry* **2007,** 79, 6473-6479.

29. Dorain, P. B.; Raben, K. U. v.; Chang, R. K., Voltage dependence of the pH at the interface of a Ag electrode: A SERS measurement of a phosphate-phosporic acid system. *Surface Science* **1984,** 148, 439-452.

30. Anderson, M. R.; Evans, D. H., Surface-Enhanced Raman-Study of the Effect of Electrode Potential and Solution Ph Upon the Interfacial Behavior of 4-Pyridinecarboxaldehyde. *Journal of the American Chemical Society* **1988,** 110, (20), 6612-6617.

31. Kuznetsov, B. A.; Byzova, N. A.; Shumakovich, G. P., The effect of the orientation of cytochrome c molecules covalently attached to the electrode surface upon the electrochemical activity. *Journal of Electroanalytical Chemistry* **1994,** 371, 85-92.

32. Iwasita, T.; Xia, X., Adsorption of water at Pt(111) electrode in HClO4 solutions. The potential of zero charge. *Journal of Electroanalytical Chemistry* **1996,** 411, 95-102.

33. Nosal-Wiercinska, A.; Fekner, Z.; Dalmata, G., The adsorption of thiourea on the mercury from neutral and acidic solutions of perchlorates. *Journal of Electroanalytical Chemistry* **2005,** 584, 192-200.

34. Cao, X. W., Study of electrode potential effect on acid-base behavior of omega-functionalized self-assembled monolayers using Fourier transform surface-enhanced Raman scattering spectroscopy. *Journal of Raman Spectroscopy* **2005,** 36, (3), 250-256.

35. Sugihara, K.; Shimazu, K.; Uosaki, K., Electrode potential effect on the surface pK(a) of a self-assembled 15-mercaptohexadecanoic acid monolayer on a gold/quartz crystal microbalance electrode. *Langmuir* **2000,** 16, (18), 7101-7105.

36. Hammond, P. T., Recent explorations in electrostatic multilayer thin film assembly. *Current Opinion in Colloid and Interface Science* **2000,** 4, 430-442.

37. Clark, S. L.; Montague, M.; Hammond, P. T., Selective deposition in multilayer assembly: SAMs as molecular templates. *Supramolecular Science* **1996,** 4, 141-146.

38. Decher, G.; Hong, J. D.; Schmitt, J., Buildup of ultrathin multilayer films by a self-assembly process: III. Consecutively alternating adsorption of anionic and cationic polyelectrolytes on charged surfaces. *Thin Solid Films* **1992,** 210/211, 831-835.

39. Jordan, C. E.; Frey, B. L.; Kornguth, S.; Corn, R. M., Characterization of poly-l-lysine adsorption onto alkanethiol-modified gold surfaces with polarization-modulation fourier transform infrared spectroscopy and surface plasmon resonance measurements. *Langmuir* **1994,** 10, 3642-3648.

40. Wu, Z.; Guan, L.; Shen, G.; Yu, R., Renewable urea sensor based on a self-assembled polyelectrolyte layer. *Analyst* **2002,** 127, 391-395.

41. Hodak, J.; Etchenique, R.; Calvo, E. J., Layer-by-layer self-assembly of glucose oxidase with a poly(allylamine)ferrocene redox mediator. *Langmuir* **1997,** 13, 2708-2716.

42. Decher, G.; Hong, J. D.; Schmitt, J., Buildup of Ultrathin Multilayer Films by a Self-Assembly Process .3. Consecutively Alternating Adsorption of Anionic and Cationic Polyelectrolytes on Charged Surfaces. *Thin Solid Films* **1992,** 210, (1-2), 831-835.

43. Jordan, C. E.; Frey, B. L.; Kornguth, S.; Korn, R. M., Characterization of poly-l-lysine adsorption onto alkanethiol-modified gold surfaces with polarization-modulation fourier transform infrared spectroscopy and surface plasmon resonance measurements. *Langmuir* **1994,** 10, 3642-3648.

44. Kotov, N. A., layer-by-layer self-assembly: the contribution of hydrophobic interactions. *Nanostructured Materials* **1999,** 12, 789-796.

45. Claesson, P. M.; Poptoshev, E.; Blomberg, E.; Dedinaite, A., Polyelectroyte-mediated surface interactions. *Advances in colloid and interface science* **2005,** 114-115, 173-187.

46. Shi, L.; Sun, J.; Liu, J.; Shen, J.; Gao, M., Site selective deposition of enyme/polyelectrolyte multilayer films on ITO electrodes controlled electric fields. *Chemistry Letters* **2002,** 12, 1168-1169.

47. Wu, F.; Hu, Z.; Wang, L.; Xu, J.; Xian, Y.; Tian, U.; Jin, L., Electric field directed layer-by-layer assembly of horseradish peroxidase nanotubes via anodic alumina oxide template. *Electrochemistry Communications* **2008,** 10, 6]30-6]34.

48. Gao, M.; Sun, J.; Dulkeith, E.; Gaponik, N.; Lemmer, U.; Feldmann, J., Lateral patterning of CdTe nanocrystal films by the electric field directed layer-by-layer assembly method. *Langmuir* **2002,** 18, 4098-4102.

49. Shi, L.; Lu, Y.; Sun, J.; Zhang, J.; Sun, C.; Liu, J.; Shen, J., Site-selective lateral multilayer assembly of bienzyme with polyelectrolyte on ITO electrode based on electric field-induced directly layer-by-layer deposition. *Biomacromolecules* **2003,** 4, 1161-1167.

50. Sun, J.; Gao, M.; Feldmann, J., Electric field directed layer-by-layer assembly of highly fluorescent CdTe nanoparticles. *Journal of Nanoscience and Nanotechnology* **2001,** 1, (2), 133-136.

51. Sun, J.; Gao, M.; Zhu, M.; Feldman, J.; Mohwald, H., Layer-by-layer depositions of polyelectrolyte/CdTe nanocrystal films controlled by electric fields. *Journal of Materials Chemistry* **2002,** 12, 1775-1778.

52. Rodriguez, M. C.; Rivas, G. A., Assembly of Glucose Oxidase and Different Polyelectrolytes by Means of Electrostatic Layer-by-Layer Adsorption on Thiolated Gold Surface. *Electroanalysis* **2004,** 16, 1717-1722.

53. Zhou, J.; Wipf, D. O., Deposition of conducting polyaniline patterns with the scanning electrochemical microscope. *Journal of The Electrochemical Society* **1997,** 144, (4), 1202-1207.

54. Fernandez-Sanchez, C.; McNeil, C. J.; Rawson, K., Electrochemical impedance spectroscopy studies of polymer degradation: application to biosensor development. *Trends in Analytical Chemistry* **2005,** 24, (1), 37-48.

55. Loveday, D.; Peterson, P.; Rodgers, B., Evaluation of Organic Coatings with Electrochemical Impedance Spectroscopy. Part 1: Fundamentals of Electrochemical Impedance Spectroscopy. *JCT Coatings Tech* **2004**, 46-52.

56. Basics of electrochemical impedance spectroscopy. *Princeton Applied Research* Application Note AC-1.

57. Park, S.-M.; Yoo, J.-S., Electrochemical Impedance Spectroscopy. *Analytical Chemistry A* **2003**, 455A-461A.

58. Jin, Z. H.; Vezenov, D. V.; Lee, Y. W.; Zull, J. E.; Sukenik, C. N.; Savinell, R. F., Alternating current impedance characterization of the structure of alkylsiloxane self-assembled monolayers on silicon. *Langmuir* **1994,** 10, 2662-2671.

59. Finklea, H. O.; Snider, D. A.; Fedyk, J., Characterization of octadecanethiol-coated gold electrodes as microarray electrodes by cyclic voltammetry and ac impedance spectroscopy. *Langmuir* **1993,** 9, 3660-3667.

60. Diao, P.; Guo, M.; Tong, R., Characterization of defects in the formation process of self-assembled thiol monolayers by electrochemical impedance spectroscopy. *Journal of Electroanalytical Chemistry* **2001,** 495, 98-105.

61. Campuzano, S.; Pedrero, M.; Montemayor, C.; Fatas, E.; Pingarron, J. M., Characterization of alkanethiol-self-assembled-monolayers-modified gold electrodes by electrochemical impedance spectroscopy. *Journal of Electroanalytical Chemistry* **2006,** 586, 112-121.

62. Ding, S.-J.; Chang, N.-W.; Wu, C.-C.; Lai, M.-F.; Chang, H.-C., Impedance spectral studies of self-assembly of alkanethiols with different chain lengths using different immobilization strategies on Au electrodes. *Analytica Chimica Acta* **2005,** 554, 43-51.

6]3. Cui, X.; Jiang, D.; Diao, P.; Li, J.; Tong, R.; Wang, X., Assesing the apparent effective thickness of alkanethiol self-assembled monolayers in different concentrations of[Fe(CN)6]3-/Fe(CN)64- by ac impedance spectroscopy. *Journal of Electroanalytical Chemistry* **1999,** 470, 9-13.

64. Saum, A. G. E.; Cumming, R. H.; Rowell, F. J., Use of substrate coated electrodes and AC impedance spectroscopy for the detection of enzyme activity. *Biosensors and Bioelectronics* **1998,** 13, 511-518.

65. Guan, J.-G.; Miao, Y.-Q.; Zhang, Q.-J., Impedimetric Biosensors. *Journal of Bioscience and Bioengineering* **2004,** 97, 219-226.

66. Patolsky, F.; Zayatas, M.; Katz, E.; Wilner, I., Precipitation of an insoluble product on enzyme monolayer electrodes for biosensor applications: characterization by faradaic impedance

spectroscopy, cyclic voltammetry, and microgravimetric quartz crystal microbalance analyses. *Analytical Chemistry* **1999,** 71, 3171-3180.

67. Komura, T.; Yamaguchi, T.; Shimatani, H.; Okushio, R., Interfacial charge-transfer resistance at ionizable thiol monolayer-modified gold electrodes as studied by impedance spectroscopy. *Electrochimica Acta* **2004,** 49, (4), 597-606.

68. Kim, K.; Kwak, J., Faradaic impedance titration of pure 3-mercaptopropionic acid and ethanethiol mixed monolayers on gold. *Journal of Electroanalytical Chemistry* **2001,** 512, 83-91.

69. Pedrosa, V. A.; Paixao, T. R. L. C.; Freire, R. S.; Bertotti, M., Studies on the electrochemical behavior of a cystine self-assembled monolayer modified electrode using ferrocyanide as a probe. *Journal of Electroanalytical Chemistry* **2007,** 602, 149-155.

70. Sanders, W.; Vargas, R.; Anderson, M., Characterization of carboxylic acid terminated self-assembled monolayers by electrochemical impedance spectroscopy and scanning electrochemical microspcopy. *Langmuir* **2008,** 24, (12), 6133-6139.

71. Janek, R. P.; Fawcett, R., Impedance spectroscopy of self-assembled monolayers on Au(111): evidence for complex double-layer structure in aqueous NaClO4 at the potential of zero charge. *Journal of Physical Chemistry B.* **1997,** 101, 8550-8558.

72. Buttry, D. A.; Ward, M. D., Measurement of Interfacial Processes at Electrode Surfaces with the Electrochemical Quartz Crystal Microbalance. *Chemical Reviews* **1992,** 92, 1355-1379.

73. Qu, D.; Morin, M., An ECQM study of the oxidative deposition of alkylthiolates on gold. *Journal of Electroanalytical Chemistry* **2001,** 517, 45-53.

74. Rocha, T. A. P.; Gomes, M. T. S. R.; Duarte, A. C.; Oliveira, J. A. B. P., Quartz crystal microbalance with gold electrodes as a sensor for monitoring gas-phase adsorption/desorption of short chain alkylthiol and alkyl sulfides. *Analytical Communications* **1998,** 35, 415-416.

75. Sabot, A.; Krause, S., Simultaneous quartz crystal microbalance impedance and electrochemical impedance measurements. Investigation into the degradation of thin polymer films. *Analytical Chemistry* **2002,** 74, 3304-3311.

76. O'Sullivan, C. K.; Guilbault, G. G., Commercial quartz crystal microbalances - theory and applications. *Biosensors and Bioelectronics* **1999,** 14, 66]3-670.

77. Wang, J.; Frostman, L. M.; Ward, M. D., Self-assembled thiol monolayers with carboxylic acid functionality: measuring pH-dependent phase transitions with the quartz crystal microbalance. *Journal of Physical Chemistry* **1992,** 96, 5224-5228.

78. Melroy, O.; Kanazawa, K.; II, J. G. G.; Buttry, D., Direct Determination of the Mass of Underpotentially Deposited Monolayer of Lead on Gold. *Langmuir* **1986,** 2, 697-700.

79. Tjipto, E.; Quinn, J. F.; Caruso, F., Assembly of multilayer films from polyelectrolytes containing weak and strong acid moieties. *Langmuir* **2005,** 21, 8785-8792.

80. Bard, A. J.; Fan, F.-R. F.; Kwak, J.; Lev, O., Scanning electrochemical microscopy. Introduction and principles. *Analytical Chemistry* **1989,** 61, 132-138.

81. Marck, C.; Borgwarth, K.; Heinze, J., Generation of polythiopene micropatterns by scanning electrochemical microscopy. *Chemistry of Materials* **2001,** 13, 747-752.

82. Wuu, Y.-M.; Fan, F.-R. F.; Bard, A. J., High resolution deposition of polyaniline on Pt with the scanning electrochemical microscope. *Journal of The Electrochemical Society* **1989,** 136, (3), 885-886.

83. Kranz, C.; Gaub, H. E.; Schuhmann, W., Polypyrrole towers grown with the scanning electrochemical microscope. *Advanced Materials* **1996,** 8, (8), 6]34-6]37.

84. Shao, Y.; Mikin, M. V., Nanometer-sized electrochemical sensors. *Analytical Chemistry* **1997,** 69, 1627-16]34.

85. Roach, D. M. Novel Applications of Scanning Electrochemical Microscopy. Virginia Polytechnic Institute and State University, Blacksburg, 2005.

86. Nagy, G.; Nagy, L., Scanning electrochemical microscopy: an new way of making electrochemical measurements. *Fresenius Journal of Analytical Chemistry* **2000,** 366, 735-744.

87. Shohat, I.; Mandler, D., Deposition of Nickel Hydroxide Structures Using the Scanning Electrochemical Microscope. *Journal of The Electrochemical Society* **1994,** 141, (4), 995-999.

88. Wittstock, G.; Hesse, R.; Schuhmann, W., Patterned self-assembled alkanethiolate monolayers on gold. Patterning and Imaging by means of scanning electrochemical microscopy. *Electroanalysis* **1997,** 9, 746-750.

89. Widrig, C. A.; Chung, C.; Porter, M. D., The electrochemical desorption of n-alkanethiol monolayers from polycrystalline Au and Ag electrodes. *Journal of Electroanalytical Chemistry* **1991,** 310, 335-359.

90. Palchetti, I.; Laschi, S.; Marrazza, G.; Mascini, M., Electrochemical imaging of localized sandwiched DNA hybridization using scanning electrochemical microscopy. *Analytical Chemistry* **2007,** 79, 7206-7213.

91. Turcu, F.; Schulte, A.; Hartwich, G.; Schuhman, W., Label-free electrochemical recognition of DNA hybridization by means of modulation of the feedback current in SECM. *Angewandte Chemie International Edition* **2004,** 43, 3482-3485.

92. Ye, J.; Liu, J.; Zhang, Z.; Hu, J.; Dong, S.; Shao, Y., Investigation of the model compounds at 4-aminobenzoic acid modified glassy carbon electrode by scanning electrochemical microscopy. *Journal of Electroanalytical Chemistry* **2001,** 508, 123-128.

93. Boldt, F.-M.; Baltes, N.; Borgwarth, K.; Heinze, J., Investigation of carboxylic-functionalized and n-alkanethiol self-assembled monolayers on gold and their application as pH-sensitive probes using scanning electrochemical microscopy. *Surface Science* **2005,** 597, 51-64.

94. Creager, S. E.; Clark, J., Contact angle titrations of mixed ω-mercpatoalkanoic acid/alkanethiol monlayers on gold. Reactive vs nonreactive spreading and chain length effects on surface pKa values. *Langmuir* **1994,** 10, 3675-3683.

95. Zhao, J.; Luo, L.; Yang, X.; Wang, E.; Dong, S., Determination of surface pKa of SAM using electrochemical titration method. *Electroanalysis* **1999,** 11, (15), 1108-1111.

96. Walczak, M. M.; Popenoe, D. D.; Deinhammer, R. S.; Lamp, B. D.; Chung, C.; Porter, M. D., Reductive desorption of alkanethiolate monolayers at gold: a measure of surface coverage. *Langmuir* **1991,** 7, 2687-2693.

97. Ebbing, D. D., *General Chemistry.* 4th ed.; Houghton Mifflin Company: Boston, 1993.

98. Lahann, J.; Mitragotri, S.; Tran, T.-N.; Kaido, H.; Sundaram, J.; Choi, I. S.; Hoffer, S.; Somorjai, G. A.; Langer, R., A reversibly switching surface. *Science* **2003,** 299, (17), 371-374.

99. Chuang, W.-H.; Lin, J.-C., Surface characterization and platelet adhesion studies for the mixed self-assembled monolayers with amine and carboxylic acid functionalities. *Journal of Biomedicals Research Part A* **2006**, 820-830.

100. Holmlin, R. E.; Chen, X.; Chapman, R. G.; Takayama, S.; Whitesides, G. M., Zwitterionic SAMs that resist nonspecific adsorption of protein from aqueous buffer. *Langmuir* **2001,** 17, 2841-2850.

101. Brigatti, M. F.; Lugli, C.; Montorsi, S.; Poppi, L., Effects of exchance cations and layer-charge location on cysteine retention by smectites. *Clay and Clay Minerals* **1999,** 47, (5), 664-671.

102. Monterroso-Marco, B.; Lopez-Ruiz, B., pH effect on cysteine and cystine behaviour at hanging mercury drop electrode. *Talanta* **2003,** 61, 733-741.

103. Wang, S.; Du, D., Studies on the Electrochemical Behavior of Hydroquinone at L-cysteine Self-Assembled Monolayers on Modified Gold Electrode. *Sensors* **2002,** 2, 41-49.

104. Quigwen, L.; Hong, G.; Yiming, W.; Guoan, L.; Jie, M., Studies on Self-Assembly Monolayers of Cysteine on Gold by XPS, QCM, and Electrochemical Techniques. *Electroanalysis* **2001,** 13, 1342-1346.

105. Brolo, A. G.; Germain, P.; Hager, G., Investigation of the Adsorption of L-Cysteine on a Polycrystalline Silver Electrode by Surface-Enhanced Raman Scattering (SERS) and Surface-Enhanced Second Harmonic Generation (SESHG). *Journal of Physical Chemistry B* **2002,** 106, 5982-5987.

106. Sato, Y.; Mizutami, F., Determination of Real Composition of 3-Mercaptopropioinic Acid and 1-Octadecanethiol Mixed Self-Assembled Monolayers Using Electrochemical and Electrochemical Quartz Crystal Microbalance Measurements. *Electroanalysis* **1998,** 10, 6]33-6]36.

107. Zhang, J.; Demetriou, A.; Welinder, A. C.; Albrecht, T.; Nichols, R. J.; Ulstrup, J., Potential-induced structural transitions of DL-homocysteine monolayers on Au(111) electrode surfaces. *Chemical Physics* **2005,** 319, 210-221.

108. Kurulugama, R. T.; Wipf, D. O.; Takacs, S. A.; Pongmayteegul, S.; Garris, P. A.; Baur, J. E., Scanning electrochemical microscopy of model neurons: constant distance imaging. *Analytical Chemistry* **2005,** 77, 1111-1117.